Eur. Phys. J. C (2021) 81:1118
https://doi.org/10.1140/epjc/s10052-021-09749-7

THE EUROPEAN PHYSICAL JOURNAL C

Check for updates

Regular Article - Experimental Physics

Search for chargino–neutralino pair production in final states with three leptons and missing transverse momentum in $\sqrt{s} = 13$ TeV pp collisions with the ATLAS detector

ATLAS Collaboration[*]

CERN, 1211 Geneva 23, Switzerland

Received: 7 June 2021 / Accepted: 12 October 2021
© CERN for the benefit of the ATLAS collaboration 2021

Abstract A search for chargino–neutralino pair production in three-lepton final states with missing transverse momentum is presented. The study is based on a dataset of $\sqrt{s} =$ 13 TeV pp collisions recorded with the ATLAS detector at the LHC, corresponding to an integrated luminosity of 139 fb^{-1}. No significant excess relative to the Standard Model predictions is found in data. The results are interpreted in simplified models of supersymmetry, and statistically combined with results from a previous ATLAS search for compressed spectra in two-lepton final states. Various scenarios for the production and decay of charginos ($\tilde{\chi}_1^{\pm}$) and neutralinos ($\tilde{\chi}_2^0$) are considered. For pure higgsino $\tilde{\chi}_1^{\pm}\tilde{\chi}_2^0$ pair-production scenarios, exclusion limits at 95% confidence level are set on $\tilde{\chi}_2^0$ masses up to 210 GeV. Limits are also set for pure wino $\tilde{\chi}_1^{\pm}\tilde{\chi}_2^0$ pair production, on $\tilde{\chi}_2^0$ masses up to 640 GeV for decays via on-shell W and Z bosons, up to 300 GeV for decays via off-shell W and Z bosons, and up to 190 GeV for decays via W and Standard Model Higgs bosons.

1 Introduction

Supersymmetry (SUSY) [1–6] postulates a symmetry between bosons and fermions, and predicts the existence of new partners for each Standard Model (SM) particle. This extension offers a solution to the hierarchy problem [7–11] and provides a candidate for dark matter as the lightest supersymmetric particle (LSP), which will be stable in the case of conserved R-parity [12].

This paper describes a search for direct production of charginos and neutralinos, mixtures of the SUSY partners of the electroweak gauge and Higgs (h) bosons, decaying to three charged leptons, and significant missing transverse momentum ($\mathbf{p}_{\mathrm{T}}^{\mathrm{miss}}$, of magnitude $E_{\mathrm{T}}^{\mathrm{miss}}$). The search uses the full Run 2 dataset of proton–proton collisions recorded between 2015 and 2018 with the ATLAS detector at the CERN Large Hadron Collider (LHC). Protons were collided at a centre-of-mass energy $\sqrt{s}$ of 13 TeV and the dataset corresponds to an integrated luminosity of 139 fb^{-1} [13]. Similar searches at the LHC have been reported by the ATLAS [14–20] and CMS collaborations [21–27].

Previous results are extended by analysing the full ATLAS Run 2 dataset, improving the signal selection strategies – particularly for intermediately compressed mass spectra, and exploiting improved particle reconstruction performance. Significant gains in lepton identification and isolation performance follow from updates in the electron reconstruction as well as from the use of a novel multivariate discriminant [28]. Furthermore, the new results are statistically combined with a previous ATLAS search [18] targeting compressed mass spectra and two-lepton final states. Finally, the paper reports updated results for a previous ATLAS search which observed excesses of three-lepton events in the partial, 36 fb^{-1}, Run 2 dataset [15]. The original analysis using the Recursive Jigsaw Reconstruction (RJR) technique [29,30] is repeated using the full Run 2 dataset, and no significant excesses relative to the SM expectation are observed. A related follow-up search emulating the RJR technique with conventional laboratory-frame variables, also using the full Run 2 dataset, was published in Ref. [16]. The updated RJR results are not included in the combination with the new results, as they are not statistically independent and not competitive with the results of the new search optimised for the full Run 2 dataset.

Section 2 introduces the target SUSY scenarios, while a brief overview of the ATLAS detector is presented in Sect. 3, followed by a description of the dataset and Monte Carlo simulation in Sect. 4. After a discussion of the event reconstruction and physics objects used in the analysis in Sects. 5, 6 covers the general analysis strategy, including the definition of signal regions, background estimation techniques, and systematic uncertainties. This is followed by Sect. 7, with details specific to the on-shell WZ selection and the

[*] e-mail: atlas.publications@cern.ch

Published online: 20 December 2021

Wh selection, and Sect. 8, with details specific to the off-shell *WZ* selection. Results are presented in Sect. 9, together with the interpretation in the context of relevant SUSY scenarios. Section 10 reports the follow-up RJR analysis, and finally Sect. 11 summarises the main conclusions.

2 Target scenarios

The bino, the winos, and the higgsinos are respectively the superpartners of the $U(1)_Y$ and $SU(2)_L$ gauge fields, and the Higgs field. In the minimal supersymmetric extension of the SM (MSSM) [31,32], M_1, M_2, and μ are the mass parameters for the bino, wino, and higgsino states, respectively. Through mixing of the superpartners, chargino ($\widetilde{\chi}^{\pm}_{1,2}$) and neutralino ($\widetilde{\chi}^{0}_{1,2,3,4}$) mass eigenstates are formed. These are collectively referred to as electroweakinos, and the subscripts indicate increasing electroweakino mass. If the $\widetilde{\chi}^{0}_{1}$ is stable, e.g. as the lightest supersymmetric particle (LSP) and with R-parity conservation assumed, it is a viable dark-matter candidate [33,34].

Two physics scenarios are considered in this search. In the first scenario, referred to as the 'wino/bino scenario', mass parameters $|M_1| < |M_2| \ll |\mu|$ are assumed such that the produced electroweakinos have a wino and/or bino nature, with the $\widetilde{\chi}^{\pm}_{1}$ and $\widetilde{\chi}^{0}_{2}$ being wino dominated, and the $\widetilde{\chi}^{0}_{1}$ LSP being bino dominated. Such a hierarchy is typically predicted by either a class of models in the framework of gaugino mass unification at the GUT scale (including mSUGRA [35,36] and cMSSM [37]), or a MSSM parameter space where the discrepancy between the measured muon anomalous magnetic moment [38], and its SM predictions [39] can be explained [40–42]. When the mass-splitting between $\widetilde{\chi}^{\pm}_{1}$ and $\widetilde{\chi}^{0}_{1}$ is 15–30 GeV, this hierarchy is also motivated by the fact that the LSP can naturally be a thermal-relic dark-matter candidate that was depleted in the early universe through co-annihilation processes to match the observed dark-matter density [43–45]. These models are poorly constrained by dark-matter direct-detection experiments, and collider searches constitute the only direct probe for $|\mu| > 800$ GeV [46].

The second scenario, referred to as the 'higgsino scenario', considers a triplet of higgsino-like states ($\widetilde{\chi}^{\pm}_{1}$, $\widetilde{\chi}^{0}_{2}$, $\widetilde{\chi}^{0}_{1}$) to be the lightest SUSY particles. This type of scenario is motivated by naturalness arguments [47,48], which suggest that $|\mu|$ should be near the weak scale [49–52], while M_1 and/or M_2 can be larger. The mass-splittings between the light higgsino states are determined by the magnitude of M_1 or M_2 relative to $|\mu|$. For the higgsino scenario this paper considers the regime where the mass-splitting between $\widetilde{\chi}^{0}_{2}$ and $\widetilde{\chi}^{0}_{1}$ is about 5–60 GeV, corresponding to cases where the wino and bino states are moderately decoupled (M_1, $M_2 > 0.5$ TeV).

Simplified SUSY models [53–55] for the two scenarios are considered for optimisation of the selections and interpretation of the results. For the wino/bino scenario, the $\widetilde{\chi}^{\pm}_{1}$ and $\widetilde{\chi}^{0}_{2}$ are assumed to be mass degenerate and purely wino, while the $\widetilde{\chi}^{0}_{1}$ is purely bino. The product of the two signed neutralino eigenmass parameters $m_{\text{eig}}(\tilde{\chi}^{0}_{2}) \times m_{\text{eig}}(\tilde{\chi}^{0}_{1})$ can be either positive or negative,[1] and the two cases are referred to as the wino/bino '(+)' or '(−)' scenario, respectively. For the higgsino scenario, the $\widetilde{\chi}^{\pm}_{1}$, $\widetilde{\chi}^{0}_{2}$ and $\widetilde{\chi}^{0}_{1}$ are purely higgsino states, and the mass of the $\widetilde{\chi}^{\pm}_{1}$ is assumed to be exactly the mean of the $\widetilde{\chi}^{0}_{1}$ and $\widetilde{\chi}^{0}_{2}$ masses. In both scenarios, all other SUSY particles are assumed to be heavier, such that they do not affect the production and decay of the $\widetilde{\chi}^{\pm}_{1}$ and $\widetilde{\chi}^{0}_{2}$.

The search targets direct pair production of the lightest chargino and the next-to-lightest neutralino, $\widetilde{\chi}^{\pm}_{1}\widetilde{\chi}^{0}_{2}$, decaying into a pair of $\widetilde{\chi}^{0}_{1}$ LSPs via an intermediate state with a W boson and a Z boson (WZ mediated), or a W boson and a SM Higgs boson (Wh mediated). Final states with three light-flavour leptons (electrons or muons, referred to as 'leptons' in the rest of this paper) are explored. One lepton originates from a leptonic decay of a W boson, and two leptons come from the direct decay of a Z boson or the indirect decay of a Higgs boson. The signatures are also characterised by the presence of $E_{\text{T}}^{\text{miss}}$ originating from the LSPs, and this $E_{\text{T}}^{\text{miss}}$ component is enhanced when hadronic initial-state radiation (ISR) is present, due to recoil between the $\widetilde{\chi}^{\pm}_{1}\widetilde{\chi}^{0}_{2}$ system and the jets.

The following three simplified model scenarios of $\widetilde{\chi}^{\pm}_{1}\widetilde{\chi}^{0}_{2}$ pair production, as illustrated in Fig. 1, are considered with dedicated selections:

- *On-shell WZ* selection: $\tilde{\chi}^{0}_{2} \to Z\tilde{\chi}^{0}_{1}$ with 100% branching ratio, where $\Delta m(\tilde{\chi}^{0}_{2}, \tilde{\chi}^{0}_{1}) \gtrsim m_Z$, for the wino/bino (+) scenario.
- *Off-shell WZ* selection: $\tilde{\chi}^{0}_{2} \to Z^{(*)}\tilde{\chi}^{0}_{1}$ with 100% branching ratio, where $\Delta m(\tilde{\chi}^{0}_{2}, \tilde{\chi}^{0}_{1}) < m_Z$, for the wino/bino (+), the wino/bino (−), and the higgsino scenarios.
- *Wh* selection: $\tilde{\chi}^{0}_{2} \to h\tilde{\chi}^{0}_{1}$ with 100% branching ratio, where $\Delta m(\tilde{\chi}^{0}_{2}, \tilde{\chi}^{0}_{1}) > m_h$, for the wino/bino (+) scenario.

A 100% branching ratio is assumed for $\tilde{\chi}^{\pm}_{1} \to W^{(*)}\tilde{\chi}^{0}_{1}$ for all models. Unless otherwise indicated, mass splitting Δm refers to $\Delta m(\tilde{\chi}^{0}_{2}, \tilde{\chi}^{0}_{1})$ in the rest of this paper. For the considered Wh-mediated scenarios, the Higgs boson has SM properties and branching fractions; and three-lepton final states

[1] The mixing matrix used to diagonalise the neutral electroweakino states can be complex, even in the absence of CP violation, but can be made real at the cost of introducing negative mass eigenstates. The sign will affect the couplings and thus the distributions in the decay under consideration. For additional discussion of this, see Ref. [56] and Appendix A of Ref. [57].

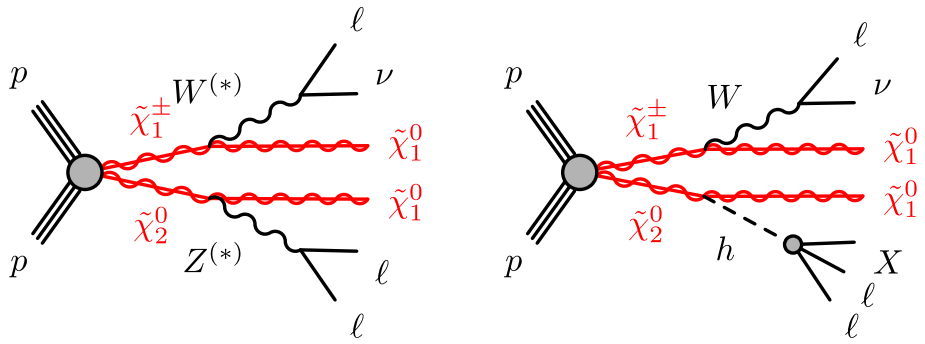

Fig. 1 Diagrams of the targeted simplified models: $\tilde{\chi}_1^{\pm}\tilde{\chi}_2^0$ pair production with subsequent decays into two $\tilde{\chi}_1^0$, via leptonically decaying W, Z and SM Higgs bosons, three leptons and a neutrino. Diagrams are shown for (left) intermediate WZ (W^*Z^*) as well as (right) intermediate Wh, with the Higgs boson decaying indirectly into leptons+X (where X denotes additional decay products) via WW, ZZ, or $\tau\tau$

are expected with one lepton coming from the W boson and the remaining two from Higgs boson decays via WW, ZZ or $\tau\tau$.

For $\widetilde{\chi}_1^{\pm}\widetilde{\chi}_2^0$ pair production with decays via WZ to 3ℓ final states, in the wino/bino (+) scenario, limits were previously set at the LHC for $\widetilde{\chi}_1^{\pm}/\widetilde{\chi}_2^0$ masses up to 500 GeV for massless $\widetilde{\chi}_1^0$, up to 200 GeV for $\Delta m \sim m_Z$, and up to 240 GeV for 50 GeV $< \Delta m < m_Z$ [21]. Limits for mass splittings $\Delta m < 50$ GeV were set in 2ℓ final states for $\widetilde{\chi}_1^{\pm}/\widetilde{\chi}_2^0$ masses up to 250 GeV[18]. For decays via Wh to 3ℓ final states (including hadronically decaying τ-leptons), limits reached 150 GeV for massless $\widetilde{\chi}_1^0$, and as high as 145 GeV for a $\widetilde{\chi}_1^0$ mass of 20 GeV[17].

For the higgsino scenario, the most stringent limits for 5 GeV $< \Delta m <$ 55 GeV were set by ATLAS using 2ℓ final states [18] where $\widetilde{\chi}_2^0$ masses up to 130–190 GeV are excluded depending on Δm. For $\Delta m >$ 55 GeV the best limits were reported by LEP [58–63,63–67], excluding $\widetilde{\chi}_1^{\pm}$ masses up to 103.5 GeV.

3 ATLAS detector

The ATLAS detector [68] is a general-purpose particle detector with almost 4π solid angle coverage around the interaction point.[2] It consists of an inner tracking system surrounded by a superconducting solenoid, sampling electromagnetic and hadronic calorimeters, and a muon spectrometer encompassing superconducting toroidal magnets.

The inner detector (ID) reconstructs charged-particle tracks in the pseudorapidity range $|\eta| < 2.5$, using silicon pixel and microstrip subsystems followed by a transition radiation tracker. For $\sqrt{s} = 13$ TeV data-taking an additional innermost layer, the insertable B-layer [69,70], was added to the pixel tracker to improve tracking performance and flavour identification of quark-initiated jets. The ID is immersed in a 2 T axial magnetic field provided by the surrounding thin, superconducting solenoid.

Beyond the ID a high-granularity lead/liquid-argon (LAr) electromagnetic sampling calorimeter (ECAL) and a steel/scintillator-tile hadronic sampling calorimeter cover $|\eta| < 3.2$ and $|\eta| < 1.7$ respectively. In the forward regions a copper/LAr endcap calorimeter extends the hadronic coverage to $1.7 < |\eta| < 3.2$, while copper/LAr and tungsten/LAr forward calorimeters are used for electromagnetic and hadronic measurements in the $3.1 < |\eta| < 4.9$ region. The muon spectrometer (MS) surrounds the calorimeters and comprises three layers of trigger and high-precision tracking chambers spanning $|\eta| < 2.4$ and $|\eta| < 2.7$, respectively. A magnetic field is provided by a system of three superconducting air-core toroidal magnets with eight coils each.

Events of interest are selected using a two-level trigger system [71] consisting of a custom hardware-based first-level (L1) trigger followed by a software-based high-level trigger (HLT). The L1 trigger accepts events from the 40 MHz bunch crossings at a rate below 100 kHz, which the high-level trigger reduces in order to record events to disk at about 1 kHz.

4 Data and Monte Carlo simulated event samples

This analysis exploits the full Run 2 $\sqrt{s} = 13$ TeV pp dataset recorded by the ATLAS experiment during stable beam conditions between 2015 and 2018. The LHC collided protons with bunch-crossing intervals of 25 ns, and the average number of interactions per crossing in data was $\langle\mu\rangle = 34$. After applying beam, detector and data-quality requirements [72],

[2] ATLAS uses a right-handed coordinate system with its origin at the nominal interaction point (IP) in the centre of the detector and the z-axis along the beam pipe. The x-axis points from the IP to the centre of the LHC ring, and the y-axis points upwards. Cylindrical coordinates (r, ϕ) are used in the transverse plane, ϕ being the azimuthal angle around the z-axis. Pseudorapidity is defined in terms of the polar angle θ as $\eta = -\ln\tan(\theta/2)$. Angular distance is measured in units of $\Delta R \equiv \sqrt{(\Delta\eta)^2 + (\Delta\phi)^2}$. Rapidity is defined by $y = \frac{1}{2}\ln[(E+p_z)/(E-p_z)]$, where E is the energy and p_z is the longitudinal component of the momentum along the beam direction.

the dataset corresponds to a total integrated luminosity of 139 fb^{-1} [13], with an uncertainty in the integrated luminosity of 1.7%, obtained using the LUCID-2 detector [73] for the primary luminosity measurements.

The expected contributions of SM processes and $\tilde{\chi}_1^{\pm}\tilde{\chi}_2^0$ SUSY signals are estimated using Monte Carlo (MC) simulation. The MC samples are used in the optimisation of event selection criteria, as well as for yield prediction and the estimation of systematic uncertainties in the yield prediction. The yield prediction for the dominant WZ background is improved by extracting normalisation factors from data in dedicated control regions, as discussed in Sect. 6.2. The background contribution from events with one or more misidentified or non-prompt leptons is estimated using a data-driven method also outlined in Sect. 6.2. For all other processes, the MC-predicted yields are used directly. The samples are produced including an ATLAS detector simulation [74] based on GEANT4 [75], or a faster simulation using a parameterised calorimeter response [76] and GEANT4 for all other detector systems. Simulated events are reconstructed in the same way as data events. Details of the MC simulation, including the generators used for the matrix element (ME) calculation and the parton shower (PS), hadronisation and underlying event (UE) modelling, the parton distribution function (PDF) sets used in the ME and PS, the set of tuned parameter values used as the UE tune, and the order of the cross-section calculations used for yield normalisation are given in Table 1 and briefly discussed below.

The SUSY $\tilde{\chi}_1^{\pm}\tilde{\chi}_2^0 \rightarrow WZ/Wh \rightarrow 3\ell$ signal samples were generated from leading-order (LO) matrix elements with up to two additional partons using MADGRAPH 2.6 and PYTHIA 8.2, for both the wino/bino and the higgsino scenarios. MADSPIN [125] was used to model off-shell WZ decays. The ME–PS matching was done using the CKKW-L prescription [126,127], with the matching scale set to one quarter of the $\tilde{\chi}_1^{\pm}/\tilde{\chi}_2^0$ mass. Samples were generated for $\tilde{\chi}_1^{\pm}/\tilde{\chi}_2^0$ masses between 100 GeV and 850 GeV, and mass splittings Δm between 5 GeV and 850 GeV. Only $\tilde{\chi}_1^{\pm}/\tilde{\chi}_2^0$ decays via bosons, which in turn decay leptonically via SM branching fractions, are considered. For the Wh samples, only Higgs boson decays via WW, ZZ and $\tau\tau$ were generated, with cross section times branching fractions corrected to match the SM Higgs branching fractions [109]. The generated signal events are required to have at least two leptons for the on-shell WZ samples, and at least three leptons for the off-shell WZ samples and the Wh samples; hadronically decaying τ-leptons are not considered in the requirement.

The only difference between the two wino/bino scenarios (positive or negative $m_{\text{eig}}(\tilde{\chi}_2^0) \times m_{\text{eig}}(\tilde{\chi}_1^0)$) is the mass lineshape of the Z boson from the $\tilde{\chi}_2^0$ decay, particularly when $\Delta m < m_Z$ and the Z boson is off-shell.[3] The samples were generated for the (+) scenario and a reweighting in $m_{Z^{(*)}}$, based on an analytic function presented in Ref. [128], was used to simulate the (−) scenario.

Inclusive production cross sections are computed at next-to-leading order (NLO) plus next-to-leading-log (NLL) precision [79–84]. For wino production the computation is performed in the limit of mass-degenerate $\tilde{\chi}_1^{\pm}$ and $\tilde{\chi}_2^0$, and with light $\tilde{\chi}_1^0$, while for higgsino production a partially degenerate case is considered, with the $\tilde{\chi}_1^{\pm}$ mass equal to the mean of the $\tilde{\chi}_1^0$ and $\tilde{\chi}_2^0$ masses; all the other supersymmetric particles (sparticles) are assumed to be heavy and decoupled. For production at a centre-of-mass energy of $\sqrt{s} = 13$ TeV, the wino (higgsino) $\tilde{\chi}_1^{\pm}\tilde{\chi}_2^0$ cross section ranges between 22.67 ± 0.97 pb (12.22 ± 0.26 pb, $\Delta m = 80$ GeV) and 3.42 ± 0.41 fb (87.2 ± 3.2 fb, $\Delta m = 20$ GeV) for $\tilde{\chi}_2^0$ masses between 100 GeV and 850 (320) GeV, with the higgsino cross section depending additionally on Δm.

Diboson, triboson and Z+jets processes were simulated with the SHERPA 2.2 generator. ME–PS matching and merging is based on Catani–Seymour dipole factorisation [122,129,130], using improved CKKW matching [131,132] extended to NLO accuracy using the MEPS@NLO prescription [130–133], and including NLO virtual QCD corrections for the ME [134,135]. The diboson samples cover dilepton masses down to 4 GeV for $p_{\text{T}}^{\ell_1}$, $p_{\text{T}}^{\ell_2} > 5$ GeV, and down to $m_{\ell\ell} > 2m_{\ell} + 250$ MeV if $p_{\text{T}}^{\ell_1} > 5$ GeV and any of $m_{\ell\ell} > 4$ GeV, $p_{\text{T}}^{\ell_1} > 20$ GeV, or $E_{\text{T}}^{\text{miss}} > 50$ GeV are satisfied. The standard multiboson samples do not include Higgs boson production. An alternative triboson sample including off-shell contributions and leptonically decaying $h \rightarrow VV$ (with $V = W$ or Z) contributions is used in the off-shell WZ selection, where W^*Z^* decays are targeted and off-shell triboson processes are non-negligible in the estimation of the SM background; dilepton masses down to 4 GeV are considered in the sample.

The $t\bar{t}$, single-top tW, t-channel, s-channel and $t\bar{t}h$ processes were modelled using POWHEG BOX 2 + PYTHIA 8. The h_{damp} parameter[4] was set to 1.5 times the top-quark mass [136]. The samples were generated employing the five-flavour scheme (four-flavour in case of single-top t-channel), and a diagram removal scheme [137] was used in the case of tW to remove interference and overlap with $t\bar{t}$ production. Other top-quark processes ($t\bar{t}V$, tZ, tWZ, $t\bar{t}VV$, $t\bar{t}\ell\ell$ ($t \rightarrow Wb + (\gamma^*/Z \rightarrow \ell\ell)$), 3-top and 4-top) were modelled using MADGRAPH5_AMC@NLO 2 + PYTHIA 8. Samples of Higgs boson production via gluon fusion, vector-

[3] See also Section 3 of Ref. [18].

[4] The h_{damp} parameter is a resummation damping factor and one of the parameters that controls the matching of POWHEG matrix elements to the parton shower and thus effectively regulates the high-p_{T} radiation against which the $t\bar{t}$ system recoils.

Table 1 Monte Carlo simulation details by physics process. The table lists the event generators used for ME and PS calculations, the accuracy of the ME calculation, the PDF sets and UE parameter tunes used, and the order in α_s of cross-section calculations used for yield normalisation ('–' if the cross section is taken directly from MC simulation)

Process	Event generator	ME accuracy	ME PDF set	Cross-section normalisation
$\tilde{\chi}_1^{\pm}\tilde{\chi}_2^0$	MadGraph 2.6 [77]	0,1,2j@LO	NNPDF2.3lo [78]	NLO+NLL [79–84]
Diboson [85]	Sherpa 2.2.2 [86]	0, 1j@NLO + 2,3j@LO	NNPDF3.0nlo [87]	–
Triboson [85]	Sherpa 2.2.2	0j@NLO + 1,2j@LO	NNPDF3.0nlo	–
Triboson (alternative) [85]	Sherpa 2.2.1	0,1j@LO	NNPDF2.3lo	–
Z+jets [88]	Sherpa 2.2.1	0,1,2j@NLO + 3,4j@LO	NNPDF3.0nlo	NNLO [89]
$t\bar{t}$ [90]	Powheg Box 2 [91–93]	NLO	NNPDF3.0nlo	NNLO+NNLL [94–100]
tW [101]	Powheg Box 2	NLO	NNPDF3.0nlo	NLO+NNLL [102,103]
single-t (t-channel [104], s-channel [105])	Powheg Box 2	NLO	NNPDF3.0nlo	NLO [106,107]
$t\bar{t}h$ [108]	Powheg Box 2	NLO	NNPDF3.0nlo	NLO [109]
$t\bar{t}V$, tZ, tWZ	MadGraph5_aMC@NLO 2.3	NLO	NNPDF3.0nlo	–
$t\bar{t}\ell\ell$ ($t \to Wb + (\gamma^*/Z \to \ell\ell)$) [110]	MadGraph5_aMC@NLO 2.3	LO	NNPDF2.3lo	–
$t\bar{t}\,VV$, 3-top, 4-top	MadGraph5_aMC@NLO 2.2	LO	NNPDF2.3lo	–
Higgs (ggF)	Powheg Box 2	NNLO+NNLL	NNPDF3.0nlo	NNNLO+NLO(EWK) [109,111–116]
Higgs (VBF)	Powheg Box 2	NLO+NNLL	NNPDF3.0nlo	NNLO+NLO(EWK) [109,117–119]
Higgs (Vh)	Powheg Box 2	NLO	NNPDF3.0nlo	NNLO+NLO(EWK) [109]

Process	PS and hadronisation	PS PDF set	UE tune
$\tilde{\chi}_1^{\pm}\tilde{\chi}_2^0$	Pythia 8.2 [120]	NNPDF2.3lo	A14 [121]
Diboson, triboson, Z+jets	Sherpa 2.2.2	default Sherpa [122]	default Sherpa
Triboson (alternative)	Sherpa 2.2.1	default Sherpa	default Sherpa
$t\bar{t}$, tW, single-t, $t\bar{t}h$	Pythia 8.2	NNPDF2.3lo	A14
$t\bar{t}V$, tZ, tWZ, $t\bar{t}\ell\ell$	Pythia 8.2	NNPDF2.3lo	A14
$t\bar{t}\,VV$, 3-top, 4-top	Pythia 8.1	NNPDF2.3lo	A14
Higgs (ggF, VBF, Vh)	Pythia 8.2	CTEQ6L1 [123]	AZNLO [124]

j jet, *LO* leading order, *NLO* next-to-leading order, *NNLO* next-to-next-to-leading order, *NNNLO* next-to- next-to-next-to-leading order, *NLL* next-to-leading-log, *NNLL* next-to-next-to-leading-log, *EWK* electroweak

boson fusion and associated production were generated using POWHEG BOX 2 + PYTHIA 8.

All background and signal samples make use of EVTGEN 1.6.0 and 1.2.0 [138] for the modelling of b- and c-hadrons, except those generated using SHERPA. The effect of additional interactions in the same and neighbouring bunch crossings (pile-up) was included by overlaying simulated minimum-bias interactions onto each hard-scatter process. The simulation was done using PYTHIA 8.2 with the A3 tune [139] and the NNPDF2.3lo set of PDFs, and the samples were reweighted such that the pile-up distribution matches the one in data.

5 Event reconstruction and preselection

The strategy for event reconstruction and preselection is defined here, where a common approach has been adopted for all regions in the analysis, unless specified otherwise. Further selection specific to individual regions is discussed in Sects. 6 to 8.

Events are chosen for the Wh and on-shell WZ selections using dilepton triggers and for the off-shell WZ selection using single-lepton, dilepton and trilepton triggers [140,141]. The off-shell WZ selection is complemented at high $E_{\mathrm{T}}^{\mathrm{miss}}$ with softer-lepton events selected using $E_{\mathrm{T}}^{\mathrm{miss}}$ triggers [142]. The lepton triggers use various p_{T} thresholds, depending on the lepton type, quality and multiplicity. To ensure trigger efficiencies are well understood in the analysis phase space, tighter quality and p_{T} requirements are applied to fully reconstructed signal leptons, as defined below. Single-electron triggers are not used, to facilitate looser signal-lepton identification criteria. The number of leptons in the event that activate the trigger must be at least as many as the number of leptons required in the trigger, and electrons (muons) activating the trigger must have a fully calibrated p_{T} above 18 GeV (27.3, 14.7 or 6.5 GeV, for increasing trigger-lepton multiplicity). For events selected by a $E_{\mathrm{T}}^{\mathrm{miss}}$ trigger, an offline requirement of $E_{\mathrm{T}}^{\mathrm{miss}} > 200$ GeV is imposed to similarly ensure well-understood trigger efficiencies in the analysis phase space.

Events are required to have at least one reconstructed pp interaction vertex [143,144] with a minimum of two associated tracks with $p_{\mathrm{T}} > 500$ MeV. In events with multiple vertices, the primary vertex is defined as the one with the highest $\sum p_{\mathrm{T}}^2$ of associated tracks.

The primary objects used in this analysis are electrons, muons and jets. To be considered, reconstructed objects must satisfy 'baseline' loose identification criteria; to be selected for the analysis regions, they must also survive a second, tighter set of 'signal' identification requirements. Additionally, a lepton 'anti-ID' requirement is defined, corresponding to leptons that satisfy the baseline criteria but not the signal criteria. These anti-ID leptons are used in the Z + jets background estimation in Sect. 6.2. Hadronically decaying τ-leptons are not considered in the analysis, and the term 'lepton' always refers to electrons or muons in this document.

Electron candidates are reconstructed from three-dimensional clustered energy deposits in the electromagnetic calorimeter (ECAL), matched to an ID track [145]. Muon candidates are reconstructed by matching MS tracks or track segments to ID tracks [146]. Electron and muon candidates are calibrated in situ [145,146], using $Z \to ee$, $J/\psi \to ee$, $Z \to \mu\mu$ and $J/\psi \to \mu\mu$ decays. Baseline electrons are required to have $p_{\mathrm{T}} > 4.5$ GeV and fall within the acceptance of the ID ($|\eta| < 2.47$). They are further required to satisfy the calorimeter- and tracking-based '*Loose and B-layer* likelihood' identification [145]. Baseline muons must have $p_{\mathrm{T}} > 3$ GeV and $|\eta| < 2.5$, and satisfy *Medium* identification criteria [146]. To suppress pile-up, both the baseline electrons and baseline muons are required to have a trajectory consistent with the primary vertex, i.e. $|z_0 \sin\theta| < 0.5$ mm.[5]

Jet candidates are reconstructed from topological energy clusters in the electromagnetic and hadronic calorimeters [147], grouped using the anti-k_t algorithm [148,149] with radius parameter $R = 0.4$. After subtracting the expected energy contribution from pile-up following the jet area technique [150], the jet energy scale (JES) and resolution (JER) are corrected to particle level using MC simulation, and then calibrated in situ using Z+jets, γ+jets and multijet events [151,152]. Baseline jets must then have $p_{\mathrm{T}} > 20$ GeV, and fall within the full calorimeter acceptance ($|\eta| < 4.5$).

Photon candidates are reconstructed from energy clusters in the ECAL provided they have no matched track, or have one or more matched tracks consistent with photon conversion origin. Baseline photons, while not used in the signal regions, are included in the calculation of missing transverse momentum, and used in SM background estimation validation. They are required to have $p_{\mathrm{T}} > 25$ GeV, fall inside the ECAL strip detector acceptance ($|\eta| < 2.37$), but outside the ECAL transition region ($|\eta| \in [1.37, 1.52]$). Candidates must also satisfy *Tight* identification criteria [145].

Ambiguities may exist between reconstructed objects. To prevent single detector signatures from being identified as multiple objects, the following overlap removal procedure is applied to baseline leptons and jets. First, all electrons sharing an ID track with a muon are discarded to remove bremsstrahlung from muons that is followed by a photon conversion. Second, all jets separated from remaining electrons by less than $\Delta R = 0.2$ are removed. Also, all jets within

[5] The transverse impact parameter, d_0, is defined as the distance of closest approach in the transverse plane between a track and the beam-line. The longitudinal impact parameter, z_0, corresponds to the z-coordinate distance between the point along the track at which the transverse impact parameter is defined and the primary vertex.

$\Delta R = 0.4$ of a muon and associated with fewer than three tracks with $p_{\mathrm{T}} \geq 500$ MeV are removed. Finally, electrons or muons separated from surviving jets by less than $\Delta R = 0.4$ are discarded to reject non-prompt leptons from decays of b- and c-hadrons.

The missing transverse momentum is defined as the negative vector sum of the transverse momenta of all baseline objects (electrons, muons, jets, and photons) and an additional soft term [153]. The soft term is constructed from all tracks that pass basic quality requirements and are associated with the primary vertex, but are not associated with any baseline object. In this way, the $\mathbf{p}_{\mathrm{T}}^{\mathrm{miss}}$ is adjusted for the calibration of the contributing objects, while maintaining robustness against pile-up [154]. Additionally, an 'object-based $E_{\mathrm{T}}^{\mathrm{miss}}$ significance' [155] is defined as $\sqrt{|\mathbf{p}_{\mathrm{T}}^{\mathrm{miss}}|^2/(\sigma_{\mathrm{L}}^2(1-\rho_{\mathrm{LT}}^2))}$. The p_{T} resolution of the contributing objects, at a given p_{T} and $|\eta|$, is determined from parameterised Monte Carlo simulation which well reproduces the resolution measured in data. The quantity σ_{L} denotes the p_{T} resolution of the system, and ρ_{LT} is a correlation factor between the resolutions of the p_{T} components parallel (L) and perpendicular (T) to $\mathbf{p}_{\mathrm{T}}^{\mathrm{miss}}$. The $E_{\mathrm{T}}^{\mathrm{miss}}$ significance is used to discriminate events where the $E_{\mathrm{T}}^{\mathrm{miss}}$ arises from undetected particles in the final state or from events where the $E_{\mathrm{T}}^{\mathrm{miss}}$ arises from poorly measured particles (and jets). It is also useful in discriminating between signal events with large $E_{\mathrm{T}}^{\mathrm{miss}}$ and e.g. Z + jets events with medium-to-low $E_{\mathrm{T}}^{\mathrm{miss}}$.

To ensure high-quality object measurement and selection purity for the analysis regions, leptons and jets must satisfy additional tighter 'signal' criteria and isolation requirements to be selected. Signal jets are selected within $|\eta| < 2.8$, and must satisfy *Loose* quality criteria to reject contamination from non-collision backgrounds or noise bursts [156]. In order to suppress jets originating from pile-up, signal jet candidates with $p_{\mathrm{T}} < 120$ GeV and $|\eta| < 2.5$ (within the ID acceptance) are further required to satisfy the *Medium* working point of the track-based jet vertex tagger (JVT) [150,157]. For jets with $|\eta| < 2.5$ a multivariate discriminant – constructed using track impact parameters, information about displaced secondary vertices, and trajectories of b- and c-hadrons inside the jet [158] – is used for the identification of b-hadron decays, referred to as b-jets. The b-tagging algorithm working point is chosen such that b-jets from simulated $t\bar{t}$ events are identified with 85% efficiency, with rejection factors of 2.7 for charm-quark jets and 25 for light-quark and gluon jets [158]. Signal electrons must satisfy *Medium* identification criteria [145]. All signal leptons are then required to be compatible with originating from the primary vertex; the significance of the transverse impact parameter must satisfy $|d_0/\sigma(d_0)| < 5$ (3) for electrons (muons), where $\sigma(d_0)$ is the track-by-track estimated impact parameter resolution.

Isolation requirements are applied to suppress contributions from conversions, semileptonic decays of heavy-flavour hadrons, or hadrons and jets wrongly identified as leptons, collectively referred as fake or non-prompt (FNP) leptons. The criteria rely on isolation energy variables calculated as $\sum p_{\mathrm{T}}$ of tracks or calo-clusters within a certain size of cone around the lepton candidate; the energy of the lepton candidate itself is not considered in this calculation. The isolation working points used in this analysis are based on those described in Refs. [145,146], including updates to improve the performance under the increased pile-up conditions encountered during 2017 and 2018 data-taking. The choice of isolation working points is optimised per selection region and per lepton-flavour to account for different levels of contribution from the FNP lepton background. The *Tight* working point is used for both electrons and muons in the on-shell WZ and Wh selections, while the looser working point *Gradient* (*Loose*) is employed for electrons (muons) in the off-shell WZ selection to maintain a reasonable efficiency down to low p_{T}.

To further suppress FNP lepton backgrounds in the off-shell WZ selection, a dedicated multivariate discriminant 'non-prompt lepton BDT' [28] is used to tighten the requirements on the lepton with the lowest p_{T} (which is commonly also the most FNP-like lepton of the three), after selecting exactly three baseline leptons in the event. The discriminant uses eight input variables including the isolation information, combined lepton and track quantities, and the b-jet likeliness calculated from the energy deposits and tracks in a cone around the lepton using the `DL1mu` or `RNNIP` algorithms [159]. The non-prompt lepton BDT selection is designed to maintain 70–90% efficiency for real leptons, for lepton p_{T} below 20 GeV, with a rejection factor of 2–3 for FNP leptons passing the isolation selection. Figure 2 shows the combined signal lepton selection efficiency (including the reconstruction, identification, isolation, vertex association and non-prompt BDT selection) for the leptons from $\widetilde{\chi}_1^{\pm}\widetilde{\chi}_2^0$ signal events, as well as the differential probability for a Z + jets event to be accompanied by a FNP lepton satisfying the signal lepton selection criteria.

To account for small efficiency differences between simulation and data, simulated events are corrected with scale factors covering lepton reconstruction, identification, isolation and trigger efficiencies, as well as jet pile-up rejection and flavour-tagging efficiencies.

A common preselection is applied for all search regions requiring exactly three signal leptons. Events are also required to have exactly three baseline leptons. This additional baseline requirement ensures orthogonality with other ATLAS SUSY analyses [18,160,161] and facilitates statistical combinations; it also simplifies the FNP lepton background estimation. Muons in the region $2.5 < |\eta| < 2.7$ are exceptionally included in this count if they satisfy all other baseline muon criteria, in order to harmonise with the definition applied in the other analyses.

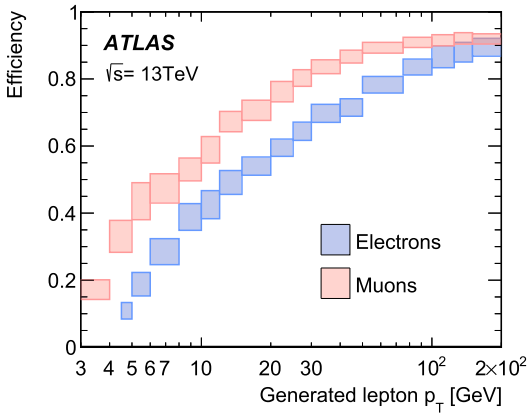

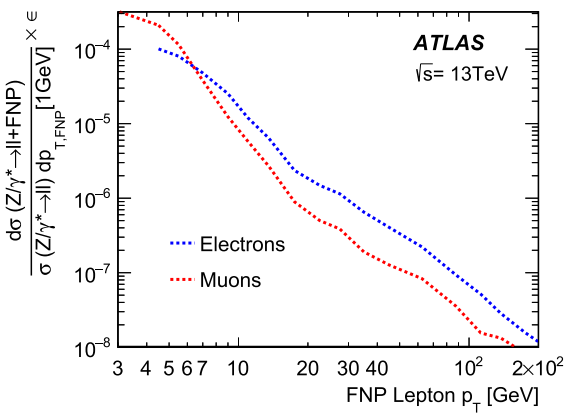

Fig. 2 The left panel shows the combined lepton selection efficiencies for the signal electron/muon requirements applied to the lowest-p_{T} lepton after selecting three baseline leptons in the off-shell WZ selection. The efficiencies are calculated using simulated samples of wino/bino (+) $\widetilde{\chi}_1^{\pm}/\widetilde{\chi}_2^0$ decays and shown as a function of the generated lepton p_{T}. The associated uncertainties represent the range of efficiencies observed across all signal samples used for the given p_{T} bin. The right panel illustrates the differential probability for a $Z+$jets event to be accompanied by a FNP lepton satisfying the signal lepton criteria, as a function of the FNP lepton p_{T}. This probability is measured using data events in a region with at least two signal leptons, with the other processes subtracted using the MC samples

6 Analysis strategy

The selections in this paper – while targeting different simplified model scenarios – all consider final states with exactly three leptons, possible ISR jets, and $E_{\mathrm{T}}^{\mathrm{miss}}$. Therefore, a common approach is used throughout most steps of the analyses. The on-shell WZ, off-shell WZ, and Wh selections are optimised independently.

This section describes the general analysis strategy, introducing the common parts of the search region definitions (Sect. 6.1), the background estimation (Sect. 6.2), and the uncertainty treatment (Sect. 6.3). The statistical methods used are outlined in Sect. 6.4. Further details specific to either the on-shell WZ selection and the Wh selection, or the off-shell WZ selection, are then discussed in dedicated Sects. 7 and 8.

6.1 Search regions

Event selections enriched in signal (signal regions or SRs) are designed independently for the three targeted models, i.e. for the on-shell WZ, off-shell WZ or Wh selections. All the SRs are optimised to the wino/bino (+) scenario, maximising the expected sensitivity using benchmark signal samples. The SRs of the on-shell WZ selection, $\mathtt{SR}^{\mathtt{WZ}}$, are optimised for $\widetilde{\chi}_1^{\pm}\widetilde{\chi}_2^0$ signals with WZ-mediated decays and mass splittings near or above the Z-boson mass, $\Delta m \gtrsim m_Z$, while the SRs of the off-shell WZ selection, $\mathtt{SR}^{\mathtt{offWZ}}$, target W^*Z^*-mediated decays and mass splittings $\Delta m < m_Z$. The SRs of the Wh selection, $\mathtt{SR}^{\mathtt{Wh}}$, are optimised for Wh-mediated decays and veto Z-boson candidates.

For SRs targeting $W^{(*)}Z^{(*)}$-mediated scenarios, two leptons are assigned to the $Z^{(*)}$-boson candidate by selecting a same-flavour opposite-charge-sign (SFOS) lepton pair in the event, and the remaining lepton is assigned to the $W^{(*)}$ boson (labelled W lepton or ℓ_{W}). If more than one SFOS lepton pair is present in the event, the invariant mass $m_{\ell\ell}$ of the SFOS lepton pairs is used to select which pair is assigned to the $Z^{(*)}$-boson candidate. The on-shell WZ selection selects the SFOS lepton pair with $m_{\ell\ell}$ nearest the Z-boson mass, $m_{\ell\ell}^{mZ}$, while the off-shell WZ selection selects the SFOS lepton pair with the smallest $m_{\ell\ell}$, $m_{\ell\ell}^{\mathrm{min}}$. In the rest of this document, these two types of lepton assignment are referred to as $m_{\ell\ell}^{mZ}$-based and $m_{\ell\ell}^{\mathrm{min}}$-based lepton assignment, and $m_{\ell\ell}$ refers to $m_{\ell\ell}^{mZ}$ unless otherwise indicated. In Wh-mediated scenarios, the opposite-sign leptons are the indirect product of the Higgs boson decay and can be of either the same or different flavour. Two subsets of SRs are defined depending on lepton flavour composition: the $\mathtt{SR}_{\mathtt{SFOS}}^{\mathtt{Wh}}$ target events with at least one SFOS pair (using $m_{\ell\ell}^{mZ}$-based lepton assignment), and the $\mathtt{SR}_{\mathtt{DFOS}}^{\mathtt{Wh}}$ target complementary events without a SFOS lepton pair.

For events with at least one SFOS lepton pair the transverse mass, m_{T}, is constructed using the W lepton and the $E_{\mathrm{T}}^{\mathrm{miss}}$, and assuming the SM WZ event hypothesis: $m_{\mathrm{T}} = \sqrt{2p_{\mathrm{T}}^{\ell_{\mathrm{W}}} E_{\mathrm{T}}^{\mathrm{miss}}(1-\cos(\Delta\phi))}$, where $\Delta\phi$ is the separation in the transverse plane between the lepton and the $E_{\mathrm{T}}^{\mathrm{miss}}$. This exploits the difference between SM WZ, which has a Jacobian peak with a sharp cut-off at $m_{\mathrm{T}} \sim m_W$ (the W-boson mass), and the targeted signals, which have relatively flat distributions.

For the initial SR segmentation, events with at least one SFOS lepton pair are divided into three $m_{\ell\ell}$ slices: below,

in, and above the Z-boson mass window, defined as $m_{\ell\ell} \in [75, 105]$ GeV. The $\mathtt{SR}^{\mathtt{offWZ}}$ and $\mathtt{SR}^{\mathtt{WZ}}$ use the first and second slice, respectively, while the $\mathtt{SR}^{\mathtt{Wh}}_{\mathtt{SFOS}}$ use the first and third slice. The $\mathtt{SR}^{\mathtt{WZ}}$ are orthogonal to the $\mathtt{SR}^{\mathtt{offWZ}}$ and the $\mathtt{SR}^{\mathtt{Wh}}_{\mathtt{SFOS}}$ through the $m_{\ell\ell}$ selection. The $\mathtt{SR}^{\mathtt{offWZ}}$ and the $\mathtt{SR}^{\mathtt{Wh}}_{\mathtt{SFOS}}$ can overlap, but are never used in the same interpretation. The $\mathtt{SR}^{\mathtt{Wh}}_{\mathtt{DFOS}}$ are orthogonal to all other SRs through lepton flavour composition.

For the final selection, a few key discriminating variables are used to further segment and refine the SRs. The $\mathtt{SR}^{\mathtt{WZ}}$ and $\mathtt{SR}^{\mathtt{Wh}}$ have a shared binning strategy aside from the $m_{\ell\ell}$ range, while $\mathtt{SR}^{\mathtt{offWZ}}$ binning focuses on $m_{\ell\ell}^{\min}$ and properties of more compressed $\widetilde{\chi}_1^{\pm}\widetilde{\chi}_2^0$ signals. Ultimately, 20, 31, 19, and 2 SR bins are defined for the $\mathtt{SR}^{\mathtt{WZ}}$, $\mathtt{SR}^{\mathtt{offWZ}}$, $\mathtt{SR}^{\mathtt{Wh}}_{\mathtt{SFOS}}$, and $\mathtt{SR}^{\mathtt{Wh}}_{\mathtt{DFOS}}$, respectively. The complete definitions of these nominal SRs are further detailed per selection in subsequent Sects. 7.1 ($\mathtt{SR}^{\mathtt{WZ}}$ and $\mathtt{SR}^{\mathtt{Wh}}$) and 8.1 ($\mathtt{SR}^{\mathtt{offWZ}}$). The bins within each subset are explicitly disjoint, and are statistically combined when calculating the constraints on the target models. A more detailed overview of the fit configuration is given in Sect. 6.4. Additionally, discovery-oriented inclusive SRs are designed by grouping sets of adjoining nominal-SR bins in order to facilitate quantifying the size of data excesses in a model-independent manner. The inclusive-SR definitions are discussed in Sect. 9.1.

6.2 Background estimation

The dominant SM background in most of the SRs in this analysis is from SM WZ events with only leptonic decays, followed in importance by $t\bar{t}$ and Z + jets processes associated with at least one FNP lepton. In $\mathtt{SR}^{\mathtt{Wh}}_{\mathtt{DFOS}}$, SM Higgs, triboson and $t\bar{t}$ production are the dominant processes.

A partially data-driven method is used for the estimation of the WZ background, which produces three real and prompt leptons. The background is predicted using MC simulation samples and normalised to data in dedicated control regions (CRs). This normalisation improves the estimation in the phase space of the selections, and constrains the systematic uncertainties. The CRs are designed to be both orthogonal and similar to the SRs, whilst also having little signal contamination; this is achieved by taking the SR definitions and inverting some of the selection criteria. Dedicated validation regions (VRs) are defined kinematically in between the CRs and SRs, and are used to assess the quality of the background estimation and its extrapolation to the SRs. The final estimation of the yields and uncertainties is performed with a simultaneous fit to the CRs and SRs, as discussed in Sect. 6.4.

The $t\bar{t}$ background is predicted using MC simulation samples and validated in VRs. It is dominated by decays with a dileptonic final state and an additional lepton from a b- or c-hadron decay. As the MC modelling is found to be of good quality, no additional corrections are applied to the MC events. Rare SM processes, including multiboson and Higgs boson production, top-pair production in association with a boson, and single-top production, are estimated from MC simulation in all analysis regions.

The $(Z/\gamma^* \to \ell\ell)+(\text{jets}/\gamma)$ background has two prompt leptons and one FNP lepton from jets or photons. In the rest of this document, 'Z + jets' is used to refer to this set of processes. As there are no invisible particles in these processes at tree level, the observed $E_{\mathrm{T}}^{\mathrm{miss}}$ is mostly due to mismeasured leptons and/or jets, or due to the $E_{\mathrm{T}}^{\mathrm{miss}}$ soft term. The FNP leptons originate from a mix of sources, including light-flavour jets faking leptons, electrons from photon conversion, and non-prompt leptons from b- or c-hadron decays. Such FNP leptons often arise from instrumental effects, hadronisation, and the underlying event, all of which are challenging to model reliably in simulation. Therefore a data-driven method, referred to as the 'fake-factor method' [162,163], is used to estimate the Z + jets background. The fake factor (FF) is defined as the ratio of the probability for a given lepton candidate to pass the signal lepton requirements to that to fulfil the anti-ID requirements. This is measured using data in a control region, $\mathtt{CRFF}$, designed to target Z + jets events with FNP leptons whose sources are representative of those expected in the SRs. Exactly three baseline leptons and at least one SFOS lepton pair are required in $\mathtt{CRFF}$. The Z-boson candidate in the event is identified as the SFOS pair yielding the invariant mass closest to the Z-boson mass, and the remaining lepton is tagged as the FNP lepton candidate. The two leptons from the Z-boson candidate must activate the dilepton trigger to ensure there is no selection bias from FNP leptons. The Z + jets prediction in a given region is obtained by applying the FFs to the events in its corresponding 'anti-ID region'. This region is defined by the same selection criteria as used for the nominal region with three signal leptons, except that at least one of the leptons is anti-ID instead of signal. Each event in the anti-ID region is scaled by a weight based on the FF assigned to each anti-ID lepton in the region. The FFs are derived separately per lepton flavour and are parameterised as a function of lepton p_{T} and lepton η or $E_{\mathrm{T}}^{\mathrm{miss}}$ in the event, depending on the analysis selection. In both the FF measurement and the FF application procedure, contributions from processes other than Z + jets are subtracted using MC simulation samples.

While sharing a common approach, the estimation and validation procedures for the main SM backgrounds were optimised independently for the different selections, which each target a different primary phase-space region with different relative background composition and importance. Details are given in Sect. 7.2 ($\mathtt{CR}^{\mathtt{WZ}}$/$\mathtt{VR}^{\mathtt{WZ}}$) and Sect. 8.2 ($\mathtt{CR}^{\mathtt{offWZ}}$/$\mathtt{VR}^{\mathtt{offWZ}}$).

6.3 Systematic uncertainties

The analysis considers uncertainties in the predicted yields of signal or background processes due to instrumental systematic uncertaintiesas well as statistical uncertaintiesand theoreticalsystematic uncertaintiesof the MC simulated samples. Uncertainties are assigned to the yield in each region, except for WZ processes constrained in CRs, in which case they are assigned to the acceptance in each SR relative to that in the CR. The uncertainty treatment is largely common to the on-shell WZ, Wh and off-shell WZ selections; exceptions are discussed in Sects. 7.2 ($\mathrm{SR}^{\mathrm{WZ}}$ and $\mathrm{SR}^{\mathrm{Wh}}$) and 8.2 ($\mathrm{SR}^{\mathrm{offWZ}}$). Relative uncertainties are illustrated in a breakdown per SR in the same sections.

The dominant instrumental uncertainties are the jet energy scale (JES) and resolution (JER). The jet uncertainties are derived as a function of p_{T} and η of the jet, as well as of the pile-up conditions and the jet flavour composition of the selected jet sample. They are determined using a combination of simulated samples and studies in data, such as measurements of the jet p_{T} balance in dijet, Z+jet and γ+jet events [151,152,164]. Another significant instrumental uncertainty is that in the modelling of $E_{\mathrm{T}}^{\mathrm{miss}}$, evaluated by propagating the uncertainties in the energy and momentum scale of each of the objects entering the calculation, as well as the uncertainties in the $E_{\mathrm{T}}^{\mathrm{miss}}$ soft-term resolution and scale [153]. Other instrumental uncertainties concerning the efficiency of the trigger selection, flavour-tagging and JVT, as well as reconstruction, identification, impact parameter selection and isolation for leptons, are found to have minor impact. Each experimental uncertainty is treated as fully correlated across the analysis regions and physics processes considered.

For the processes estimated using the MC simulation, the predicted yield is also affected by different sources of theoretical modelling uncertainty. All theoretical uncertainties are treated as fully correlated across analysis regions, except those related to MC statistics. The uncertaintiesfor the dominant background processes, WZ, ZZ, and $t\bar{t}$, are derived using MC simulation samples. For the WZ background, which is normalised to data in CRs, these uncertainties are implemented as transfer factor uncertainties that reflect differences in the SR-to-CR or VR-to-CR ratio of yields, and therefore provide an uncertainty in the assumed shape of MC distributions across analysis regions. The uncertaintiesrelated to the choice of QCD renormalisation and factorisation scales are represented by three Gaussian nuisance parameters in the fit (see Sect. 6.4): the first varies the renormalisation scale up and down, where a one-sigma deviation represents varying that scale up or down by a factor of two, while the factorisation scale is fixed to its nominal value; the second varies the factorisation scale in the same way while fixing the renormalisation scale; and the third nuisance coherently varies both the renormalisation and factorisation scales. There is no nuisance parameter to account for anti-correlated configurations of the renormalisation and factorisation scales, as these are deemed unphysical. For the WZ and ZZ samples, the uncertaintiesdue to the resummation and matching scales between ME and PS as well as the PS recoil scheme are evaluated by varying the corresponding parameters in SHERPA. For $t\bar{t}$, modelling uncertainties at ME and PS level are determined by comparing the predictions of nominal and alternative generators, considering POWHEG BOX versus MADGRAPH5_AMC@NLO and PYTHIA 8 versus HERWIG 7 [165,166], respectively. Uncertainties in the $t\bar{t}$ prediction due to ISR and final-state radiation (FSR) uncertainties are evaluated by varying the relevant generator parameters. The uncertainties associated with the choice of PDF set (NNPDF [78,87]) and the uncertainty in the strong coupling constant, α_{s}, are also considered for the major backgrounds. Uncertainties in the cross section of 13%, 12%, 10% and 20% are applied for minor backgrounds $t\bar{t}W$, $t\bar{t}Z$, $t\bar{t}h$, and triboson, respectively [109]; for all other rare top processes a conservative uncertainty of 50% is applied.

The data-driven $Z+$jets estimation is subject to the statistical uncertainty due to the limited data sample size in CRFF or in the anti-ID regions used when applying the FF method, the uncertainty due to varying choice of parameterisation, and the uncertainty in the subtraction of non-$Z+$jets processes. The uncertainties are evaluated by considering the variations in the FF and propagating the effects to the estimated yields. The prescription applied for the estimation in the off-shell WZ selection is different from that in the on-shell WZ and Wh selections, reflecting the higher presence of $Z+$jets in $\mathrm{SR}^{\mathrm{offWZ}}$. Details are included in Sects. 7.2 and 8.2.

Uncertainties in the expected yields for SUSY signals are estimated by varying by a factor of two the MADGRAPH5_AMC@NLO parameters corresponding to the renormalisation, factorisation and CKKW-L matching scales, as well as the PYTHIA8 shower tune parameters. The overall uncertainties in the signal acceptance range from 5% to 20% depending on the analysis region. Uncertainties are smallest in jet-veto regions and slightly larger for higher $E_{\mathrm{T}}^{\mathrm{miss}}$ and jet-inclusive regions. This uncertainty estimates match the results of a dedicated study using data and MC $Z \to \mu\mu$ events in Ref. [18].

In the following results, the uncertainties related to experimental effects are grouped and shown as 'Experimental' uncertainty. This uncertainty is applied for all processes whose yield is estimated from simulation. The 'Modelling' uncertainty groups the uncertainties due to the theoretical uncertainties, including the WZ transfer factor uncertainties. The 'Fakes' group represents the uncertainties for FNP background processes whose yield is estimated from data. 'MC stat' stands for the statistical uncertainties of the simulated event samples. Finally, the 'Normalisation' group describes

the uncertainties related to the normalisation factors derived from the CRs.

6.4 Statistical analysis

Final background estimates are obtained by performing a profile log-likelihood fit [167], implemented in the HistFitter [168] framework, simultaneously on all CRs and SRs relevant to a given interpretation. The statistical and systematic uncertainties are implemented as nuisance parameters in the likelihood; Poisson constraints are used to estimate the uncertainties arising from limited numbers of events in the MC samples or in the data-driven $Z+$jets estimation, whilst Gaussian constraints are used for experimental and theoretical systematic uncertainties. Neither the VRs, which solely serve to validate the background estimation in the SRs, nor the CRs used for data-driven $Z+$jets estimation, are included in any of the fits.

Three types of fit configuration are used to derive the results.

- A '*background-only fit*' is performed considering only the CRs and assuming no signal presence. The normalisation of the WZ background is allowed to float and is constrained by the WZ CRs. The normalisation factors and nuisance parameters are adjusted by maximising the likelihood. The background prediction as obtained from this fit is compared with data in the VRs to assess the quality of the background modelling, as well as in the SRs. The significance of the difference between the observed and expected yields is calculated with the profile likelihood method from Ref. [169], adding a minus sign if the yield is below the prediction.
- A '*discovery fit*' is performed to derive model-independent constraints, setting upper limits on the new-physics cross section. The fit considers the target single-bin SR and the associated CRs, constraining the backgrounds by following the same method as in the background-only fit. Considering only one SR at a time avoids introducing a dependence on the signal model, which may arise from correlations across multiple SR bins. A signal contribution is allowed only in the SR, and a non-negative signal-strength parameter assuming generic beyond-the-SM (BSM) signals is derived.
- An '*exclusion fit*' is performed to set exclusion limits on the target models. The backgrounds are again constrained by following the same method as in the background-only fit, considering the CRs and the SRs, and the signal contribution to each region participating in the fit is taken into account according to the model predictions.

For each discovery or exclusion fit, the compatibility of the observed data with the signal-plus-background hypotheses is checked using the $\mathrm{CL_s}$ prescription [170], and limits on the cross section are set at 95% confidence level (CL).

Following the independent optimisation of the CRs and SRs, the simultaneous fits are performed separately for the different selections: once for the on-shell WZ and Wh selections combined, and once for the off-shell WZ selection. The results are presented in Sect 9.

The new results of the on-shell and off-shell WZ searches, as well as the results of a previous ATLAS search for electroweak SUSY with compressed mass spectra [18], are statistically combined and interpreted in the simplified models discussed in Sect. 1. Exclusion limits are calculated by statistically combining the results from the signal regions of the contributing searches, which are designed to be orthogonal. The combination is implemented in the `pyhf` framework [171,172], which was validated against the HistFitter framework [173]. The results are presented in Sect. 9.2.

7 On-shell WZ and Wh selections

The following subsections discuss the implementation specific to the on-shell WZ selection and the Wh selection, expanding on the general strategy outlined in Sect. 6. The selection is applied on top of the common preselection as defined in Sect. 5, and the SRs are optimised to the wino/bino (+) scenario.

7.1 Search regions

The $\mathtt{SR}^{\mathtt{WZ}}$ and $\mathtt{SR}^{\mathtt{Wh}}$ selections as introduced in Sect. 6.1 are further refined, taking into consideration differences in signal and background kinematics and composition. Driven by the p_{T} thresholds of the dilepton triggers used in this selection, the leading and sub-leading leptons in the event must satisfy $p_{\mathrm{T}} > 25, 20$ GeV, while the third lepton must satisfy $p_{\mathrm{T}} > 10$ GeV. To reduce SM backgrounds with little to no real $E_{\mathrm{T}}^{\mathrm{miss}}$, events are required to have $E_{\mathrm{T}}^{\mathrm{miss}} > 50$ GeV. To suppress the contribution of $t\bar{t}$ events and single-boson production in association with a $t\bar{t}$ pair, events with at least one b-jet are rejected.

To reduce the contribution from processes with low-mass dilepton resonances, events are vetoed if they contain a SFOS lepton pair with an invariant mass below 12 GeV. Additionally, in events with a SFOS pair, the three-lepton invariant mass $m_{3\ell}$ is required to be inconsistent with the mass of a Z boson, $|m_{3\ell} - m_Z| > 15$ GeV, in order to suppress contributions from asymmetric photon conversions from the $Z+$jets process with $Z \to \ell\ell\gamma^{(*)}$ and $\gamma^{(*)} \to \ell\ell$, where one of the leptons is out of acceptance.

Events with at least one SFOS lepton pair are divided into three $m_{\ell\ell}$ bins, in order to separate processes that include a Z boson in the decay chain from processes where a SM

Table 2 Summary of the common selection criteria applied in the SRs of the on-shell WZ and Wh selections. In rows where only one value is given it applies to all regions. '–' indicates no requirement is applied for a given variable/region

Variable	Common selection requirements		
	$\mathrm{SR}^{\mathrm{WZ}}$	$\mathrm{SR}^{\mathrm{Wh}}_{\mathrm{SFOS}}$	$\mathrm{SR}^{\mathrm{Wh}}_{\mathrm{DFOS}}$
$n^{\mathrm{baseline}}_{\mathrm{lep}}, n^{\mathrm{signal}}_{\mathrm{lep}}$		= 3	
Trigger		dilepton	
$p^{\ell_1}_{\mathrm{T}}, p^{\ell_2}_{\mathrm{T}}, p^{\ell_3}_{\mathrm{T}}$ [GeV]		> 25, 20, 10	
$E^{\mathrm{miss}}_{\mathrm{T}}$ [GeV]		> 50	
$n_{b\text{-jets}}$		= 0	
Resonance veto $m_{\ell\ell}$ [GeV]	> 12	> 12	–
n_{SFOS}	≥ 1	≥ 1	= 0
$m_{\ell\ell}$ [GeV]	∈ [75, 105]	∉ [75, 105]	–
$\lvert m_{3\ell} - m_Z \rvert$ [GeV]	> 15	> 15	–

Higgs boson is involved. The first bin is defined as the Z-boson mass window ($m_{\ell\ell} \in [75, 105]$ GeV), and is used for the $\mathrm{SR}^{\mathrm{WZ}}$ selection. The second and third bins are defined below and above the Z-boson mass ($m_{\ell\ell} \leq 75$ GeV and $m_{\ell\ell} \geq 105$ GeV), and are used for the $\mathrm{SR}^{\mathrm{Wh}}_{\mathrm{SFOS}}$ selection. The Z-boson mass window bin is expected to contain a larger irreducible SM background contribution than the other bins. A summary of the common selection criteria is presented in Table 2. The $\mathrm{SR}^{\mathrm{WZ}}$ and $\mathrm{SR}^{\mathrm{Wh}}$ regions are further segmented as discussed below, and indexed with `-i`.

Each $m_{\ell\ell}$ bin is further divided into m_{T} and $E^{\mathrm{miss}}_{\mathrm{T}}$ bins, which enhances the sensitivity to various Δm scenarios. The m_{T} distribution falls steeply in the region around the W-boson mass, and facilitates discrimination against the background from SM WZ production. Three m_{T} bins, $m_{\mathrm{T}} < 100$, $100 \leq m_{\mathrm{T}} \leq 160$, and $m_{\mathrm{T}} > 160$ GeV, are defined to separate processes with and without a leptonic W-boson decay. The lower and upper bounds on the $E^{\mathrm{miss}}_{\mathrm{T}}$ bins vary with the $m_{\ell\ell}$ and m_{T} thresholds. The SM background contribution is expected to be higher in low m_{T} and $E^{\mathrm{miss}}_{\mathrm{T}}$ bins, while the signal populates different m_{T} and $E^{\mathrm{miss}}_{\mathrm{T}}$ bins, depending on the mass splitting. Signals with smaller Δm tend to have more events in the lower $E^{\mathrm{miss}}_{\mathrm{T}}$ and m_{T} range, shifting to higher $E^{\mathrm{miss}}_{\mathrm{T}}$ and m_{T} bins as the mass difference increases.

Furthermore, events are separated by jet multiplicity, with jet-veto ($n_{\mathrm{jets}} = 0$; $\mathrm{SR}^{\mathrm{WZ}}$-1 to 8, $\mathrm{SR}^{\mathrm{Wh}}_{\mathrm{SFOS}}$-1 to 7 and 17 to 19) and jet-inclusive ($n_{\mathrm{jets}} > 0$; $\mathrm{SR}^{\mathrm{WZ}}$-9 to 20, $\mathrm{SR}^{\mathrm{Wh}}_{\mathrm{SFOS}}$-8 to 16) SRs. The ISR topology is exploited further in the jet-inclusive regions of $\mathrm{SR}^{\mathrm{WZ}}$ and $\mathrm{SR}^{\mathrm{Wh}}_{\mathrm{SFOS}}$ by categorising the events with at least one jet according to their H_{T}, the scalar p_{T} sum of the jets with $p_{\mathrm{T}} > 20$ GeV. At higher H_{T}, signals with mass splitting $\Delta m \approx m_Z$ tend to have more events at high values of $E^{\mathrm{miss}}_{\mathrm{T}}$ and m_{T} than the SM background, due to the recoil against ISR jets. In the high H_{T} ($H_{\mathrm{T}} > 200$ GeV) regions, softer lepton-p_{T} spectra are expected for the signal because of the presence of a massive $\widetilde{\chi}^0_1$, which carries most of the transverse momenta of the boosted $\widetilde{\chi}^{\pm}_1\widetilde{\chi}^0_2$ system. Therefore $H^{\mathrm{lep}}_{\mathrm{T}}$, the scalar p_{T} sum of the three selected leptons, is required to be less than 350 GeV. The H_{T} categorisation is applied in regions with $m_{\ell\ell} < 105$ GeV. Finally, in the high-mass off-peak region ($m_{\ell\ell} \geq 105$ GeV), only jet-veto events are considered. The full set of 20 $\mathrm{SR}^{\mathrm{WZ}}$ and 19 $\mathrm{SR}^{\mathrm{Wh}}_{\mathrm{SFOS}}$ signal regions is summarised in Tables 3 and 4.

In the $\mathrm{SR}^{\mathrm{Wh}}_{\mathrm{DFOS}}$ regions, events are required to have one same-flavour same-charge-sign (SFSS) lepton pair as well as a third lepton which has a different flavour and opposite sign to the SFSS pair, and is referred to as the DFOS lepton. After this selection, $t\bar{t}$ production dominates the SM background and is minimised by keeping events with low jet multiplicity ($n_{\mathrm{jets}} < 3$). These are then further split into two SR bins, one with $n_{\mathrm{jets}} = 0$ ($\mathrm{SR}^{\mathrm{Wh}}_{\mathrm{DFOS}}$-1) and the other satisfying $n_{\mathrm{jets}} \in [1, 2]$ ($\mathrm{SR}^{\mathrm{Wh}}_{\mathrm{DFOS}}$-2). Due to the presence of the $\widetilde{\chi}^0_1$, signals tend to have higher $E^{\mathrm{miss}}_{\mathrm{T}}$ significance than the SM background, and therefore the events are required to have $E^{\mathrm{miss}}_{\mathrm{T}}$ significance > 8. The third lepton in $t\bar{t}$ production usually arises from a heavy flavour quark decay and is typically lower in p_{T} than the third lepton in the SUSY signal scenarios. To reduce this contribution the lower bound on the third lepton's p_{T} is increased to 15 and 20 GeV in the $\mathrm{SR}^{\mathrm{Wh}}_{\mathrm{DFOS}}$-1 and $\mathrm{SR}^{\mathrm{Wh}}_{\mathrm{DFOS}}$-2 regions, respectively. Angular proximity between leptons coming from a Higgs-boson decay is used for further event separation, using the variable $\Delta R_{\mathrm{OS,near}}$, defined as the ΔR between the DFOS lepton and the SFSS lepton nearest in ϕ. The signal is expected to populate the lower range in $\Delta R_{\mathrm{OS,near}}$, while the SM background tends to have a flatter distribution. Events in $\mathrm{SR}^{\mathrm{Wh}}_{\mathrm{DFOS}}$-1 are required to satisfy $\Delta R_{\mathrm{OS,near}} < 1.2$. To suppress the higher $t\bar{t}$ contribution in the $\mathrm{SR}^{\mathrm{Wh}}_{\mathrm{DFOS}}$-2, a tighter selection on $\Delta R_{\mathrm{OS,near}}$ is imposed. A complete summary of the selection criteria in $\mathrm{SR}^{\mathrm{Wh}}_{\mathrm{DFOS}}$ is presented in Table 5.

For the WZ-mediated $\widetilde{\chi}^{\pm}_1\widetilde{\chi}^0_2$ signal sample with NLSP mass of 600 GeV and massless $\widetilde{\chi}^0_1$, the $\mathrm{SR}^{\mathrm{WZ}}_{\mathrm{0j}}$ and $\mathrm{SR}^{\mathrm{WZ}}_{\mathrm{nj}}$ regions have selection acceptance times efficiency values of 2.0×10^{-3} and 3.0×10^{-3}, respectively. For the Wh-mediated $\widetilde{\chi}^{\pm}_1\widetilde{\chi}^0_2$ signal sample with NLSP mass of 200 GeV and mass-

Table 3 Summary of the selection criteria for the SRs targeting events with at least one SFOS lepton pair and $m_{\ell\ell} \in [75, 105]$ GeV, for the on-shell WZ search regions. Region selections are binned by m_{T} (rows) and $E_{\mathrm{T}}^{\mathrm{miss}}$ for the two sets of regions, where each set has different n_{jets} and H_{T} requirements. $\mathtt{SR^{WZ}}$ common selection criteria are applied (Table 2)

Selection requirements				
$m_{\ell\ell} \in [75, 105]$ GeV, $n_{\mathrm{jets}} = 0$				
m_{T} [GeV]	$E_{\mathrm{T}}^{\mathrm{miss}}$ [GeV]			
[100, 160]	$\mathtt{SR^{WZ}}$-1: [50, 100]	$\mathtt{SR^{WZ}}$-2: [100, 150]	$\mathtt{SR^{WZ}}$-3: [150, 200]	$\mathtt{SR^{WZ}}$-4: > 200
> 160	$\mathtt{SR^{WZ}}$-5: [50, 150]	$\mathtt{SR^{WZ}}$-6: [150, 200]	$\mathtt{SR^{WZ}}$-7: [200, 350]	$\mathtt{SR^{WZ}}$-8: > 350
$m_{\ell\ell} \in [75, 105]$ GeV, $n_{\mathrm{jets}} > 0$, $H_{\mathrm{T}} < 200$ GeV				
m_{T} [GeV]	$E_{\mathrm{T}}^{\mathrm{miss}}$ [GeV]			
[100, 160]	$\mathtt{SR^{WZ}}$-9: [100, 150]	$\mathtt{SR^{WZ}}$-10: [150, 250]	$\mathtt{SR^{WZ}}$-11: [250, 300]	$\mathtt{SR^{WZ}}$-12: > 300
> 160	$\mathtt{SR^{WZ}}$-13: [50, 150]	$\mathtt{SR^{WZ}}$-14: [150, 250]	$\mathtt{SR^{WZ}}$-15: [250, 400]	$\mathtt{SR^{WZ}}$-16: > 400
$m_{\ell\ell} \in [75, 105]$ GeV, $n_{\mathrm{jets}} > 0$, $H_{\mathrm{T}} > 200$ GeV, $H_{\mathrm{T}}^{\mathrm{lep}} < 350$ GeV				
m_{T} [GeV]	$E_{\mathrm{T}}^{\mathrm{miss}}$ [GeV]			
> 100	$\mathtt{SR^{WZ}}$-17: [150, 200]	$\mathtt{SR^{WZ}}$-18: [200, 300]	$\mathtt{SR^{WZ}}$-19: [300, 400]	$\mathtt{SR^{WZ}}$-20: > 400

Table 4 Summary of the selection criteria for the SRs targeting events with at least one SFOS lepton pair and $m_{\ell\ell} \notin [75, 105]$ GeV, for the Wh search regions. Region selections are binned by m_{T} (rows) and $E_{\mathrm{T}}^{\mathrm{miss}}$ for the three sets of regions, where each set has different $m_{\ell\ell}$, n_{jets}, and H_{T} requirements. $\mathtt{SR^{Wh}_{SFOS}}$ common selection criteria are applied (Table 2)

Selection requirements			
$m_{\ell\ell} \leq 75$ GeV, $n_{\mathrm{jets}} = 0$			
m_{T} [GeV]	$E_{\mathrm{T}}^{\mathrm{miss}}$ [GeV]		
[0, 100]	$\mathtt{SR^{Wh}_{SFOS}}$-1: [50, 100]	$\mathtt{SR^{Wh}_{SFOS}}$-2: [100, 150]	$\mathtt{SR^{Wh}_{SFOS}}$-3 > 150
[100, 160]	$\mathtt{SR^{Wh}_{SFOS}}$-4: [50, 100]	$\mathtt{SR^{Wh}_{SFOS}}$-5: > 100	
> 160	$\mathtt{SR^{Wh}_{SFOS}}$-6: [50, 100]	$\mathtt{SR^{Wh}_{SFOS}}$-7: > 100	
$m_{\ell\ell} \leq 75$ GeV, $n_{\mathrm{jets}} > 0$, $H_{\mathrm{T}} < 200$ GeV			
m_{T} [GeV]	$E_{\mathrm{T}}^{\mathrm{miss}}$ [GeV]		
[0, 50]	$\mathtt{SR^{Wh}_{SFOS}}$-8: [50, 100]		
[50, 100]	$\mathtt{SR^{Wh}_{SFOS}}$-9: [50, 100]		
[0, 100]	$\mathtt{SR^{Wh}_{SFOS}}$-10: [100, 150]	$\mathtt{SR^{Wh}_{SFOS}}$-11: > 150	
[100, 160]	$\mathtt{SR^{Wh}_{SFOS}}$-12: [50, 100]	$\mathtt{SR^{Wh}_{SFOS}}$-13: [100, 150]	$\mathtt{SR^{Wh}_{SFOS}}$-14: > 150
> 160	$\mathtt{SR^{Wh}_{SFOS}}$-15: [50, 150]	$\mathtt{SR^{Wh}_{SFOS}}$-16: > 150	
$m_{\ell\ell} \geq 105$ GeV, $n_{\mathrm{jets}} = 0$			
m_{T} [GeV]	$E_{\mathrm{T}}^{\mathrm{miss}}$ [GeV]		
> 100	$\mathtt{SR^{Wh}_{SFOS}}$-17: [50, 100]	$\mathtt{SR^{Wh}_{SFOS}}$-18: [100, 200]	$\mathtt{SR^{Wh}_{SFOS}}$-19: > 200

Table 5 Summary of the selection criteria for the SRs targeting events with a DFOS lepton pair, for the Wh selection. $\mathtt{SR^{Wh}_{DFOS}}$ common selection criteria are applied (Table 2)

Variable	Selection requirements	
	$\mathtt{SR^{Wh}_{DFOS}}$-1	$\mathtt{SR^{Wh}_{DFOS}}$-2
n_{jets}	$= 0$	$\in [1, 2]$
$E_{\mathrm{T}}^{\mathrm{miss}}$ significance	> 8	> 8
$p_{\mathrm{T}}^{\ell_3}$ [GeV]	> 15	> 20
$\Delta R_{\mathrm{OS,near}}$	< 1.2	< 1.0

less $\tilde{\chi}_1^0$, the $\mathtt{SR^{Wh}_{low\text{-}m_{ll}\text{-}0j}}$, $\mathtt{SR^{Wh}_{low\text{-}m_{ll}\text{-}nj}}$, and $\mathtt{SR^{Wh}_{DFOS}}$ regions have selection acceptance times efficiency values of 9.1×10^{-5}, 1.0×10^{-4}, and 3.7×10^{-5}, respectively.

7.2 Background estimation

The normalisation of the WZ background is measured in CRs characterised by moderate values of the $E_{\mathrm{T}}^{\mathrm{miss}}$ and m_{T} variables. The CRs contain only events with at least one SFOS pair with an invariant mass of $75 < m_{\ell\ell} < 105$ GeV, targeting on-shell decays. Additional requirements of $50 < E_{\mathrm{T}}^{\mathrm{miss}} < 100$ GeV and $20 < m_{\mathrm{T}} < 100$ GeV improve the WZ purity, the upper bound on m_{T} at 100 GeV also ensures orthogonality between the WZ CRs and $\mathtt{SR^{WZ}}$. To address the possible mis-modelling of the jet multiplicity in the WZ simulated samples, the cross-section normalisation factor is extracted separately in each jet multiplicity and H_{T} category, using $\mathtt{CRWZ^{WZ}_{0j}}$, $\mathtt{CRWZ^{WZ}_{low\text{-}H_T}}$, and $\mathtt{CRWZ^{WZ}_{high\text{-}H_T}}$. The estimation is cross-checked in kinematically similar, orthogonal VRs: $\mathtt{VRWZ^{WZ}_{0j}}$, $\mathtt{VRWZ^{WZ}_{low\text{-}H_T}}$, and $\mathtt{VRWZ^{WZ}_{high\text{-}H_T}}$. A summary of the selection criteria defining the WZ CRs and VRs is presented in Table 6. The WZ purity is about 80% in all CRs and VRs. The signal contamination is almost negligible in the CRs and increases to 10% in the VRs.

Performing the simultaneous background-only fit for the on-shell WZ and Wh selections, normalisation factors for WZ of 1.07 ± 0.02 ($\mathtt{CRWZ^{WZ}_{0j}}$), 0.94 ± 0.03 ($\mathtt{CRWZ^{WZ}_{low\text{-}H_T}}$) and 0.85 ± 0.05 ($\mathtt{CRWZ^{WZ}_{high\text{-}H_T}}$) are found.

A good description of the m_{T} and $E_{\mathrm{T}}^{\mathrm{miss}}$ distributions in the WZ simulation is crucial in this analysis, especially in the

Table 6 Summary of the selection criteria for the CRs and VRs for WZ, for the on-shell WZ and Wh selections. In rows where only one value is given it applies to all regions. '–' indicates no requirement is applied for a given variable/region

Variable	$\texttt{CRWZ}^{\texttt{WZ}}$			$\texttt{VRWZ}^{\texttt{WZ}}$		
	0j	low-H_T	high-H_T	0j	low-H_T	high-H_T
$n_{\text{lep}}^{\text{baseline}}, n_{\text{lep}}^{\text{signal}}$		$= 3$			$= 3$	
Trigger		Dilepton			Dilepton	
$p_{\text{T}}^{\ell_1}, p_{\text{T}}^{\ell_2}, p_{\text{T}}^{\ell_3}$ [GeV]		$> 25, 20, 10$			$> 25, 20, 10$	
$n_{b\text{-jets}}$		$= 0$			$= 0$	
n_{SFOS}		≥ 1			≥ 1	
m_{T} [GeV]		$\in [20, 100]$			$\in [20, 100]$	
$m_{\ell\ell}$ [GeV]		$\in [75, 105]$			$\in [75, 105]$	
$\lvert m_{3\ell} - m_Z \rvert$ [GeV]		> 15			> 15	
$E_{\text{T}}^{\text{miss}}$ [GeV]		$\in [50, 100]$			> 100	
n_{jets}	$= 0$	≥ 1	≥ 1	$= 0$	≥ 1	≥ 1
H_{T} [GeV]	-	< 200	> 200	–	< 200	> 200

high-m_{T} and high-$E_{\text{T}}^{\text{miss}}$ tails where new physics may appear. The tail of the m_{T} distribution is a result of, in decreasing order of importance: the use of a wrong pair of leptons to compute the mass of the Z-boson candidate and the m_{T} of the W-boson candidate ('mis-pairing' of the leptons), the $E_{\text{T}}^{\text{miss}}$ resolution, and the W-boson width. The prediction of lepton mis-pairing in simulation is validated in a control sample in data similar to the one used to calculate the cross-section normalisation factor, but only allowing events with a SFOS pair of different flavour than the W lepton. The Z-boson candidate can then be identified unambiguously, and a mis-paired control sample is obtained using the DFOS pair in the $m_{\ell\ell}$ computation and using the third lepton to calculate m_{T}. Finally, the modelling of the m_{T} and $E_{\text{T}}^{\text{miss}}$ distributions is validated in a $W+\gamma$ control sample. The $W+\gamma$ and WZ processes have very similar m_{T} shapes because their production mechanisms are similar, with the exception that the FSR production diagram of $W+\gamma$ is much more common than the corresponding diagram in WZ, which is doubly suppressed due to the mass of the Z boson and its weak coupling to leptons. Furthermore, a photon is a good proxy for a leptonically decaying Z boson since photons and leptons are reconstructed with comparable resolutions, and no large extra mismeasurements are expected. The enhancement of the FSR diagram in the $W+\gamma$ process leads to differences in the m_{T} distribution shapes between WZ and $W+\gamma$. When a photon is radiated, leptons lose energy, resulting in a lower m_{T}. In order to use the $W+\gamma$ m_{T} shape to validate the WZ MC prediction, the FSR contribution in the $W+\gamma$ control region has to be suppressed. This is done by placing threshold requirements on the p_{T} of the photon, $p_{\text{T}}^{\gamma} > 50$ GeV, and the separation between the lepton and the photon, $\Delta R(\ell, \gamma) > 0.4$, in $W+\gamma$ events, as FSR photons are expected to be close to the lepton radiating them and also tend to have low p_{T}. The distribution shapes of m_{T} and $E_{\text{T}}^{\text{miss}}$, as well as other kinematic variables, are compared in data and MC events in the $W+\gamma$ region. The m_{T} distribution in the validation region with mis-paired leptons and the $W+\gamma$ validation region are shown in Fig. 3. Good agreement in both control samples is observed and no extra corrections or scale factors are applied to correct the m_{T} distribution for the WZ background.

The $t\bar{t}$ MC modelling is validated in VRs, enhancing the $t\bar{t}$ contribution by requiring a DFOS lepton pair and using a moderate $E_{\text{T}}^{\text{miss}} > 50$ GeV selection. The main VR, $\texttt{VRt}\bar{\texttt{t}}^{\texttt{WZ}}$, requires the presence of one or two b-jets, further increasing the $t\bar{t}$ contribution. To validate the modelling in the $n_{\text{jets}} = 0$ region as well, an additional VR inclusive in b-jets, $\texttt{VRt}\bar{\texttt{t}}^{\texttt{WZ}}_{\text{incl}}$, is considered, with a $E_{\text{T}}^{\text{miss}}$ significance < 8 requirement to ensure orthogonality with the $\texttt{SR}^{\texttt{Wh}}_{\text{DFOS}}$ regions. The $t\bar{t}$ purity is about 80% in the $\texttt{VRt}\bar{\texttt{t}}^{\texttt{WZ}}$ and 72% in the $\texttt{VRt}\bar{\texttt{t}}^{\texttt{WZ}}_{\text{incl}}$. The selection requirements for the $t\bar{t}$ VRs are summarised in Table 7.

The Z + jets estimation uses the FF method as described in Sect. 6.2. For measurement region $\texttt{CRFF}^{\texttt{WZ}}$, the Z-boson candidate mass must be compatible with the Z-boson mass within 15 GeV, and low $E_{\text{T}}^{\text{miss}}$ and m_{T} are required to minimise WZ contributions. The typical value of FFs varies from 0.2 to 0.4, depending on the lepton p_{T} and η. The Z + jets estimation is then validated in $\texttt{VRFF}^{\texttt{WZ}}$, considering the intermediate $E_{\text{T}}^{\text{miss}}$ range closer to, but orthogonal to, the SRs, and adding a $m_{3\ell}$ lower bound to reduce WZ contamination. The selection criteria for $\texttt{CRFF}^{\texttt{WZ}}$ as well as those of $\texttt{VRFF}^{\texttt{WZ}}$ are summarised in Table 7.

Figure 3 presents the m_{T} distribution in $\texttt{VRWZ}^{\texttt{WZ}}_{\text{high-}H_{\text{T}}}$, and the $E_{\text{T}}^{\text{miss}}$ distribution in $\texttt{VRt}\bar{\texttt{t}}^{\texttt{WZ}}$, showing good agreement between the observed data and the estimated background. The comparisons between the expected and observed yields in the $\texttt{CRWZ}^{\texttt{WZ}}$ and all $\texttt{VR}^{\texttt{WZ}}$ are given in Fig. 4.

The systematic uncertainties considered in the on-shell WZ and the Wh SRs follow the approach discussed in Sect. 6.3. The relative composition of FNP muons is similar

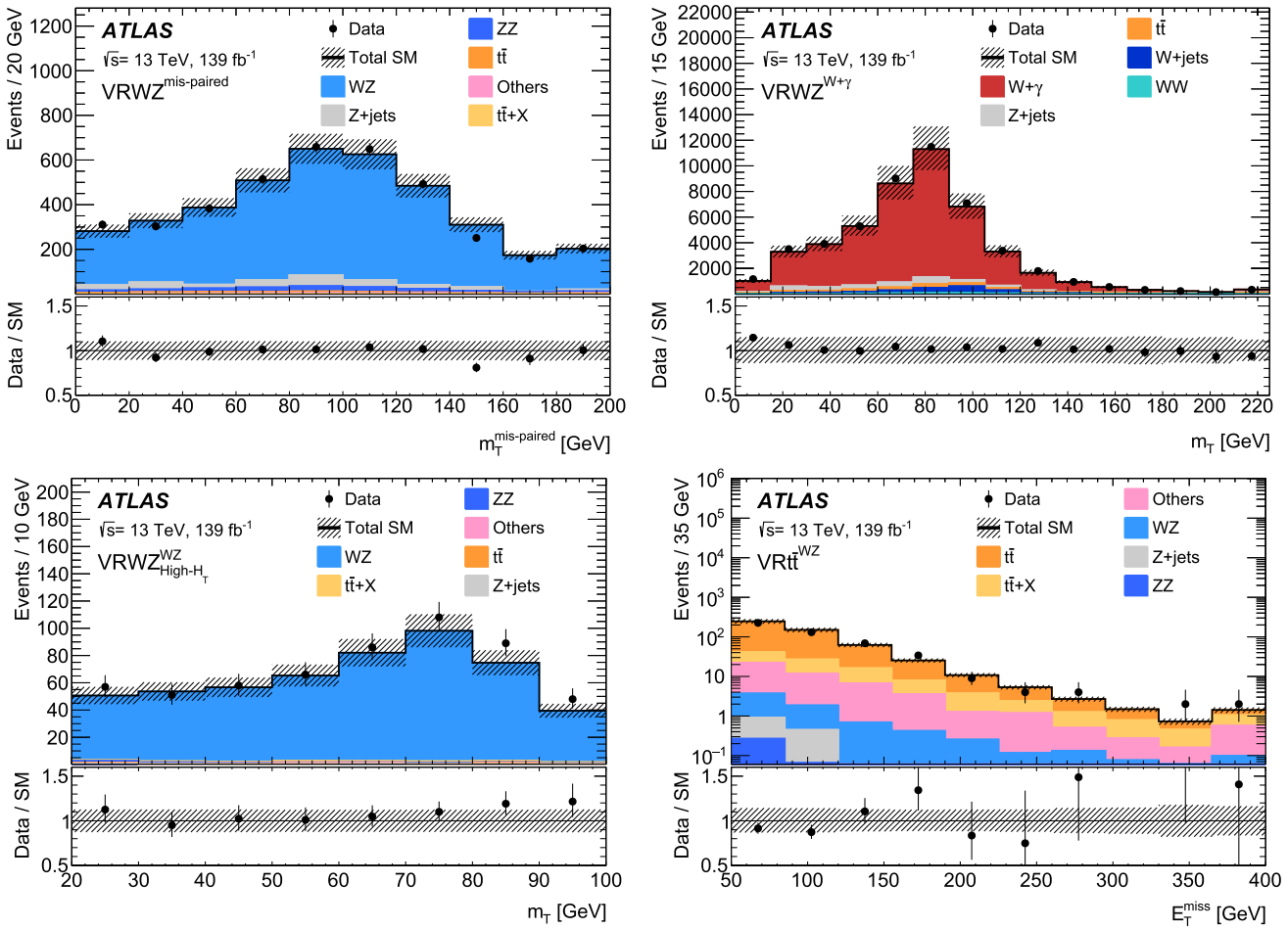

Fig. 3 Distributions of m_{T} showing the data and the pre-fit expected background in (top left) the mis-paired lepton validation region and (top right) the $W+\gamma$ validation region, used to validate the WZ background. Distributions of (bottom left) m_{T} in $\mathtt{VRWZ}^{\mathtt{WZ}}_{\mathtt{high\text{-}H_T}}$ and (bottom right) $E_{\mathrm{T}}^{\mathrm{miss}}$ in $\mathtt{VRt\bar{t}}^{\mathtt{WZ}}$, showing the data and the post-fit expected background in each region. The last bin includes overflow. The 'Others' category contains backgrounds from single-top, WW, triboson, Higgs and rare top processes. The bottom panel shows the ratio of the observed data to the predicted yields. The hatched bands indicate the combined theoretical, experimental, and MC statistical uncertainties

Table 7 Summary of the selection criteria for the CRs and VRs for $t\bar{t}$ and $Z+$ jets, for the on-shell WZ and Wh selections. The corresponding anti-ID regions used for the $Z+$ jets prediction follow the same selection criteria, except that at least one of the leptons is anti-ID instead of signal. '–' indicates no requirement is applied for a given variable/region

Variable	$\mathtt{VRt\bar{t}}^{\mathtt{WZ}}$	$\mathtt{VRt\bar{t}}^{\mathtt{WZ}}_{\mathtt{incl}}$	$\mathtt{CRFF}^{\mathtt{WZ}}$	$\mathtt{VRFF}^{\mathtt{WZ}}$
$n_{\mathrm{lep}}^{\mathrm{baseline}}$, $n_{\mathrm{lep}}^{\mathrm{signal}}$	$= 3$	$= 3$	$= 3$	$= 3$
n_{SFOS}	$= 0$	$= 0$	≥ 1	≥ 1
Trigger	dilepton	dilepton	dilepton	dilepton
$n_{b\text{-jets}}$	$\in [1, 2]$	–	$= 0$	$= 0$
$\lvert m_{\ell\ell} - m_Z \rvert$ [GeV]	–	–	< 15	< 15
$p_{\mathrm{T}}^{\ell_{Z1}}$, $p_{\mathrm{T}}^{\ell_{Z2}}$ [GeV]	–	–	$> 25, > 20$	–
$E_{\mathrm{T}}^{\mathrm{miss}}$ [GeV]	> 50	> 50	$\in [20, 50]$	$\in [50, 100]$
$E_{\mathrm{T}}^{\mathrm{miss}}$ significance	–	< 8	–	–
m_{T} [GeV]	–	–	< 20	< 20
$m_{3\ell}$ [GeV]	–	–	–	$\in [105, 160]$

between the CRFF and $\mathtt{SR}^{\mathtt{WZ}}$, whereas for FNP electrons the main source in the $\mathtt{SR}^{\mathtt{WZ}}$ is photon conversions, while in the CRFF the heavy-flavour decay contribution dominates. An additional source of uncertainty that is considered accounts for the different FNP lepton compositions in the CRFF and $\mathtt{SR}^{\mathtt{WZ}}$. This uncertainty arises from the method's performance

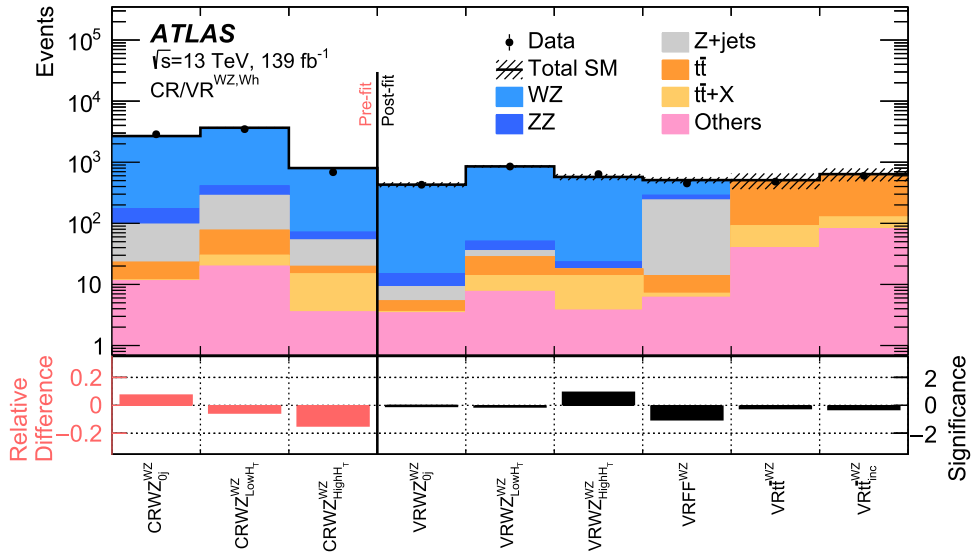

Fig. 4 Comparison of the observed data and expected SM background yields in the CRs (pre-fit) and VRs (post-fit) of the on-shell WZ and Wh selections. The 'Others' category contains the single-top, WW, triboson, Higgs and rare top processes. The hatched band indicates the combined theoretical, experimental, and MC statistical uncertainties. The bottom panel shows the relative difference between the observed data and expected yields for the CRs and the significance of the difference for the VRs, calculated with the profile likelihood method from Ref. [169], adding a minus sign if the yield is below the prediction

in the simulation (closure) in various regions of parameter space and is given by the differences between the estimated and simulated yields of events in the given region. In the DFOS region where the triboson contribution becomes dominant, the uncertainties related to the QCD renormalisation and factorisation scales are also evaluated for this background component, in the same way as previously described for diboson and $t\bar{t}$. A summary of the considered systematic uncertainties is presented in Fig. 5, with uncertainties grouped as discussed in Sect. 6.3.

Bin-to-bin fluctuations in the statistical uncertainty as well as the experimental uncertainty reflect the difference in expected yields in the various search regions, which varies by an order of magnitude. These uncertainties become the dominant ones in $\mathrm{SR}^{\mathrm{WZ}}$-3-4, 6-8, 11-12 and 15-16 of the on-shell WZ selection, and $\mathrm{SR}^{\mathrm{Wh}}_{\mathrm{SFOS}}$-5, $\mathrm{SR}^{\mathrm{Wh}}_{\mathrm{SFOS}}$-14, and $\mathrm{SR}^{\mathrm{Wh}}_{\mathrm{SFOS}}$-19 of the Wh selection, due to limited number of MC events at high $E_{\mathrm{T}}^{\mathrm{miss}}$ and m_{T}. Although the FNP lepton uncertainty is negligible in the majority of the search bins, its relative size reaches 30% in $\mathrm{SR}^{\mathrm{Wh}}_{\mathrm{DFOS}}$-2, due to the small number of events in the corresponding anti-ID sample.

8 Off-shell WZ selection

The following subsections discuss the implementation specific to the off-shell WZ selection, expanding on the general strategy outlined in Sect. 6. The selection is applied on top of the common preselection as defined in Sect. 5, and the SRs are optimised to the wino/bino (+) scenario.

8.1 Search regions

The $\mathrm{SR}^{\mathrm{offWZ}}$ selection targets the off-shell WZ region by requiring $m_{\ell\ell}^{\mathrm{min}}, m_{\ell\ell}^{\mathrm{max}} < 75$ GeV. The $m_{\ell\ell}^{\mathrm{max}}$ is the largest SFOS lepton pair invariant mass in the event, and the double requirement helps to maximally suppress combinatorial backgrounds with an on-shell Z boson. Further variables used in the off-shell WZ selection assume $m_{\ell\ell}^{\mathrm{min}}$-based lepton assignment to the Z^*- and W^*-boson candidates unless otherwise indicated. The common event selection vetoes events with a b-jet to reduce contamination from $t\bar{t}$, requires the three leptons to be well separated in min $\Delta R_{3\ell} = \min[\Delta R(\ell_i, \ell_j)$; for all lepton pairs $(\ell_i, \ell_j)]$, and requires a lower bound on $m_{\ell\ell}^{\mathrm{min}}$ of 1 GeV to remove events with collimated leptons for which FNP lepton background estimation is challenging. Finally, $m_{\ell\ell}^{\mathrm{min}}$ mass ranges of [3.0, 3.2] and [9, 12] GeV are vetoed to avoid contributions from J/ψ and Υ resonance backgrounds associated with a FNP lepton, except in the jet-inclusive high $E_{\mathrm{T}}^{\mathrm{miss}}$ regions ($E_{\mathrm{T}}^{\mathrm{miss}} > 200$ GeV) where the contribution is negligible.

Preselected events are further divided into four categories based on the multiplicity of jets with $p_{\mathrm{T}} > 30$ GeV ($n_{\mathrm{jets}}^{30\ \mathrm{GeV}}$), and on $E_{\mathrm{T}}^{\mathrm{miss}}$. Jet-veto categories $\mathrm{SR}^{\mathrm{offWZ}}_{\mathrm{low}\not{E}_{\mathrm{T}}}$-0j and $\mathrm{SR}^{\mathrm{offWZ}}_{\mathrm{high}\not{E}_{\mathrm{T}}}$-0j reject events containing jets and select low and high $E_{\mathrm{T}}^{\mathrm{miss}}$, respectively. Jet-inclusive categories $\mathrm{SR}^{\mathrm{offWZ}}_{\mathrm{low}\not{E}_{\mathrm{T}}}$-nj

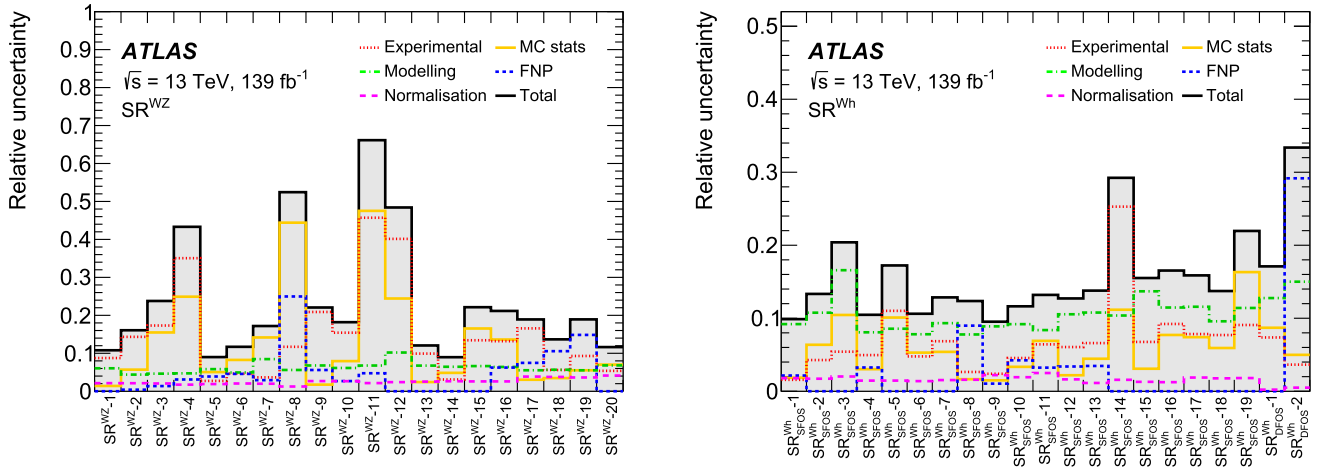

Fig. 5 Breakdown of the total systematic uncertainties in the background prediction for the SRs of (left) the on-shell WZ selection and (right) the Wh selection

and $\mathrm{SR}^{\mathrm{offWZ}}_{\mathrm{high}\not{E}_{\mathrm{T}}}\text{-nj}$ require at least one jet and also separate the events with low and high $E_{\mathrm{T}}^{\mathrm{miss}}$. As the $E_{\mathrm{T}}^{\mathrm{miss}}$ is harder in the jet-inclusive categories, due to the recoil between the $\widetilde{\chi}_1^{\pm}\widetilde{\chi}_2^0$ system and the jets, the boundary between the low and high $E_{\mathrm{T}}^{\mathrm{miss}}$ bins is set at 50 GeV for the jet-veto categories and at 200 GeV for the jet-inclusive categories. The $\mathrm{SR}^{\mathrm{offWZ}}_{\mathrm{low}\not{E}_{\mathrm{T}}}\text{-0j}$, $\mathrm{SR}^{\mathrm{offWZ}}_{\mathrm{low}\not{E}_{\mathrm{T}}}\text{-nj}$ and $\mathrm{SR}^{\mathrm{offWZ}}_{\mathrm{high}\not{E}_{\mathrm{T}}}\text{-0j}$ primarily target signals with moderate mass splitting ($\Delta m \sim [40, 90]$ GeV), and rely mostly on moderate kinematics and lepton triggers. The $\mathrm{SR}^{\mathrm{offWZ}}_{\mathrm{high}\not{E}_{\mathrm{T}}}\text{-nj}$ also target signals with highly compressed mass spectra ($\Delta m \lesssim 40$ GeV) – resulting in events with very soft leptons – by exploiting events with large $E_{\mathrm{T}}^{\mathrm{miss}}$ recoiling against hard hadronic activity. Initial lepton p_{T} requirements are kept as loose as possible, $p_{\mathrm{T}} > 10$ GeV for $\mathrm{SR}^{\mathrm{offWZ}}_{\mathrm{low}\not{E}_{\mathrm{T}}}\text{-0j}$, $\mathrm{SR}^{\mathrm{offWZ}}_{\mathrm{low}\not{E}_{\mathrm{T}}}\text{-nj}$, and $\mathrm{SR}^{\mathrm{offWZ}}_{\mathrm{high}\not{E}_{\mathrm{T}}}\text{-0j}$, and $p_{\mathrm{T}} > 4.5$ (3.0) GeV for e (μ) in $\mathrm{SR}^{\mathrm{offWZ}}_{\mathrm{high}\not{E}_{\mathrm{T}}}\text{-nj}$; however, the selection is restricted by the trigger requirements (Sect. 5) and some further requirements are applied in the bin-by-bin SR optimisation as discussed in the following.

Further common selection criteria are applied to reduce the contamination from Z + jets. First, a lower bound is set to ensure $E_{\mathrm{T}}^{\mathrm{miss}}$ significance $>$ 1.5 or 3.0, depending on the SR category. For $\mathrm{SR}^{\mathrm{offWZ}}_{\mathrm{low}\not{E}_{\mathrm{T}}}$, events are then treated separately for different flavours of the lepton from the W-boson decay (ℓ_{W}), selected using $m_{\ell\ell}^{mZ}$-based lepton assignment to best capture the SM background topology for rejection. To suppress the contribution from $Z(+\gamma) \to \ell\ell ee$ caused by bremsstrahlung from prompt electrons and subsequent photon conversions, if ℓ_{W} is an electron, the trilepton invariant mass $m_{3\ell}$ is required to be off the Z-boson peak ($|m_{3\ell} - m_Z| > 20$ GeV), and the minimum angular distance between all SFOS lepton pairs must be within $\min \Delta R_{\mathrm{SFOS}} \in [0.6, 2.4]$, with $\min \Delta R_{\mathrm{SFOS}}$ defined as $\min[\Delta R(\ell_i, \ell_j)$; for all SFOS lepton pairs $(\ell_i, \ell_j)]$. The common selection criteria and categorisation are summarised in Table 8.

The primary discriminant in $\mathrm{SR}^{\mathrm{offWZ}}$ is $m_{\ell\ell}^{\mathrm{min}}$. This variable serves as a proxy for the mass splitting of the targeted signals, and displays a characteristic kinematic edge at their mass-splitting value: $m_{\ell\ell}^{\mathrm{min}} = \Delta m$, as demonstrated in Fig. 6. A shape fit over the $m_{\ell\ell}^{\mathrm{min}}$ spectrum is performed in each SR category. Seven $m_{\ell\ell}^{\mathrm{min}}$ bins are defined with boundaries at 1, 12, 15, 20, 30, 40, 60 and 75 GeV, and labelled `'a'` to `'g'`; the $m_{\ell\ell}^{\mathrm{min}}$ bin labels are added to the region names as defined above. Signal regions `'a'` are dropped everywhere except in $\mathrm{SR}^{\mathrm{offWZ}}_{\mathrm{high}\not{E}_{\mathrm{T}}}\text{-nj}$, to avoid low-mass resonance backgrounds.

A second, similar kinematic edge is present in stransverse mass m_{T2} [174,175], reflecting the kinematic constraint originating from the $\widetilde{\chi}_1^{\pm} \to W^*\widetilde{\chi}_1^0$ decay chain. In this selection, m_{T2} is constructed by assigning the dilepton system providing $m_{\ell\ell}^{\mathrm{min}}$ $(\ell_1\ell_2)$ to one visible particle leg, and the remaining lepton (ℓ_3) to the other leg:

$$m_{\mathrm{T2}}^{m_\chi}\left(\mathbf{p}_{\mathrm{T}}^{\ell_1\ell_2}, \mathbf{p}_{\mathrm{T}}^{\ell_3}, \mathbf{p}_{\mathrm{T}}^{\mathrm{miss}}\right) = \min_{\mathbf{q}_{\mathrm{T}}}\Big(\max\Big[m_{\mathrm{T}}\left(\mathbf{p}_{\mathrm{T}}^{\ell_1\ell_2}, \mathbf{q}_{\mathrm{T}}, m_\chi\right), m_{\mathrm{T}}\left(\mathbf{p}_{\mathrm{T}}^{\ell_3}, \mathbf{p}_{\mathrm{T}}^{\mathrm{miss}} - \mathbf{q}_{\mathrm{T}}, m_\chi\right)\Big]\Big),$$

where the transverse mass m_{T} in this m_{T2} formula is defined by

$$m_{\mathrm{T}}\left(\mathbf{p}_{\mathrm{T}}^{\ell}, \mathbf{q}_{\mathrm{T}}, m_\chi\right) = \sqrt{m_\ell^2 + m_\chi^2 + 2\left(\sqrt{(p_{\mathrm{T}}^{\ell})^2 + m_\ell^2}\sqrt{q_{\mathrm{T}}^2 + m_\chi^2} - \mathbf{p}_{\mathrm{T}}^{\ell}\cdot\mathbf{q}_{\mathrm{T}}\right)}.$$

A hypothesised mass m_χ is assigned to each invisible particle leg, corresponding to the $\widetilde{\chi}_1^0$ mass; m_χ is fixed to 100 GeV in this selection.[6] The kinematic edge for signals appears at

[6] The dependency of the performance on hypothetical invisible particle mass m_χ is generally small except when assuming $m_\chi \sim 0$ GeV for

Table 8 Summary of the common selection criteria applied in the SRs of the off-shell WZ selection. In rows where only one value is given it applies to all regions. '-' indicates no requirement is applied for a given variable/region

	Common selection requirements			
Variable	$\text{SR}^{\text{offWZ}}_{\text{low}\not{E}_T}$-0j	$\text{SR}^{\text{offWZ}}_{\text{low}\not{E}_T}$-nj	$\text{SR}^{\text{offWZ}}_{\text{high}\not{E}_T}$-0j	$\text{SR}^{\text{offWZ}}_{\text{high}\not{E}_T}$-nj
$n_{\text{lep}}^{\text{baseline}}$, $n_{\text{lep}}^{\text{signal}}$	$= 3$			
n_{SFOS}	≥ 1			
$m_{\ell\ell}^{\text{max}}$ [GeV]	< 75			
$m_{\ell\ell}^{\text{min}}$ [GeV]	$\in [1, 75]$			
$n_{b\text{-jets}}$	$= 0$			
min $\Delta R_{3\ell}$	> 0.4			
Resonance veto $m_{\ell\ell}^{\text{min}}$ [GeV]	$\notin [3, 3.2], \notin [9, 12]$			-
Trigger	(multi-)lepton		((multi-)lepton $\|\|$ $E_{\text{T}}^{\text{miss}}$)	
$n_{\text{jets}}^{30\text{ GeV}}$	$= 0$	≥ 1	$= 0$	≥ 1
$E_{\text{T}}^{\text{miss}}$ [GeV]	< 50	< 200	> 50	> 200
$E_{\text{T}}^{\text{miss}}$ significance	> 1.5	> 3.0	> 3.0	> 3.0
$p_{\text{T}}^{\ell_1}, p_{\text{T}}^{\ell_2}, p_{\text{T}}^{\ell_3}$ [GeV]	> 10			$> 4.5(3.0)$ for $e(\mu)$
$\lvert m_{3\ell} - m_Z \rvert$ [GeV]	> 20 ($\ell_{\text{W}} = e$ only)		-	
min ΔR_{SFOS}	$[0.6, 2.4]$ ($\ell_{\text{W}} = e$ only)		-	

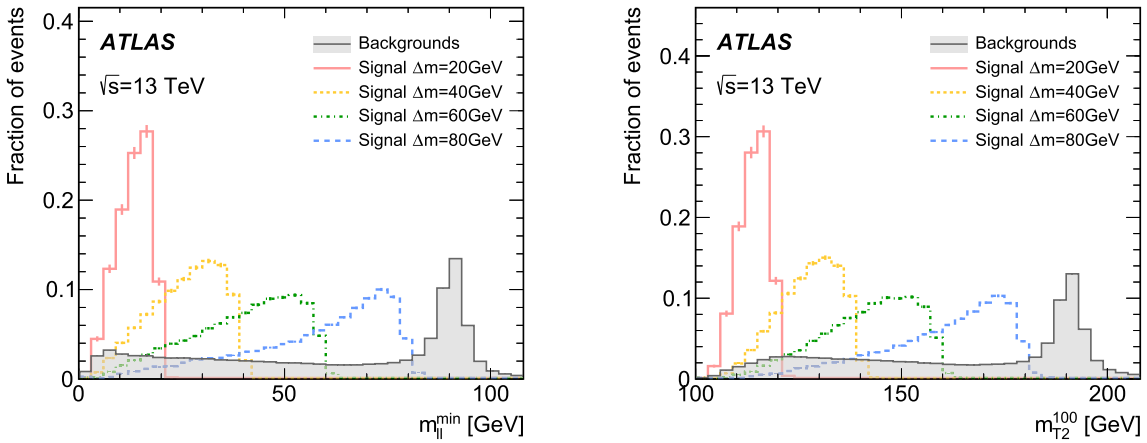

Fig. 6 Distributions of (left) $m_{\ell\ell}^{\text{min}}$ and (right) m_{T2}^{100} showing the expected SM background as well as signals with various mass splittings $\Delta m(\tilde{\chi}_2^0, \tilde{\chi}_1^0)$ ($m(\tilde{\chi}_1^{\pm}) = m(\tilde{\chi}_2^0) = 200$ GeV), for a selection of exactly three baseline and signal leptons. The distributions are normalised to unity. Signals demonstrate a cut-off in both variables matching the mass splitting, while backgrounds do not. The dominant background in this selection is WZ, with the Z-boson mass peak visible in both distributions

$m_{\text{T2}}^{100} = \Delta m(\tilde{\chi}_2^0, \tilde{\chi}_1^0) + 100$ GeV as illustrated in Fig. 6. To take advantage of this feature, a sliding cut is applied per $m_{\ell\ell}^{\text{min}}$ bin, requiring m_{T2}^{100} to be smaller than the upper $m_{\ell\ell}^{\text{min}}$ bin edge + 100 GeV. SM backgrounds can exceed the boundary and are suppressed, while a large fraction of the signal contribution targeted by a given bin is retained. The cut is particularly effective in the lowest $m_{\ell\ell}^{\text{min}}$ bins, targeting the smallest mass splittings: e.g. in $\text{SR}^{\text{offWZ}}_{\text{high}\not{E}_T}$-nja ($m_{\ell\ell}^{\text{min}} \in [1, 12]$ GeV) the total background is reduced by a factor of three following $m_{\text{T2}}^{100} < 112$ GeV, while the efficiency for $\Delta m = 10$ GeV signals is $> 95\%$.

Event selection is tightened further by employing various background rejection criteria, optimised separately for each SR^{offWZ} category and each $m_{\ell\ell}^{\text{min}}$ bin. The discriminating variables used and the detailed bin-by-bin cut values are summarised in Table 9.

In order to reduce the FNP lepton background contributions from Z + jets and $t\bar{t}$, lepton p_{T} thresholds are raised in $\text{SR}^{\text{offWZ}}_{\text{low}\not{E}_T}$-0j, $\text{SR}^{\text{offWZ}}_{\text{low}\not{E}_T}$-nj and $\text{SR}^{\text{offWZ}}_{\text{high}\not{E}_T}$-0j. In these same three categories, the transverse mass $m_{\text{T}}^{\text{mllmin}}$ is used to suppress the SM WZ contribution; the $m_{\text{T}}^{\text{mllmin}}$ variable is con-

signals with finite $\tilde{\chi}_1^0$ mass, where the signal kinematic edges become significantly smeared.

Table 9 Summary of the selection criteria for SRs for the off-shell WZ selection. $\mathtt{SR}^{\mathtt{offWZ}}$ common selection criteria are applied (Table 8). '–' indicates no requirement is applied for a given variable/region, while × is marked for regions that aren't considered

	Selection requirements								
Variable	a	b	c	d	e	f1	f2	g1	g2
$m_{\ell\ell}^{\min}$ [GeV]	[1, 12]	[12, 15]	[15, 20]	[20, 30]	[30, 40]	[40, 60]		[60, 75]	
	$\mathtt{SR}^{\mathtt{offWZ}}_{\mathtt{low}\not{E}_T}$ common								
$m_{\ell\ell}^{\max}$ [GeV]	×	< 60	< 60	< 60	< 60	-	-	-	-
$m_{\mathrm{T}}^{\mathrm{mllmin}}$ [GeV]	×	< 50	< 50	< 50	< 60	< 60	> 90	< 60	> 90
m_{T2}^{100} [GeV]	×	< 115	< 120	< 130	-	-	-	-	-
$\min \Delta R_{\mathrm{SFOS}}$	×	< 1.6	< 1.6	< 1.6	-	-	-	-	-
$p_{\mathrm{T}}^{\ell_1}, p_{\mathrm{T}}^{\ell_2}, p_{\mathrm{T}}^{\ell_3}$ [GeV]	×	> 10	> 10	> 10	> 10	> 15	> 15	> 15	> 15
	$\mathtt{SR}^{\mathtt{offWZ}}_{\mathtt{low}\not{E}_T}$-0j								
$\lvert\mathbf{p}_{\mathrm{T}}^{\mathrm{lep}}\rvert / E_{\mathrm{T}}^{\mathrm{miss}}$	×	< 1.1	< 1.1	< 1.1	< 1.3	< 1.4	< 1.4	< 1.4	< 1.4
$m_{3\ell}$ [GeV]	×	-	-	-	-	> 100	> 100	> 100	> 100
	$\mathtt{SR}^{\mathtt{offWZ}}_{\mathtt{low}\not{E}_T}$-nj								
$\lvert\mathbf{p}_{\mathrm{T}}^{\mathrm{lep}}\rvert / E_{\mathrm{T}}^{\mathrm{miss}}$	×	< 1.0	< 1.0	< 1.0	< 1.0	< 1.2	< 1.2	< 1.2	< 1.2
	$\mathtt{SR}^{\mathtt{offWZ}}_{\mathtt{high}\not{E}_T}$ common								
m_{T2}^{100} [GeV]	< 112	< 115	< 120	< 130	< 140	< 160	< 160	< 175	< 175
	$\mathtt{SR}^{\mathtt{offWZ}}_{\mathtt{high}\not{E}_T}$-0j								
$p_{\mathrm{T}}^{\ell_1}, p_{\mathrm{T}}^{\ell_2}, p_{\mathrm{T}}^{\ell_3}$ [GeV]	×	> 25, > 15, > 10							
$m_{\mathrm{T}}^{\mathrm{mllmin}}$ [GeV]	×	< 50	< 50	< 60	< 60	< 70	> 90	< 70	> 90
	$\mathtt{SR}^{\mathtt{offWZ}}_{\mathtt{high}\not{E}_T}$-nj								
						f		g	
$p_{\mathrm{T}}^{\ell_1}, p_{\mathrm{T}}^{\ell_2}, p_{\mathrm{T}}^{\ell_3}$ [GeV]	> 4.5 (3.0) for e (μ)								
$\lvert\mathbf{p}_{\mathrm{T}}^{\mathrm{lep}}\rvert / E_{\mathrm{T}}^{\mathrm{miss}}$	< 0.2	< 0.2	< 0.3	< 0.3	< 0.3	< 1.0		< 1.0	

structed using the W lepton after $m_{\ell\ell}^{\min}$-based lepton assignment and marked with 'mllmin' to distinguish it from the m_{T} variable in the on-shell WZ selection. The SRs target phase space either below or above the SM W-boson peak present at $m_{\mathrm{T}}^{\mathrm{mllmin}} \sim m_W$. An upper bound of $m_{\mathrm{T}}^{\mathrm{mllmin}} < 50$–$70$ GeV is applied in low $m_{\ell\ell}^{\min}$ bins, while the `'f'` and `'g'` bins are split into two parts below (`'f1'`, `'g1'`) and above (`'f2'`, `'g2'`) the Jacobian peak of SM WZ.

In $\mathtt{SR}^{\mathtt{offWZ}}_{\mathtt{low}\not{E}_T}$, the selection on $\min \Delta R_{\mathrm{SFOS}}$ is tightened in the low $m_{\ell\ell}^{\min}$ bins, exploiting the topology with a relatively boosted Z^* in the target signatures, and a lower bound on $m_{3\ell}$ is applied for the high $m_{\ell\ell}^{\min}$ bins to reject the SM $Z \to 4\ell$ background peaking at $m_{3\ell} \sim m_Z$. The ratio of the magnitude of a vectorial p_{T} sum of the three leptons, $|\mathbf{p}_{\mathrm{T}}^{\mathrm{lep}}|$, to $E_{\mathrm{T}}^{\mathrm{miss}}$, is labelled $|\mathbf{p}_{\mathrm{T}}^{\mathrm{lep}}|/E_{\mathrm{T}}^{\mathrm{miss}}$ and represents the extent to which the transverse momentum of the hard-scatter $\widetilde{\chi}_1^{\pm}\widetilde{\chi}_2^0$ system, recoiling against ISR jets, is converted into leptons as opposed to $E_{\mathrm{T}}^{\mathrm{miss}}$. Due to the presence of a massive $\widetilde{\chi}_1^0$, contributing to the $E_{\mathrm{T}}^{\mathrm{miss}}$, signals tend to populate lower parts of the $|\mathbf{p}_{\mathrm{T}}^{\mathrm{lep}}|/E_{\mathrm{T}}^{\mathrm{miss}}$ spectrum than SM backgrounds, particularly for the compressed signals in the high $E_{\mathrm{T}}^{\mathrm{miss}}$ regions where the $E_{\mathrm{T}}^{\mathrm{miss}}$ is almost fully generated by the ISR jets. A tight upper bound $|\mathbf{p}_{\mathrm{T}}^{\mathrm{lep}}|/E_{\mathrm{T}}^{\mathrm{miss}}$ is therefore imposed in the low $m_{\ell\ell}^{\min}$ bins of $\mathtt{SR}^{\mathtt{offWZ}}_{\mathtt{high}\not{E}_T}$-nj.

After applying the selection criteria, for the wino/bino (+) model $\widetilde{\chi}_1^{\pm}\widetilde{\chi}_2^0$ signal sample with NLSP masses of 200 GeV and a mass splitting of $\Delta m = 20$ GeV, the $\mathtt{SR}^{\mathtt{offWZ}}_{\mathtt{low}\not{E}_T}$-0j, $\mathtt{SR}^{\mathtt{offWZ}}_{\mathtt{low}\not{E}_T}$-nj, $\mathtt{SR}^{\mathtt{offWZ}}_{\mathtt{high}\not{E}_T}$-0j, and $\mathtt{SR}^{\mathtt{offWZ}}_{\mathtt{high}\not{E}_T}$-nj regions (taking the union of the bins inside each region) have acceptance times efficiency values of 2.2×10^{-5}, 1.1×10^{-5}, 3.4×10^{-6}, and 6.0×10^{-5}, respectively. Similarly, for a mass splitting of $\Delta m = 60$ GeV, values of 1.6×10^{-4}, 1.7×10^{-4}, 2.8×10^{-4}, and 7.9×10^{-5} are found. The acceptance times efficiency values for the wino/bino (−) and higgsino model signal samples are typically 15–55% and 20–60% lower, depending on the region.

8.2 Background estimation

The selection criteria for the CRs and the VRs for WZ estimation are summarised in Table 10. An on-shell Z boson ($m_{\ell\ell} \in [81, 101]$ GeV) is required to ensure orthogonality to the $\mathtt{SR}^{\mathtt{offWZ}}$, and an upper bound on $E_{\mathrm{T}}^{\mathrm{miss}}$ ensures orthogonality to the $\mathtt{SR}^{\mathtt{WZ}}$. A lower bound on m_{T} is applied to suppress the Z + jets background. The CRs are further split into two

Table 10 Summary of the selection criteria for the CRs and VRs for WZ and $t\bar{t}$, for the off-shell WZ selection. In rows where only one value is given it applies to all regions. '–' indicates no requirement is applied for a given variable/region

Variable	$\texttt{CRWZ}^{\texttt{offWZ}}_{\texttt{0j}}$	$\texttt{CRWZ}^{\texttt{offWZ}}_{\texttt{nj}}$	$\texttt{VRWZ}^{\texttt{offWZ}}_{\texttt{0j}}$	$\texttt{VRWZ}^{\texttt{offWZ}}_{\texttt{nj}}$	$\texttt{VRWZ}^{\texttt{offWZ}}_{\texttt{nj-lowm}_{\ell\ell}}$	$\texttt{VRt}\bar{\texttt{t}}^{\texttt{offWZ}}$
$n_{\text{lep}}^{\text{baseline}}$, $n_{\text{lep}}^{\text{signal}}$			= 3			
n_{SFOS}			≥ 1			
Trigger			((multi-)lepton ∥ $E_{\text{T}}^{\text{miss}}$)			
min $\Delta R_{3\ell}$			> 0.4			
$n_{b\text{-jets}}$	= 0		= 0			≥ 1
$m_{\ell\ell}$ [GeV]	∈ [81, 101]		< 75			< 75
$n_{\text{jets}}^{30\text{ GeV}}$	= 0	≥ 1	= 0	≥ 1	≥ 1	-
$E_{\text{T}}^{\text{miss}}$ [GeV]	< 50	< 50	< 50	< 80	> 80	> 50
$E_{\text{T}}^{\text{miss}}$ significance	-		> 1.5	> 1.5	> 1.5	-
m_{T} [GeV]	> 50	> 50	∈ [60, 90]		> 30	-
$m_{\ell\ell}^{\text{min}}$ [GeV]	-		∈ [12, 75]		∈ [1, 12]	∈ [1, 75]
Resonance veto $m_{\ell\ell}^{\text{min}}$ [GeV]	-		-	-	∉ [3, 3.2], ∉ [9, 12]	∉ [3, 3.2], ∉ [9, 12]
$p_{\text{T}}^{\ell_1}$, $p_{\text{T}}^{\ell_2}$, $p_{\text{T}}^{\ell_3}$ [GeV]	> 10		> 10	> 10	-	-
min ΔR	-		[0.6, 2.4] ($\ell_{\text{W}} = e$ only)		-	-
$\lvert m_{3\ell} - m_Z \rvert$ [GeV]	-		> 20 ($\ell_{\text{W}} = e$ only)		-	-
$m_{\text{W}}^{\text{reco WZ}}$ [GeV]	-		> 75	-	-	-
$\Delta R(\ell_{\text{W}}, E_{\text{T}}^{\text{miss}})$	-		> 2.6	-	-	-
$\lvert \mathbf{p}_{\text{T}}^{\text{lep}} \rvert / E_{\text{T}}^{\text{miss}}$	-		-	-	> 0.3	-

Table 11 Summary of the selection criteria for the CRs and VRs for Z + jets, for the off-shell WZ selection. The corresponding anti-ID regions used for the Z + jets prediction follow the same selection criteria, except that at least one of the leptons is anti-ID instead of signal. '–' indicates no requirement is applied for a given variable/region

Variable	$\texttt{CRFF}^{\texttt{offWZ}}$	$\texttt{CRt}\bar{\texttt{t}}^{\texttt{offWZ}}_{\text{anti-ID}}$	$\texttt{VRFF}^{\texttt{offWZ}}_{\texttt{0j}}$	$\texttt{VRFF}^{\texttt{offWZ}}_{\texttt{nj}}$	$\texttt{VRFF}^{\texttt{offWZ}}_{\texttt{nj-lowp}_{\text{T}}}$
$n_{\text{lep}}^{\text{baseline}}$, $n_{\text{lep}}^{\text{signal}}$		= 3			
min $\Delta R_{3\ell}$		> 0.4			
Trigger	dilepton	((multi-)lepton ∥ $E_{\text{T}}^{\text{miss}}$)			
n_{SFOS}	≥ 1	= 0		≥ 1	
$n_{b\text{-jets}}$	= 0	= 0 or ≥ 1		= 0	
$m_{\ell\ell}$ [GeV]	∈ [m_Z − 15, m_Z + 15]	-		< 75	
$n_{\text{jets}}^{30\text{ GeV}}$	≤ 1 if $p_{\text{T}}^{\ell_{\text{W}}=\mu}$ > 30 GeV = 0 otherwise	-	= 0	≥ 1	≥ 1
$E_{\text{T}}^{\text{miss}}$ [GeV]	< 40	> 50	< 50	< 200	∈ [50, 200]
$E_{\text{T}}^{\text{miss}}$ significance	-	-	∈ [0.5, 1.5]	∈ [0.5, 3.0]	∈ [0.5, 3.0]
$p_{\text{T}}^{\ell_1}$, $p_{\text{T}}^{\ell_2}$, $p_{\text{T}}^{\ell_3}$ [GeV]	-	> 10	> 10	> 10	< 10
$m_{\ell\ell}^{\text{min}}$ [GeV]	-	-	∈ [12, 75]	∈ [12, 75]	∈ [1, 75]
m_{T} [GeV]	< 30	-		< 50	
min ΔR	-	-	[0.6, 2.4] ($\ell_{\text{W}} = e$ only)		
$m_{3\ell}$ [GeV]	> 105	-	[81.2, 101.2] ($\ell_{\text{W}} = e$ only)		

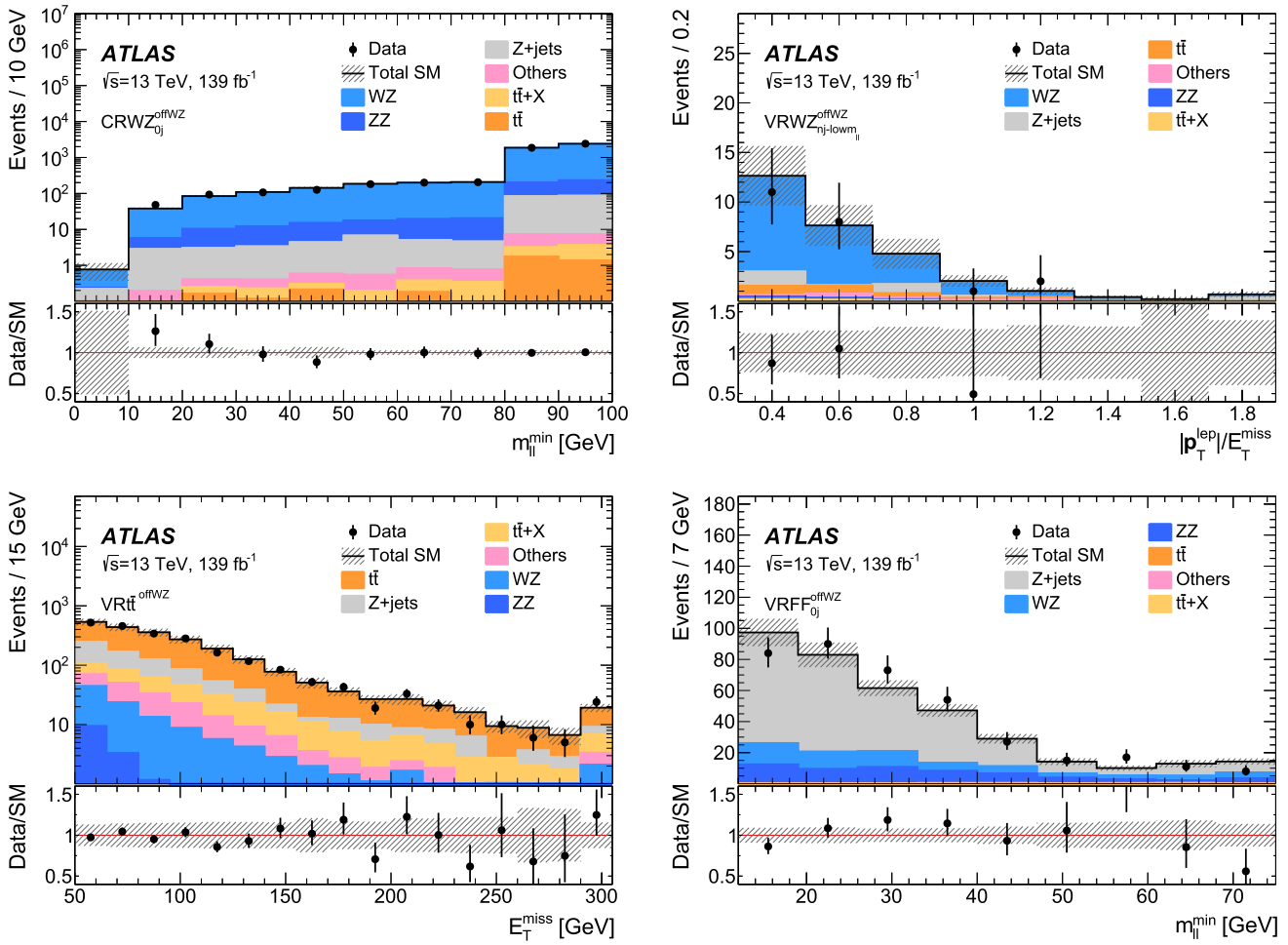

Fig. 7 Example kinematic distributions after the background-only fit, showing the data and the post-fit expected background, in regions of the off-shell WZ selection. The figure shows (top left) the $m_{\ell\ell}^{\text{min}}$ distribution in $\texttt{CRWZ}_{0j}^{\texttt{offWZ}}$, (top right) the $|\mathbf{p}_{\text{T}}^{\text{lep}}|/E_{\text{T}}^{\text{miss}}$ distribution in $\texttt{VRWZ}_{\texttt{nj-lowm}_{ll}}^{\texttt{offWZ}}$, (bottom left) the $E_{\text{T}}^{\text{miss}}$ distribution in $\texttt{VRt}\bar{\texttt{t}}^{\texttt{offWZ}}$, and (bottom right) the $m_{\ell\ell}^{\text{min}}$ distribution in $\texttt{VRFF}_{0j}^{\texttt{offWZ}}$. The last bin includes overflow. The 'Others' category contains backgrounds from single-top, WW, triboson, Higgs and rare top processes. The bottom panel shows the ratio of the observed data to the predicted yields. The hatched bands indicate the combined theoretical, experimental, and MC statistical uncertainties. The slope change in the bottom left $E_{\text{T}}^{\text{miss}}$ distribution illustrates the selection extension with $E_{\text{T}}^{\text{miss}}$ triggered events, which start contributing at $E_{\text{T}}^{\text{miss}} \gtrsim 200$ GeV

bins ($\texttt{CRWZ}_{0j}^{\texttt{offWZ}}$ and $\texttt{CRWZ}_{nj}^{\texttt{offWZ}}$), based on the absence or presence of jets, to constrain WZ events without or with hard ISR jets separately with individual normalisation factors.

Three validation regions are defined in the region with $m_{\ell\ell}^{\text{min}}$, $m_{\ell\ell} < 75$ GeV, similar to $\texttt{SR}^{\texttt{offWZ}}$. First, $\texttt{VRWZ}_{0j}^{\texttt{offWZ}}$ and $\texttt{VRWZ}_{nj}^{\texttt{offWZ}}$ are designed to validate the WZ estimation in the $\texttt{SR}_{\texttt{low}\not{E}_{\text{T}}}^{\texttt{offWZ}}$ phase space. A window in m_{T} around the Jacobian peak ($m_{\text{T}} \in [60, 90]$ GeV) is selected to enhance WZ, as well as to ensure the orthogonality with respect to the SRs. Further kinematic selection criteria similar to those in $\texttt{SR}_{\texttt{low}\not{E}_{\text{T}}}^{\texttt{offWZ}}$ are applied. Two additional variables are employed in the $\texttt{VRWZ}_{0j}^{\texttt{offWZ}}$ to suppress the signal contamination in the region. The W-boson mass, $m_{\text{W}}^{\text{reco WZ}}$, is reconstructed assuming the WZ topology and balanced longitudinal momenta of the W and Z bosons, and $\Delta R(\ell_{\text{W}}, E_{\text{T}}^{\text{miss}})$ is defined by $\sqrt{\eta_{\ell_{\text{W}}}^2 + \Delta\phi(\ell_{\text{W}}, E_{\text{T}}^{\text{miss}})^2}$ where leptons are assigned according to the $m_{\ell\ell}^{\text{min}}$ approach, and ℓ_{W} is the lepton associated with the W boson. Since $m_{\text{W}}^{\text{reco WZ}}$ peaks around m_W with a long tail to higher masses for WZ background, while signals tend to have a flatter distribution, $m_{\text{W}}^{\text{reco WZ}} > 75$ GeV is found to effectively reduce signal contamination.

In the very low $m_{\ell\ell}^{\text{min}}$ region, $\texttt{VRWZ}_{\texttt{nj-lowm}_{ll}}^{\texttt{offWZ}}$ is used to validate the WZ estimation in the $\texttt{SR}_{\texttt{high}\not{E}_{\text{T}}}^{\texttt{offWZ}}$ phase space. This region has the low-mass resonance veto applied and a lower bound on $|\mathbf{p}_{\text{T}}^{\text{lep}}|/E_{\text{T}}^{\text{miss}}$ to ensure orthogonality with the SRs. Other kinematic cuts are loosened relative to $\texttt{SR}_{\texttt{high}\not{E}_{\text{T}}}^{\texttt{offWZ}}$, or removed entirely, to increase the number of data events in the region. The WZ purity is 85–90% in the CRs and 70–

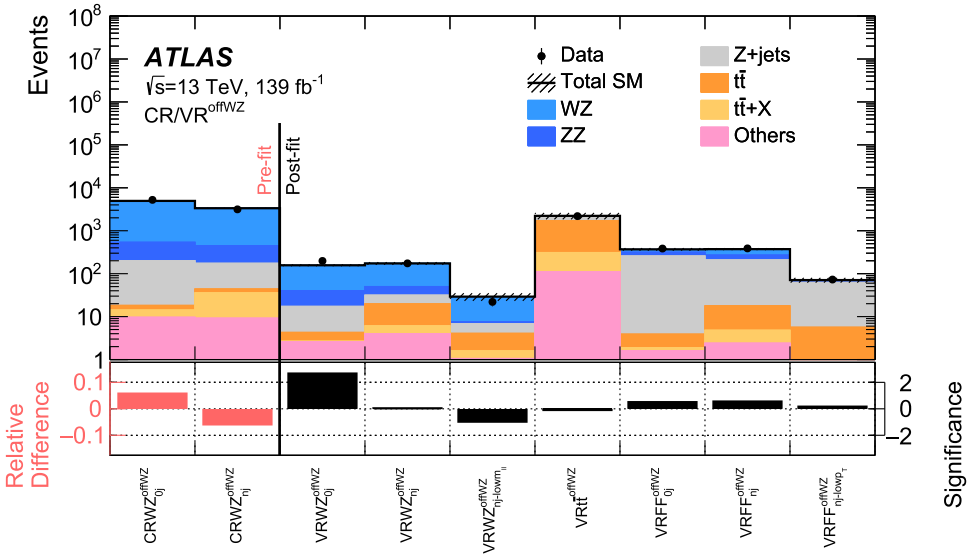

Fig. 8 Comparison of the observed data and expected SM background yields in the CRs and VRs of the off-shell WZ selection. The SM prediction is taken from the background-only fit. The 'Others' category contains the single-top, WW, triboson, Higgs and rare top processes. The hatched band indicates the combined theoretical, experimental, and MC statistical uncertainties. The bottom panel shows the significance of the difference between the observed and expected yields, calculated with the profile likelihood method from Ref. [169], adding a minus sign if the yield is below the prediction

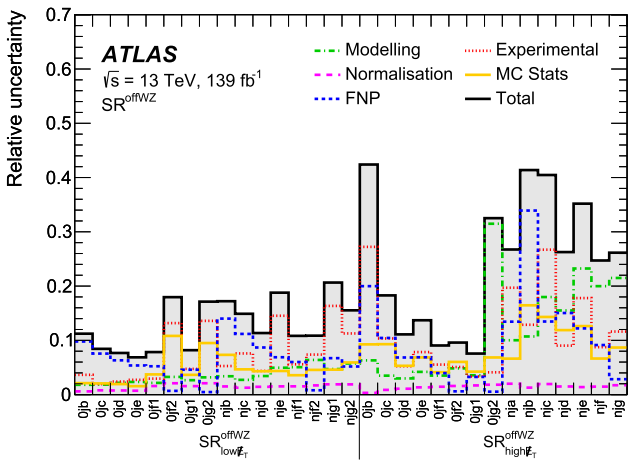

Fig. 9 Breakdown of the total systematic uncertainties in the background prediction for the SRs of the off-shell WZ selection

75% in the VRs. The contamination from the benchmark signals is negligible in the CRs and below 15% in the VRs.

The $\texttt{VRtt}^{\texttt{offWZ}}$ selection criteria are summarised in Table 10. At least one b-jet is required to maintain orthogonality with the SRs, $E_{\mathrm{T}}^{\mathrm{miss}} > 50$ GeV is required to suppress the $Z+$jets contribution, and the low-mass resonance background veto is applied. The $t\bar{t}$ purity in this region is approximately 65%.

The $Z+$jets background is estimated using the FF method as described in Sect. 6.2. The FF measurement region for the off-shell WZ selection, $\texttt{CRFF}^{\texttt{offWZ}}$, is summarised in Table 11. The Z-boson candidate is selected by requiring $|m_{\ell\ell} - m_Z| < 15$ GeV, and $E_{\mathrm{T}}^{\mathrm{miss}} < 40$ GeV and $m_{\mathrm{T}} < 30$ GeV are applied to reject contamination from WZ. Additionally $m_{3\ell} > 105$ GeV is applied to suppress $Z \to 4\ell$. To increase the number of FNP lepton candidates at high p_{T}, the overlap removal procedure described in Sect. 5 is modified for this FF measurement so that muons overlapping with jets are always kept. Finally, a jet veto is applied except for events where the FNP lepton candidate is a muon with $p_{\mathrm{T}} > 30$ GeV, in which case $n_{\mathrm{jets}}^{30\ \mathrm{GeV}} \leq 1$ is required in order to account for the special muon-vs-jet overlap-removal treatment applied to this region.

The FFs are derived separately per lepton flavour of FNP lepton candidates and per signal lepton criterion, i.e. with or without applying the non-prompt BDT, and are parameterised as a function of lepton p_{T} and $E_{\mathrm{T}}^{\mathrm{miss}}$ in the event. Typical FF values are 0.2–0.4 (0.2–0.6) without the BDT applied, and 0.05–0.2 (0.07–0.2) when applying the BDT, for electrons (muons) in a p_{T} range of 4.5–30 (3.0–30) GeV. The parameterisation in $E_{\mathrm{T}}^{\mathrm{miss}}$ is used to reflect the variation of FNP lepton source with $E_{\mathrm{T}}^{\mathrm{miss}}$, which is required in order to model the shape of fake $E_{\mathrm{T}}^{\mathrm{miss}}$ correctly. Typically the fraction of FNP leptons originating from heavy-flavour decays varies with $E_{\mathrm{T}}^{\mathrm{miss}}$, in the range 20–30% (60–70%) for electrons (muons), because of the neutrinos from the leptonic b-/c-decays.

The contribution of non-$Z+$jets processes is subtracted using MC simulated samples. A small normalisation correction is applied to the $t\bar{t}$ events in the simulated anti-ID

Table 12 Observed and expected yields after the background-only fit in the SRs for the on-shell WZ selection. The normalisation factors of the WZ sample are extracted separately for the 0j, low-H_T and high-H_T regions, and are treated separately in the combined fit. The 'Others' category contains the single-top, WW, triboson, Higgs and rare top processes. Combined statistical and systematic uncertainties are presented

Regions	SR^{WZ}-1	SR^{WZ}-2	SR^{WZ}-3	SR^{WZ}-4	SR^{WZ}-5	SR^{WZ}-6	SR^{WZ}-7
Observed	331	31	3	2	42	7	3
Fitted SM	314 ± 33	35 ± 6	4.1 ± 1.0	1.2 ± 0.5	58 ± 5	8.0 ± 0.9	5.8 ± 1.0
WZ	294 ± 31	32 ± 5	3.7 ± 0.9	0.9 ± 0.5	48 ± 4	7.1 ± 0.8	5.0 ± 0.9
ZZ	12.1 ± 3.1	0.66 ± 0.35	0.08 ± 0.04	0.04 ± 0.02	2.3 ± 0.6	0.12 ± 0.04	0.08 ± 0.03
$t\bar{t}$	2.8 ± 0.8	0.36 ± 0.26	0.04 ± 0.01	$0.00 \pm^{0.01}_{0.00}$	1.4 ± 0.4	$0.00 \pm^{0.01}_{0.00}$	0.04 ± 0.02
Z + jets	0.01 ± 0.01	0.14 ± 0.14	0.05 ± 0.06	0.06 ± 0.04	2.8 ± 2.3	0.3 ± 0.4	0.26 ± 0.17
$t\bar{t}+X$	0.16 ± 0.06	0.13 ± 0.05	0.03 ± 0.04	0.01 ± 0.01	0.10 ± 0.06	0.05 ± 0.03	0.01 ± 0.01
Others	5.1 ± 0.8	1.1 ± 0.4	0.21 ± 0.06	0.17 ± 0.06	3.2 ± 0.5	0.38 ± 0.11	0.34 ± 0.10
Regions	SR^{WZ}-8	SR^{WZ}-9	SR^{WZ}-10	SR^{WZ}-11	SR^{WZ}-12	SR^{WZ}-13	SR^{WZ}-14
Observed	1	77	11	0	0	111	19
Fitted SM	0.8 ± 0.4	90 ± 20	13.4 ± 2.4	0.5 ± 0.4	0.49 ± 0.24	89 ± 11	16.0 ± 1.4
WZ	0.44 ± 0.32	77 ± 19	11.3 ± 2.4	0.37 ± 0.31	0.38 ± 0.22	72 ± 9	13.4 ± 1.3
ZZ	0.01 ± 0.01	1.9 ± 0.9	0.24 ± 0.13	0.01 ± 0.01	0.01 ± 0.01	5.8 ± 2.8	0.39 ± 0.18
$t\bar{t}$	$0.00 \pm^{0.01}_{0.00}$	3.3 ± 0.9	0.45 ± 0.28	$0.00 \pm^{0.01}_{0.00}$	$0.00 \pm^{0.01}_{0.00}$	6.0 ± 1.4	0.24 ± 0.17
Z + jets	0.28 ± 0.20	4 ± 5	0.2 ± 0.4	0.02 ± 0.03	0.02 ± 0.03	0.02 ± 0.03	0.02 ± 0.03
$t\bar{t}+X$	0 ± 0	1.3 ± 0.4	0.40 ± 0.14	0.05 ± 0.04	0.02 ± 0.01	1.6 ± 0.5	0.56 ± 0.16
Others	0.08 ± 0.06	2.3 ± 0.5	0.79 ± 0.22	0.08 ± 0.05	0.08 ± 0.03	3.5 ± 0.7	1.37 ± 0.33
Regions	SR^{WZ}-15	SR^{WZ}-16	SR^{WZ}-17	SR^{WZ}-18	SR^{WZ}-19	SR^{WZ}-20	
Observed	5	1	13	9	3	1	
Fitted SM	2.8 ± 0.6	1.30 ± 0.27	13.7 ± 2.6	9.2 ± 1.3	2.3 ± 0.4	1.09 ± 0.13	
WZ	2.3 ± 0.6	1.07 ± 0.24	10.2 ± 1.9	6.7 ± 0.8	1.58 ± 0.24	0.87 ± 0.12	
ZZ	0.07 ± 0.04	0.04 ± 0.03	0.13 ± 0.06	0.10 ± 0.04	0.02 ± 0.01	0.02 ± 0.01	
$t\bar{t}$	$0.00 \pm^{0.01}_{0.00}$	$0.00 \pm^{0.01}_{0.00}$	0.77 ± 0.32	0.45 ± 0.26	$0.00 \pm^{0.01}_{0.00}$	$0.00 \pm^{0.01}_{0.00}$	
Z + jets	0.02 ± 0.02	0.07 ± 0.08	1 ± 1	0.7 ± 1.0	0.25 ± 0.34	0.02 ± 0.02	
$t\bar{t}+X$	0.07 ± 0.03	$0.00 \pm^{0.03}_{0.00}$	0.53 ± 0.17	0.33 ± 0.10	0.07 ± 0.04	0.03 ± 0.02	
Others	0.37 ± 0.11	0.12 ± 0.04	1.1 ± 0.8	0.9 ± 0.7	0.27 ± 0.07	0.18 ± 0.05	

region to account for the different anti-ID lepton efficiencies in data and MC simulation. Normalisation factors are derived separately depending on the ℓ_W flavour and the b-jet multiplicity in the event. They are measured using the data events in a $t\bar{t}$-enriched control region, $CRt\bar{t}^{offWZ}_{anti\text{-}ID}$, and are found to be between 0.88 and 0.95. The $CRt\bar{t}^{offWZ}_{anti\text{-}ID}$ selection requires there to be no SFOS lepton pair in the event, as well as $p_T^{\ell_3} > 10$ GeV and $E_T^{miss} > 50$ GeV to enhance the $t\bar{t}$ purity.

Two sources of uncertainty specific to the estimation in SR^{offWZ} are considered in addition to those described in Sect. 6.3. The FF parameterisation uncertainty is evaluated from the effect of using a different E_T^{miss} binning ($E_T^{miss} < 50$ GeV, 50% larger bin size), or a 3D parameterisation in lepton p_T, E_T^{miss} and lepton η, additionally taking into account the dependency on lepton η. The impact on the Z + jets background yields in the CRs is $\sim 5\%$, and 1–7% in the SRs/VRs. The uncertainty from disabling the muon-vs-jet overlap removal procedure in the FF measurement region is assessed by comparing those FFs with alternative FFs measured with muon-vs-jet overlap removal applied for events with a FNP muon candidate of $p_T < 30$ GeV. The variation in the estimated Z + jets yields in the SRs/CRs/VRs is found to be 5–15%.

The yields predicted by the FF method are cross-checked in dedicated VRs enriched in FNP lepton backgrounds, as summarised in Table 11. The E_T^{miss} significance selection is inverted with respect to the SRs to ensure orthogonality. First, $VRFF^{offWZ}_{0j}$ and $VRFF^{offWZ}_{nj}$ are designed to validate the yields in $SR^{offWZ}_{lowE_T}$-0j and $SR^{offWZ}_{lowE_T}$-nj, respectively, while $VRFF^{offWZ}_{nj\text{-}lowp_T}$ aims to cross-check the modelling of FNP leptons with $p_T < 10$ GeV specifically. The Z + jets purity is

Table 13 Observed and expected yields after the background-only fit in the SRs for the *Wh* selection. The normalisation factors of the *WZ* sample are extracted separately for the 0j, low-H_T and high-H_T regions, and are treated separately in the combined fit. The 'Others' category contains the single-top, WW, $t\bar{t}+X$ and rare top processes. Combined statistical and systematic uncertainties are presented

Regions	SR^{Wh}_{SFOS}-1	SR^{Wh}_{SFOS}-2	SR^{Wh}_{SFOS}-3	SR^{Wh}_{SFOS}-4	SR^{Wh}_{SFOS}-5	SR^{Wh}_{SFOS}-6	SR^{Wh}_{SFOS}-7
Observed	152	14	8	47	6	15	19
Fitted SM	136 ± 13	13.5 ± 1.7	4.3 ± 0.9	50 ± 5	4.3 ± 0.7	20.2 ± 2.1	16.0 ± 2.1
WZ	107 ± 12	10.2 ± 1.7	3.8 ± 0.8	32 ± 4	2.7 ± 0.6	12.3 ± 1.6	10.8 ± 1.7
$t\bar{t}$	10.3 ± 2.5	1.6 ± 0.6	0.13 ± 0.12	7.7 ± 1.9	0.74 ± 0.34	3.5 ± 1.0	2.5 ± 0.7
Z + jets	2.5 ± 2.9	$0.00 \pm^{0.02}_{0.00}$	$0.00 \pm^{0.02}_{0.00}$	2.0 ± 1.6	$0.00 \pm^{0.04}_{0.00}$	$0.00 \pm^{0.04}_{0.00}$	$0.00 \pm^{0.02}_{0.00}$
Higgs	5.7 ± 0.6	0.69 ± 0.07	0.20 ± 0.03	3.12 ± 0.31	0.26 ± 0.05	1.29 ± 0.14	0.81 ± 0.09
Triboson	1.9 ± 0.5	0.22 ± 0.07	0.07 ± 0.02	1.4 ± 0.4	0.28 ± 0.09	0.61 ± 0.18	0.83 ± 0.24
Others	8.6 ± 1.9	0.84 ± 0.11	0.08 ± 0.05	4.0 ± 0.5	0.23 ± 0.24	2.54 ± 0.22	1.11 ± 0.15
Regions	SR^{Wh}_{SFOS}-8	SR^{Wh}_{SFOS}-9	SR^{Wh}_{SFOS}-10	SR^{Wh}_{SFOS}-11	SR^{Wh}_{SFOS}-12	SR^{Wh}_{SFOS}-13	SR^{Wh}_{SFOS}-14
Observed	113	184	28	5	82	16	4
Fitted SM	108 ± 13	180 ± 17	31 ± 4	6.6 ± 0.9	90 ± 11	18.7 ± 2.6	2.5 ± 0.7
WZ	54 ± 6	127 ± 13	19.3 ± 2.3	5.3 ± 0.8	47 ± 6	6.8 ± 1.7	1.26 ± 0.26
$t\bar{t}$	21 ± 6	33 ± 10	8.2 ± 2.3	0.7 ± 0.5	28 ± 8	8.0 ± 2.2	0.9 ± 0.5
Z + jets	19 ± 10	2.3 ± 1.9	1.0 ± 1.3	0.10 ± 0.21	2.1 ± 3.1	1.2 ± 0.7	$0.00 \pm^{0.12}_{0.00}$
Higgs	1.91 ± 0.19	3.63 ± 0.35	0.67 ± 0.06	0.15 ± 0.02	2.98 ± 0.25	0.61 ± 0.07	0.07 ± 0.07
Triboson	0.79 ± 0.24	1.4 ± 0.4	0.41 ± 0.13	0.12 ± 0.05	1.6 ± 0.5	0.56 ± 0.18	0.13 ± 0.05
Others	11.1 ± 2.2	12.2 ± 2.2	1.8 ± 0.4	0.22 ± 0.05	9.0 ± 1.1	1.6 ± 0.7	0.10 ± 0.05
Regions	SR^{Wh}_{SFOS}-15	SR^{Wh}_{SFOS}-16	SR^{Wh}_{SFOS}-17	SR^{Wh}_{SFOS}-18	SR^{Wh}_{SFOS}-19	SR^{Wh}_{DFOS}-1	SR^{Wh}_{DFOS}-2
Observed	51	5	37	7	4	10	10
Fitted SM	46 ± 7	9.8 ± 1.6	43 ± 7	12.6 ± 1.7	1.8 ± 0.4	4.5 ± 0.8	7.0 ± 2.3
WZ	18.9 ± 2.2	3.9 ± 0.8	35 ± 6	9.8 ± 1.6	1.44 ± 0.32	0.44 ± 0.14	1.05 ± 0.20
$t\bar{t}$	18 ± 6	3.2 ± 1.3	1.00 ± 0.34	0.33 ± 0.17	$0.00 \pm^{0.01}_{0.00}$	1.0 ± 0.6	1.7 ± 1.1
Z + jets	$0.00 \pm^{0.12}_{0.00}$	$0.00 \pm^{0.12}_{0.00}$	$0.00 \pm^{0.12}_{0.00}$	$0.00 \pm^{0.12}_{0.00}$	$0.00 \pm^{0.12}_{0.00}$	$0.00 \pm^{0.20}_{0.00}$	2.5 ± 2.0
Higgs	2.06 ± 0.23	0.36 ± 0.05	1.02 ± 0.12	0.44 ± 0.05	0.05 ± 0.05	1.59 ± 0.22	0.96 ± 0.11
Triboson	1.5 ± 0.4	0.53 ± 0.17	2.5 ± 0.7	1.3 ± 0.4	0.2 ± 0.1	0.66 ± 0.15	0.64 ± 0.16
Others	5.0 ± 0.6	1.8 ± 0.5	3.0 ± 0.7	0.73 ± 0.15	0.14 ± 0.05	0.81 ± 0.09	0.21 ± 0.07

in the VRs is 50–80%, while the contamination from signals is negligible.

Performing the background-only fit, WZ normalisation factors of 1.06 ± 0.03 ($CRWZ^{offWZ}_{0j}$) and 0.93 ± 0.03 ($CRWZ^{offWZ}_{nj}$) are determined. Examples of kinematic distributions in the CRs and VRs, demonstrating good agreement, are presented in Fig. 7. Observed and expected yields for all CRs and VRs are summarised in Fig. 8.

The systematic uncertainties considered in the off-shell WZ selection are summarised in Fig. 9, grouped as discussed in Sect. 6.3. As the expected yields can vary by an order of magnitude throughout the regions, bin-to-bin fluctuations are expected in both the statistical and experimental uncertainty; these uncertainties are often dominant in bins with limited MC statistics in the phase space of the selection. The FNP lepton uncertainty is naturally more important in bins with larger FNP lepton background contributions, and can fluctuate in bins with few events in the corresponding anti-ID sample, such as $SR^{offWZ}_{high\not{E}_T}$-0jb and $SR^{offWZ}_{high\not{E}_T}$-njb. The modelling uncertainty is larger in the presence of ISR jets and at higher values of E_T^{miss}; the fluctuation in $SR^{offWZ}_{low\not{E}_T}$-njg2 originates from the effect of the QCD scale uncertainty on the WZ background.

9 Results

The observed data in the on-shell WZ, off-shell WZ, and Wh SRs are compared with the background expectation obtained from the background-only fits described in Sect. 6.4. The results are summarised in Tables 12 and 13 as well as visualised in Figs. 10 and 11 for the SR^{WZ} and SR^{Wh} regions, and in Tables 14 and 15 and Fig. 12 for the SR^{offWZ}. Post-fit distributions of key kinematic observables are shown for the

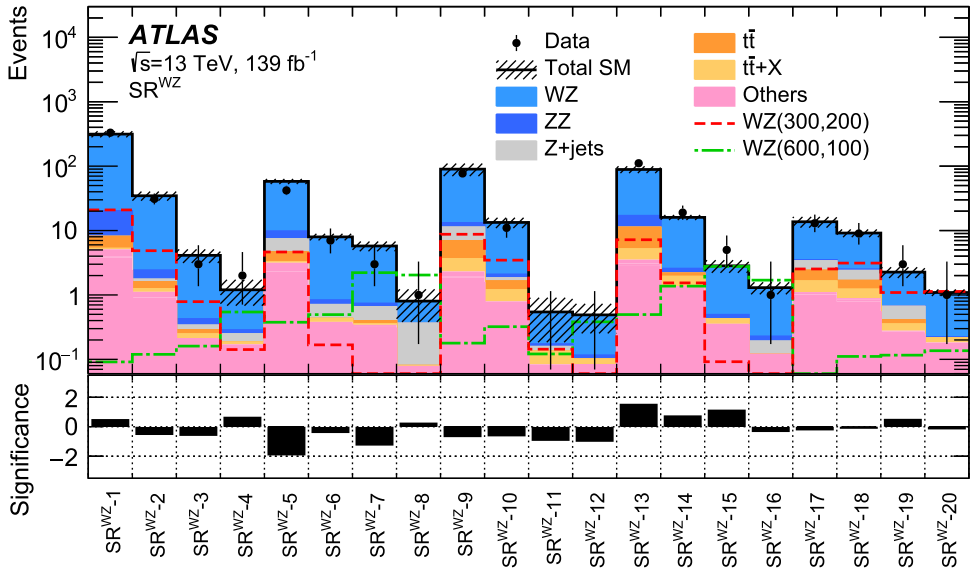

Fig. 10 Comparison of the observed data and expected SM background yields in the SRs of the on-shell WZ selection. The SM prediction is taken from the background-only fit. The 'Others' category contains the single-top, WW, triboson, Higgs and rare top processes. The hatched band indicates the combined theoretical, experimental, and MC statistical uncertainties. Distributions for wino/bino (+) $\tilde{\chi}_1^{\pm}\tilde{\chi}_2^0 \rightarrow WZ$ signals are overlaid, with mass values given as $(m(\tilde{\chi}_1^{\pm}), m(\tilde{\chi}_1^0))$ GeV. The bottom panel shows the significance of the difference between the observed and expected yields, calculated with the profile likelihood method from Ref. [169], adding a minus sign if the yield is below the prediction

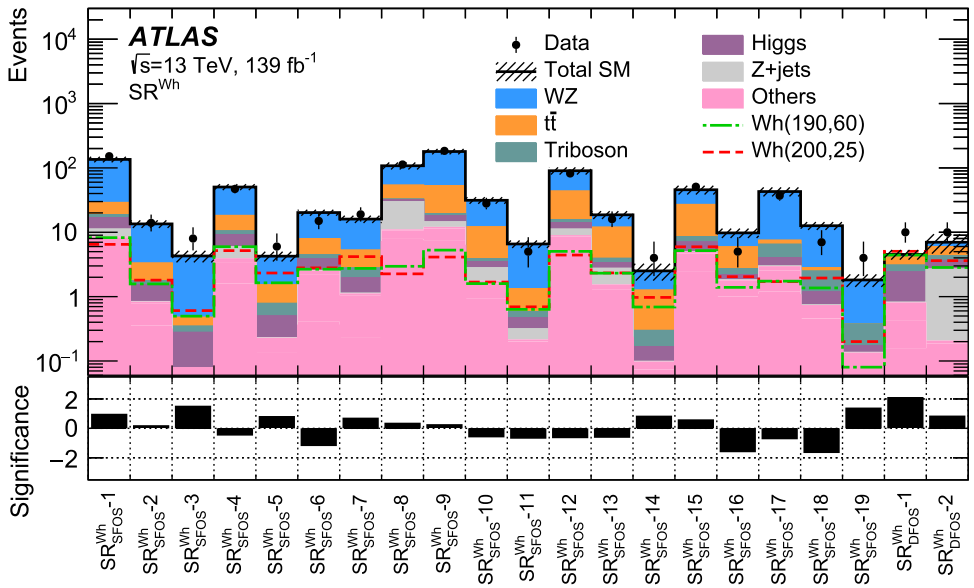

Fig. 11 Comparison of the observed data and expected SM background yields in the SRs of the Wh selection. The SM prediction is taken from the background-only fit. The 'Others' category contains the single-top, WW, $t\bar{t}+X$ and rare top processes. The hatched band indicates the combined theoretical, experimental, and MC statistical uncertainties. Distributions for wino/bino (+) $\tilde{\chi}_1^{\pm}\tilde{\chi}_2^0 \rightarrow Wh$ signals are overlaid, with mass values given as $(m(\tilde{\chi}_1^{\pm}), m(\tilde{\chi}_1^0))$ GeV. The bottom panel shows the significance of the difference between the observed and expected yields, calculated with the profile likelihood method from Ref. [169], adding a minus sign if the yield is below the prediction

$\mathrm{SR}^{\mathrm{WZ}}$ and $\mathrm{SR}^{\mathrm{Wh}}$ regions in Fig. 13 and for the $\mathrm{SR}^{\mathrm{offWZ}}$ regions in Fig. 14.

To illustrate the sensitivity to various $\tilde{\chi}_1^{\pm}\tilde{\chi}_2^0$ signals throughout the regions, representative signal MC predictions are overlaid on the figures. The sensitivity to WZ-mediated models, when the mass difference between the $\tilde{\chi}_1^{\pm}/\tilde{\chi}_2^0$ and $\tilde{\chi}_1^0$ is large, is driven by the $\mathrm{SR}^{\mathrm{WZ}}$ with large m_{T} and $E_{\mathrm{T}}^{\mathrm{miss}}$ values. On the other hand, when the mass splitting is close to the Z-boson mass, the sensitivity is dominated by the high H_{T} region and moderate m_{T} and $E_{\mathrm{T}}^{\mathrm{miss}}$ bins of the $n_{\mathrm{jets}} = 0$ and

Table 14 Observed and expected yields after the background-only fit in $\mathrm{SR}^{\mathrm{offWZ}}_{\mathrm{low}\not{E}_{\mathrm{T}}}$. The normalisation factors of the WZ sample are extracted separately for 0j and nj, and are treated separately in the combined fit. The 'Others' category contains the single-top, WW, triboson, Higgs and rare top processes. Combined statistical and systematic uncertainties are presented

Region	$\mathrm{SR}^{\mathrm{offWZ}}_{\mathrm{low}\not{E}_{\mathrm{T}}}$-0jb	$\mathrm{SR}^{\mathrm{offWZ}}_{\mathrm{low}\not{E}_{\mathrm{T}}}$-0jc	$\mathrm{SR}^{\mathrm{offWZ}}_{\mathrm{low}\not{E}_{\mathrm{T}}}$-0jd	$\mathrm{SR}^{\mathrm{offWZ}}_{\mathrm{low}\not{E}_{\mathrm{T}}}$-0je	$\mathrm{SR}^{\mathrm{offWZ}}_{\mathrm{low}\not{E}_{\mathrm{T}}}$-0jf1	$\mathrm{SR}^{\mathrm{offWZ}}_{\mathrm{low}\not{E}_{\mathrm{T}}}$-0jf2
Observed	25	42	77	101	33	7
Fitted SM events	32 ± 4	44 ± 4	54 ± 4	91 ± 6	32.2 ± 2.5	5.9 ± 1.1
WZ	7.6 ± 0.9	13.8 ± 1.3	16.3 ± 1.9	25.6 ± 1.8	20.1 ± 1.5	4.9 ± 1.0
ZZ	5.5 ± 1.3	7.4 ± 1.2	9.6 ± 1.6	21.8 ± 3.2	2.7 ± 1.1	0.43 ± 0.14
Z + jets	19.1 ± 3.2	22.7 ± 3.4	26.5 ± 3.5	40 ± 5	7.2 ± 1.7	$0.00 \pm ^{0.04}_{0.00}$
$t\bar{t}$	0.05	$^{0.18}_{0.05} \pm 0.11$	$^{0.17}_{0.11} \pm 0.38$	0.22 ± 1.1	0.4 ± 0.78	$0.29 \pm 0.08^{0.10}_{0.08}$
$t\bar{t}+X$	$0.007 \pm ^{0.019}_{0.007}$	$0.002 \pm ^{0.008}_{0.002}$	$0.009 \pm ^{0.019}_{0.009}$	$0.019 \pm ^{0.026}_{0.019}$	0.026 ± 0.026	$0.010 \pm ^{0.015}_{0.010}$
Others	0.045 ± 0.031	0.30 ± 0.12	1.3 ± 0.6	1.9 ± 0.6	1.4 ± 0.4	0.51 ± 0.18

Region	$\mathrm{SR}^{\mathrm{offWZ}}_{\mathrm{low}\not{E}_{\mathrm{T}}}$-0jg1	$\mathrm{SR}^{\mathrm{offWZ}}_{\mathrm{low}\not{E}_{\mathrm{T}}}$-0jg2	$\mathrm{SR}^{\mathrm{offWZ}}_{\mathrm{low}\not{E}_{\mathrm{T}}}$-njb	$\mathrm{SR}^{\mathrm{offWZ}}_{\mathrm{low}\not{E}_{\mathrm{T}}}$-njc	$\mathrm{SR}^{\mathrm{offWZ}}_{\mathrm{low}\not{E}_{\mathrm{T}}}$-njd	$\mathrm{SR}^{\mathrm{offWZ}}_{\mathrm{low}\not{E}_{\mathrm{T}}}$-nje
Observed	34	9	6	13	17	14
Fitted SM events	34.7 ± 2.8	6.3 ± 1.1	3.5 ± 0.6	8.0 ± 1.2	13.5 ± 1.5	18.2 ± 3.4
WZ	21.4 ± 2.1	5.2 ± 1.0	1.62 ± 0.30	3.2 ± 0.6	6.0 ± 0.8	8.6 ± 1.3
ZZ	4.7 ± 1.4	0.45 ± 0.14	0.45 ± 0.13	0.72 ± 0.22	1.00 ± 0.28	1.4 ± 0.9
Z + jets	6.6 ± 1.6	$0.001 \pm ^{0.029}_{0.001}$	1.2 ± 0.5	3.7 ± 0.9	4.5 ± 1.2	3.3 ± 1.3
$t\bar{t}$	0.8 ± 0.4	0.36 ± 0.21	0.15 ± 0.13	0.28 ± 0.14	1.5 ± 0.4	3.3 ± 0.9
$t\bar{t}+X$	0.039 ± 0.025	$0.003 \pm ^{0.008}_{0.003}$	0.030 ± 0.013	0.052 ± 0.019	0.24 ± 0.06	0.33 ± 0.07
Others	1.16 ± 0.27	0.27 ± 0.09	0.006 ± 0.004	$0.14 \pm ^{0.34}_{0.14}$	0.21 ± 0.06	$1.3 \pm ^{1.8}_{1.3}$

Region	$\mathrm{SR}^{\mathrm{offWZ}}_{\mathrm{low}\not{E}_{\mathrm{T}}}$-njf1	$\mathrm{SR}^{\mathrm{offWZ}}_{\mathrm{low}\not{E}_{\mathrm{T}}}$-njf2	$\mathrm{SR}^{\mathrm{offWZ}}_{\mathrm{low}\not{E}_{\mathrm{T}}}$-njg1	$\mathrm{SR}^{\mathrm{offWZ}}_{\mathrm{low}\not{E}_{\mathrm{T}}}$-njg2
Observed	25	20	22	12
Fitted SM events	23.4 ± 2.5	17.9 ± 1.9	17.0 ± 3.5	12.4 ± 1.9
WZ	11.1 ± 1.2	9.4 ± 1.1	10.0 ± 1.2	7.3 ± 1.3
ZZ	4.0 ± 1.6	0.66 ± 0.25	$1.1 \pm ^{2.6}_{1.1}$	0.34 ± 0.11
Z + jets	2.2 ± 1.4	$0.00 \pm ^{0.14}_{0.00}$	1.8 ± 1.1	$0.0 \pm ^{0.6}_{0.0}$
$t\bar{t}$	4.6 ± 1.1	5.7 ± 1.2	3.0 ± 0.8	2.9 ± 0.7
$t\bar{t}+X$	0.44 ± 0.09	0.72 ± 0.11	0.36 ± 0.08	0.44 ± 0.09
Others	1.0 ± 0.4	1.4 ± 0.9	0.71 ± 0.21	1.4 ± 0.6

low H_{T} regions. For the Wh-mediated scenarios the sensitivity is driven by $\mathrm{SR}^{\mathrm{Wh}}_{\mathrm{SFOS}}$ and $\mathrm{SR}^{\mathrm{Wh}}_{\mathrm{DFOS}}$ regions, with $\mathrm{SR}^{\mathrm{Wh}}_{\mathrm{DFOS}}$-1 contributing the most.

For the WZ-mediated models targeted with the $\mathrm{SR}^{\mathrm{offWZ}}$, with mass differences between the $\tilde{\chi}_1^{\pm}/\tilde{\chi}_2^0$ and $\tilde{\chi}_1^0$ smaller than the Z-boson mass, the sensitivity to signals with different Δm depends on the $m_{\ell\ell}^{\mathrm{min}}$ range of the bins. The bins with larger (smaller) $m_{\ell\ell}^{\mathrm{min}}$ values are sensitive to signals with larger (smaller) mass splittings; for the lowest mass-splitting signals, only $\mathrm{SR}^{\mathrm{offWZ}}_{\mathrm{high}\not{E}_{\mathrm{T}}}$-nja has sensitivity.

No significant deviation from the SM background prediction is found in any of the SRs, and none of the deviations agree with any of the benchmark signal hypotheses. The maximum deviation of the data from the background expectation is in $\mathrm{SR}^{\mathrm{offWZ}}_{\mathrm{low}\not{E}_{\mathrm{T}}}$-0jd with a 2.3σ data excess, followed by a 2.1σ deficit in $\mathrm{SR}^{\mathrm{offWZ}}_{\mathrm{high}\not{E}_{\mathrm{T}}}$-0jf2, a 2.0σ excess in $\mathrm{SR}^{\mathrm{Wh}}_{\mathrm{DFOS}}$-1, and a 2.0σ deficit in $\mathrm{SR}^{\mathrm{WZ}}$-5; the significances are computed following the profile likelihood method in Ref. [169].

9.1 Model-independent limits on new physics in inclusive regions

Model-independent upper limits and discovery p-values in the SRs are derived by performing the discovery fits as described in Sect. 6.4. The set of single-bin signal regions used in the fits, referred to as 'inclusive SRs', is constructed by logically grouping adjoining, disjoint, nominal SRs of the on-shell WZ, Wh and off-shell WZ selections. Multiple, sometimes overlapping, regions are defined to capture signatures with different unknown $m_{\ell\ell}^{\mathrm{min}}$ shapes and jet multiplicities inclusively. Based on the best expected discovery sensitivity and using a number of signal points covering both the WZ- and Wh-mediated scenarios and different

Table 15 Observed and expected yields after the background-only fit in $\mathrm{SR}^{\mathrm{offWZ}}_{\mathrm{high}\not{E}_{\mathrm{T}}}$. The normalisation factors of the WZ sample are extracted separately for 0j and nj, and are treated separately in the combined fit. The 'Others' category contains the single-top, WW, triboson, Higgs and rare top processes. Combined statistical and systematic uncertainties are presented

Region	$\mathrm{SR}^{\mathrm{offWZ}}_{\mathrm{high}\not{E}_{\mathrm{T}}}$-0jb	$\mathrm{SR}^{\mathrm{offWZ}}_{\mathrm{high}\not{E}_{\mathrm{T}}}$-0jc	$\mathrm{SR}^{\mathrm{offWZ}}_{\mathrm{high}\not{E}_{\mathrm{T}}}$-0jd	$\mathrm{SR}^{\mathrm{offWZ}}_{\mathrm{high}\not{E}_{\mathrm{T}}}$-0je	$\mathrm{SR}^{\mathrm{offWZ}}_{\mathrm{high}\not{E}_{\mathrm{T}}}$-0jf1
Observed	1	4	11	13	37
Fitted SM events	1.5 ± 0.7	4.3 ± 0.8	14.0 ± 1.6	11.5 ± 1.6	35.7 ± 3.2
WZ	$0.20 \pm^{0.27}_{0.20}$	1.5 ± 0.5	6.0 ± 0.9	6.1 ± 1.1	20.5 ± 2.1
ZZ	0.5 ± 0.5	0.31 ± 0.12	1.8 ± 0.8	0.89 ± 0.24	3.1 ± 1.0
Z + jets	0.81 ± 0.31	1.7 ± 0.4	4.4 ± 1.0	1.1 ± 0.8	4.3 ± 1.4
$t\bar{t}$	0.05 ± 0.05	0.45 ± 0.17	0.64 ± 0.28	1.8 ± 0.6	4.4 ± 1.0
$t\bar{t}+X$	$0.003 \pm^{0.014}_{0.003}$	$0.009 \pm^{0.013}_{0.009}$	0.029 ± 0.015	0.08 ± 0.04	0.11 ± 0.05
Others	$0.014 \pm^{0.018}_{0.014}$	$0.3 \pm^{0.4}_{0.3}$	1.1 ± 0.4	1.6 ± 0.4	3.3 ± 0.8
Region	$\mathrm{SR}^{\mathrm{offWZ}}_{\mathrm{high}\not{E}_{\mathrm{T}}}$-0jf2	$\mathrm{SR}^{\mathrm{offWZ}}_{\mathrm{high}\not{E}_{\mathrm{T}}}$-0jg1	$\mathrm{SR}^{\mathrm{offWZ}}_{\mathrm{high}\not{E}_{\mathrm{T}}}$-0jg2	$\mathrm{SR}^{\mathrm{offWZ}}_{\mathrm{high}\not{E}_{\mathrm{T}}}$-nja	$\mathrm{SR}^{\mathrm{offWZ}}_{\mathrm{high}\not{E}_{\mathrm{T}}}$-njb
Observed	14	43	17	3	2
Fitted SM events	25.5 ± 2.4	39.5 ± 3.0	21 ± 7	6.0 ± 1.6	1.4 ± 0.6
WZ	16.0 ± 2.3	26.4 ± 2.2	15 ± 7	3.8 ± 1.2	0.57 ± 0.18
ZZ	0.95 ± 0.35	3.0 ± 0.9	0.58 ± 0.17	0.044 ± 0.023	0.009 ± 0.005
Z + jets	$0.00 \pm^{0.15}_{0.00}$	3.4 ± 1.3	$0.00 \pm^{0.11}_{0.00}$	1.5 ± 0.8	0.5 ± 0.5
$t\bar{t}$	4.4 ± 1.0	4.3 ± 0.9	3.1 ± 0.7	0.6 ± 0.5	$0.14 \pm^{0.15}_{0.14}$
$t\bar{t}+X$	0.109 ± 0.030	0.16 ± 0.05	0.09 ± 0.04	0.16 ± 0.06	$0.014 \pm^{0.025}_{0.014}$
Others	4.0 ± 1.0	2.3 ± 0.8	2.0 ± 0.5	0.038 ± 0.030	0.22 ± 0.22
Region	$\mathrm{SR}^{\mathrm{offWZ}}_{\mathrm{high}\not{E}_{\mathrm{T}}}$-njc	$\mathrm{SR}^{\mathrm{offWZ}}_{\mathrm{high}\not{E}_{\mathrm{T}}}$-njd	$\mathrm{SR}^{\mathrm{offWZ}}_{\mathrm{high}\not{E}_{\mathrm{T}}}$-nje	$\mathrm{SR}^{\mathrm{offWZ}}_{\mathrm{high}\not{E}_{\mathrm{T}}}$-njf	$\mathrm{SR}^{\mathrm{offWZ}}_{\mathrm{high}\not{E}_{\mathrm{T}}}$-njg
Observed	2	2	2	11	4
Fitted SM events	2.1 ± 0.8	5.4 ± 1.4	3.0 ± 1.1	9.9 ± 2.5	6.8 ± 1.8
WZ	1.25 ± 0.25	2.5 ± 0.4	1.31 ± 0.25	4.5 ± 0.7	3.7 ± 0.6
ZZ	0.020 ± 0.011	0.014 ± 0.013	0.029 ± 0.014	0.081 ± 0.033	0.050 ± 0.020
Z + jets	$0.04 \pm^{0.28}_{0.04}$	$0.7 \pm^{0.8}_{0.7}$	$0.0 \pm^{0.4}_{0.0}$	$0.6 \pm^{0.9}_{0.6}$	$0.00 \pm^{0.19}_{0.00}$
$t\bar{t}$	0.6 ± 0.5	1.3 ± 0.8	1.2 ± 1.0	3.4 ± 2.0	2.5 ± 1.6
$t\bar{t}+X$	0.027 ± 0.023	0.08 ± 0.08	0.09 ± 0.04	0.31 ± 0.08	0.21 ± 0.07
Others	$0.14 \pm^{0.36}_{0.14}$	0.8 ± 0.6	0.33 ± 0.21	1.0 ± 0.4	$0.3 \pm^{0.4}_{0.3}$

mass splittings, 12 inclusive SRs are formed by merging $\mathrm{SR}^{\mathrm{WZ}}$ and $\mathrm{SR}^{\mathrm{Wh}}$ regions, creating $\mathrm{incSR}^{\mathrm{WZ}}$ and $\mathrm{incSR}^{\mathrm{Wh}}$, respectively. They are summarised in Table 16. Similarly, 17 inclusive SRs are formed by merging $\mathrm{SR}^{\mathrm{offWZ}}$ regions, creating $\mathrm{incSR}^{\mathrm{offWZ}}$; their definitions are summarised in Table 17. For $\mathrm{incSR}^{\mathrm{offWZ}}$, contiguous jet-veto regions are merged with jet-inclusive regions, as the $m_{\ell\ell}^{\mathrm{min}}$ shape of a signal is assumed to be insensitive to jet multiplicity. The $\mathrm{SR}^{\mathrm{offWZ}}_{\mathrm{low}\not{E}_{\mathrm{T}}}$ and $\mathrm{SR}^{\mathrm{offWZ}}_{\mathrm{high}\not{E}_{\mathrm{T}}}$ regions are kept separate, while the $\mathrm{SR}^{\mathrm{offWZ}}_{\mathrm{high}\not{E}_{\mathrm{T}}}$-nj regions are considered separately for $m_{\ell\ell}^{\mathrm{min}} < 20$ GeV, as this selection provides the best sensitivity to low-mass-splitting models.

The 95% CL upper limits on the generic BSM cross section are calculated by performing a discovery fit for each target SR and its associated CRs, using pseudo-experiments. Results are reported in Tables 18 and 19 for the on-shell WZ and Wh analysis selections (off-shell WZ selection). The tables list the observed (N_{obs}) and expected (N_{exp}) yields in the inclusive SRs, the upper limits on the observed (S^{95}_{obs}) and expected (S^{95}_{exp}) number of BSM events, and the visible cross section ($\sigma^{95}_{\mathrm{vis}}$) reflecting the product of the production cross section, the acceptance, and the selection efficiency for a BSM process; the p-value and significance (Z) for the background-only hypothesis are also presented.

9.2 Constraints on WZ- and Wh-mediated models

Constraints on the target simplified models are derived using the nominal SRs discussed in Sects. 7.1 and 8.1. The results are statistically combined with the previous results for the electroweakino regions (SR-E) of the two-lepton search targeting compressed mass spectra [18], referred to as the compressed selection. Model-dependent 95% CL exclusion limits are calculated by performing the exclusion fits as

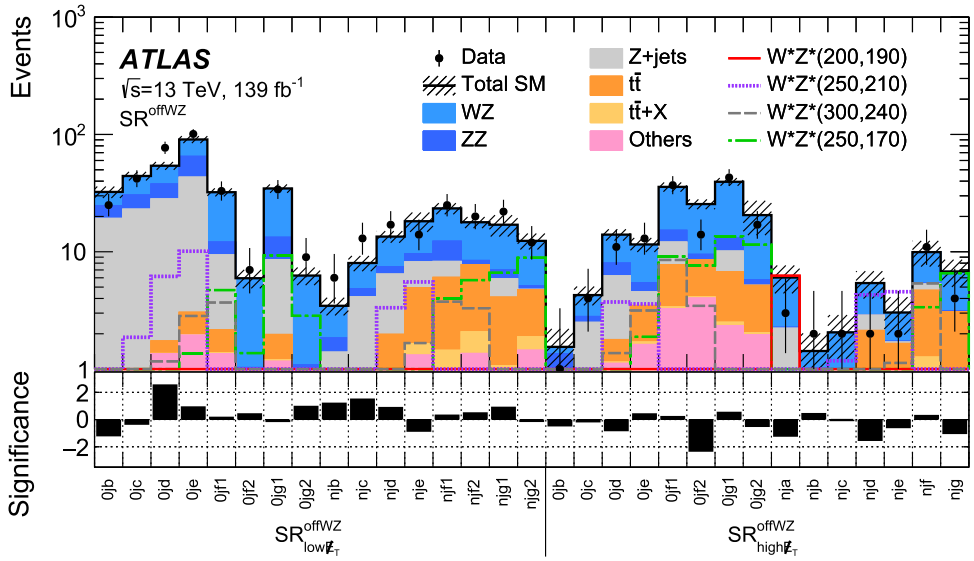

Fig. 12 Comparison of the observed data and expected SM background yields in the SRs of the off-shell WZ selection. The SM prediction is taken from the background-only fit. The 'Others' category contains the single-top, WW, triboson, Higgs and rare top processes. The hatched band indicates the combined theoretical, experimental, and MC statistical uncertainties. Distributions for wino/bino (+) $\tilde{\chi}_1^{\pm}\tilde{\chi}_2^0 \to W^*Z^*$ signals are overlaid, with mass values given as $(m(\tilde{\chi}_1^{\pm}), m(\tilde{\chi}_1^0))$ GeV. The bottom panel shows the significance of the difference between the observed and expected yields, calculated with the profile likelihood method from Ref. [169], adding a minus sign if the yield is below the prediction

described in Sect. 6.4. When performing the combination, common experimental uncertainties are treated as correlated between regions and processes. Theoretical uncertainties of the background and signal are treated as correlated between regions only, while statistical uncertainties are considered uncorrelated between regions and processes.

All regions of the on-shell WZ, off-shell WZ, and compressed selections were explicitly designed to be orthogonal, allowing a statistical combination of the results. The on-shell and off-shell WZ selections are orthogonal due to the $m_{\ell\ell}$ and $E_{\mathrm{T}}^{\mathrm{miss}}$ requirements, while the off-shell WZ and compressed selections are orthogonal by lepton multiplicity. Results are combined where greater exclusion power is expected over the individual results, ignoring contributions from search regions that do not add sensitivity in a given region of phase space. This approach results in multiple pairwise combinations of the on-shell and off-shell WZ selections, and the off-shell WZ and compressed selections, in bands of the $(\Delta m,\ m(\tilde{\chi}_2^0))$ plane.

Four separate fits are performed to obtain constraints for the following simplified models:

- the wino/bino (+) WZ-mediated model combining the on-shell WZ, off-shell WZ, and compressed selections,
- the wino/bino (+) Wh-mediated model using the Wh selection only,
- the wino/bino (−) WZ-mediated model combining the off-shell WZ and compressed selections,
- the higgsino WZ-mediated model combining the off-shell WZ and compressed selections.

For the WZ-mediated model in the wino/bino (+) scenario, only the $\mathrm{SR}^{\mathrm{WZ}}$ are sensitive for mass splittings Δm above 100 GeV. Conversely, the $\mathrm{SR}^{\mathrm{offWZ}}$ dominate the intermediate mass-splitting region, with sensitivity in the $\Delta m = [5, 100]$ GeV range. In the most compressed region, the SR−E are important, driving the result for Δm below 10 GeV and adding sensitivity up to $\Delta m = 50$ GeV. Given these contributions, the Δm range is split into five bands to make optimal use of the different channels, and the combination considers respectively the SR−E only, the SR−E and $\mathrm{SR}^{\mathrm{offWZ}}$, the $\mathrm{SR}^{\mathrm{offWZ}}$ only, the $\mathrm{SR}^{\mathrm{offWZ}}$ and $\mathrm{SR}^{\mathrm{WZ}}$, and the $\mathrm{SR}^{\mathrm{WZ}}$ only. In the wino/bino (−) an

d higgsino scenarios, the on-shell WZ selection is not considered, and only three bands are defined for the combination. The exact Δm ranges used are illustrated for the different scenarios in Fig. 15.

Expected and observed exclusion contours are reported as a function of the $\tilde{\chi}_1^0$ and $\tilde{\chi}_1^{\pm}/\tilde{\chi}_2^0$ masses, and shown in Fig. 16 (WZ-mediated model) and Fig. 17 (Wh-mediated model). The combined results are shown together with the individual contributions. For each mass point, a $\mathrm{CL_s}$ value is derived to assess the probability of compatibility between the observed data and the signal-plus-background prediction obtained by the exclusion fit. For the WZ-mediated model, the results are obtained by statistically combining the $\mathrm{SR}^{\mathrm{WZ}}$,

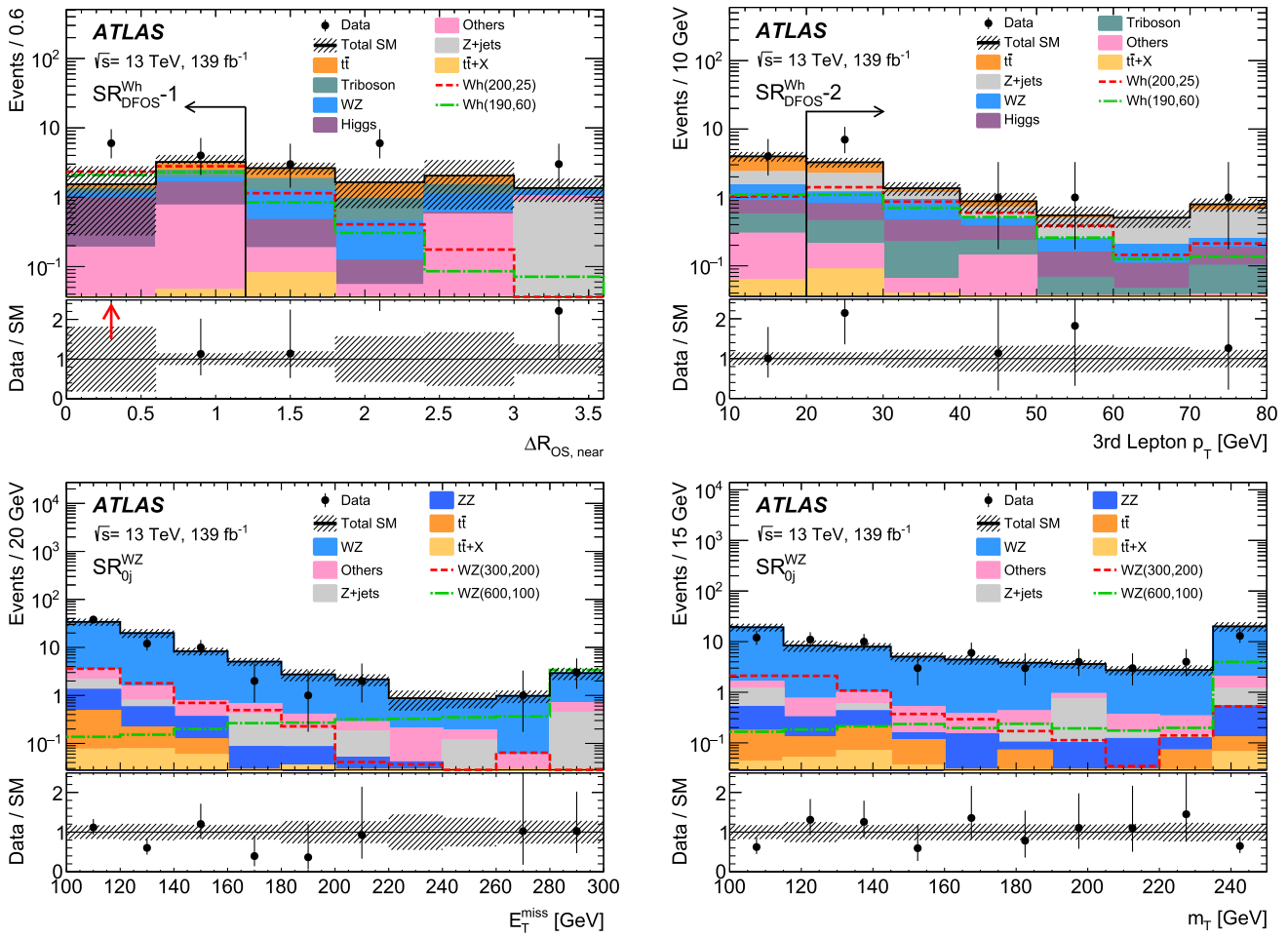

Fig. 13 Kinematic distributions after the background-only fit showing the data and the post-fit expected background, in SRs of the on-shell WZ and Wh selections. The figure shows (top left) the $\Delta R_{\mathrm{OS,near}}$ distribution in $\mathrm{SR}^{\mathrm{Wh}}_{\mathrm{DFOS}}\text{-}1$, (top right) the 3rd leading lepton's p_{T} in $\mathrm{SR}^{\mathrm{Wh}}_{\mathrm{DFOS}}\text{-}2$, and the (bottom left) $E_{\mathrm{T}}^{\mathrm{miss}}$ and (bottom right) m_{T} distributions in $\mathrm{SR}^{\mathrm{WZ}}_{0\mathrm{j}}$ (with all SR-i bins of $\mathrm{SR}^{\mathrm{WZ}}_{0\mathrm{j}}$ summed). The SR selections are applied for each distribution, except for the variable shown, for which the selection is indicated by a black arrow. The last bin includes overflow. The 'Others' category contains backgrounds from single-top, WW, triboson, Higgs and rare top processes, except in the top panels, where triboson and Higgs production contributions are shown separately, and $t\bar{t}+X$ is merged into Others. Distributions for wino/bino (+) $\widetilde{\chi}_1^{\pm}\widetilde{\chi}_2^0 \rightarrow WZ/Wh$ signals are overlaid, with mass values given as $(m(\widetilde{\chi}_1^{\pm}), m(\widetilde{\chi}_1^0))$ GeV. The bottom panel shows the ratio of the observed data to the predicted yields. Ratio values outside the graph range are indicated by a red arrow. The hatched bands indicate the combined theoretical, experimental, and MC statistical uncertainties

$\mathrm{SR}^{\mathrm{offWZ}}$ and $\mathrm{SR}\text{-}\mathrm{E}$ contributions, following the prescription outlined above. For the Wh-mediated model, the results are taken from a simultaneous fit of the 19 bins of $\mathrm{SR}^{\mathrm{Wh}}$.

For the wino/bino (+) WZ-mediated model, shown in Fig. 16 (top panels), observed (expected) lower limits for equal-mass $\widetilde{\chi}_1^{\pm}/\widetilde{\chi}_2^0$ are set at 640 (660) GeV for massless $\widetilde{\chi}_1^0$, and up to 300 (300) GeV for scenarios with mass splittings Δm near m_Z, driven by the on-shell WZ selection. The exclusion for the scenarios with $\Delta m < m_Z$ is driven by the off-shell WZ selection. For $\widetilde{\chi}_1^{\pm}$ and $\widetilde{\chi}_2^0$ decaying via off-shell WZ bosons, observed and expected limits are set at values up to 300 GeV for $\Delta m > 35$ GeV, and up to 210–300 GeV for $\Delta m = 20$–35 GeV. Below $\Delta m = 15$ GeV the observed and expected limits are extended by the combination with the compressed selection, up to 240 GeV for $\Delta m = 10$ GeV, and down to as low as $\Delta m = 2$ GeV for a $\widetilde{\chi}_1^{\pm}/\widetilde{\chi}_2^0$ mass of 100 GeV. Furthermore, constraints are calculated in the bino–wino co-annihilation dark-matter scenario by determining the area in the two-dimensional mass plane that yields a thermal dark-matter relic density equal to the observed value [176]. Figure 16 (top right) shows this area in blue, with the over- and under-abundant regions marked above and below; $\widetilde{\chi}_1^{\pm}/\widetilde{\chi}_2^0$ ($\widetilde{\chi}_1^0$) masses are excluded in this dark-matter scenario up to 210 (195) GeV.

The obtained wino/bino (+) exclusion limits are greatly improved compared to the previous equivalent search presented by the ATLAS experiment using the Run 1, 8 TeV dataset [17] (shown as a light grey shaded area in Fig. 16, top panels), due to a combination of increased production cross section

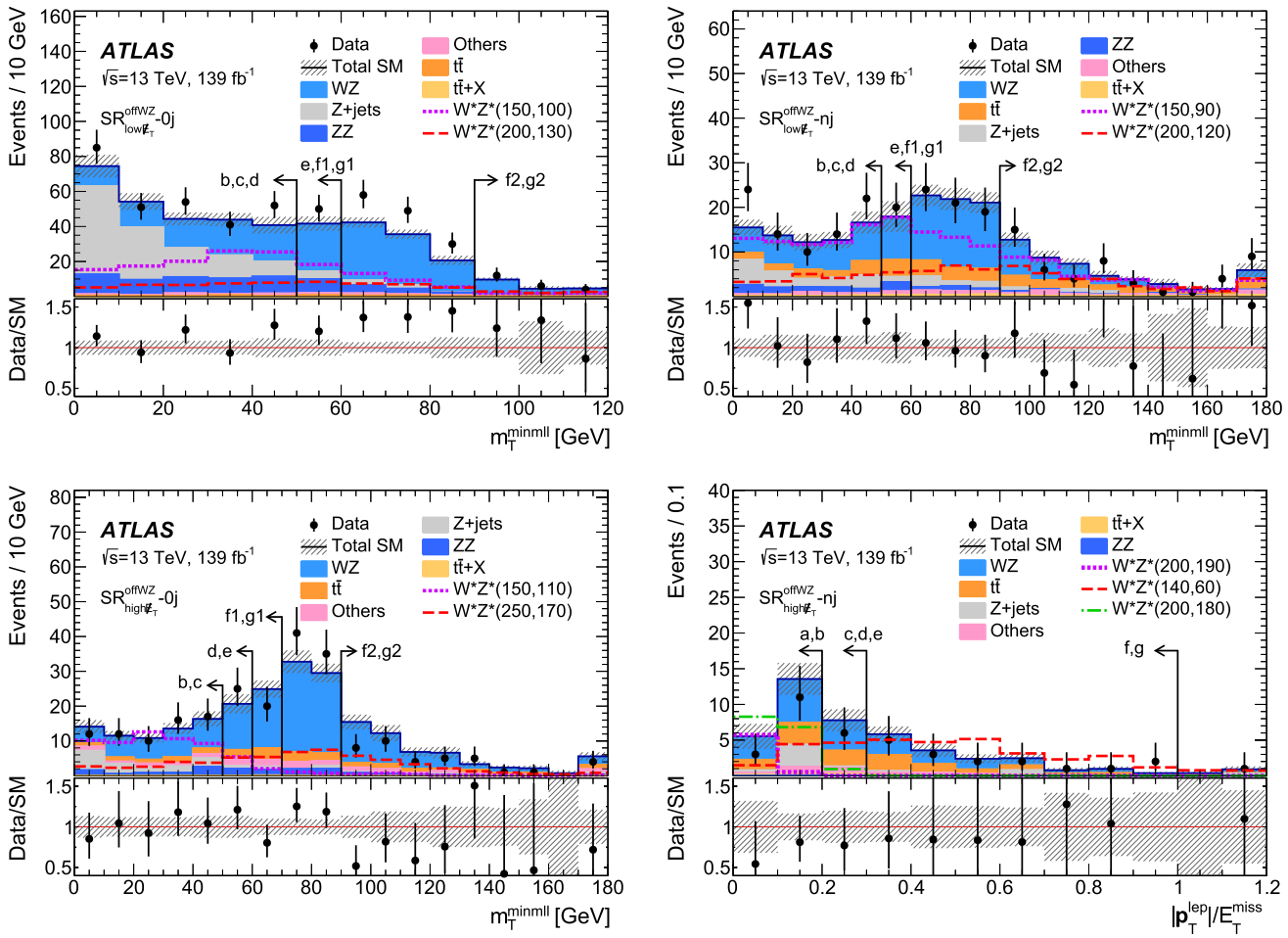

Fig. 14 Kinematic distributions after the background-only fit showing the data and the post-fit expected background, in SRs of the off-shell WZ selection. The figure shows the $m_{\mathrm{T}}^{\mathrm{mllmin}}$ distribution in (top left) $\mathtt{SR}^{\mathtt{offWZ}}_{\mathrm{low}\not{E}_{\mathrm{T}}}\mathtt{-0j}$, (top right) $\mathtt{SR}^{\mathtt{offWZ}}_{\mathrm{low}\not{E}_{\mathrm{T}}}\mathtt{-nj}$ and (bottom left) $\mathtt{SR}^{\mathtt{offWZ}}_{\mathrm{high}\not{E}_{\mathrm{T}}}\mathtt{-0j}$, and the $|\mathbf{p}_{\mathrm{T}}^{\mathrm{lep}}|/E_{\mathrm{T}}^{\mathrm{miss}}$ distribution in (bottom right) $\mathtt{SR}^{\mathtt{offWZ}}_{\mathrm{high}\not{E}_{\mathrm{T}}}\mathtt{-nj}$. The contributing $m_{\ell\ell}^{\mathrm{min}}$ mass bins within each $\mathtt{SR}^{\mathtt{offWZ}}$ category are summed. The SR selections are applied for each distribution, except for the variable shown, for which the selection is indicated by a black arrow. The last bin includes overflow. The 'Others' category contains backgrounds from single-top, WW, triboson, Higgs and rare top processes. Distributions for wino/bino (+) $\widetilde{\chi}_1^{\pm}\widetilde{\chi}_2^0 \to WZ$ signals are overlaid, with mass values given as $(m(\widetilde{\chi}_1^{\pm}),\ m(\widetilde{\chi}_1^0))$ GeV. The bottom panel shows the ratio of the observed data to the predicted yields. The hatched bands indicate the combined theoretical, experimental, and MC statistical uncertainties

at the increased collision centre-of-mass energy, larger data sample, and improved analysis techniques.

Expected and observed exclusion contours are also derived for the WZ-mediated model in the wino/bino (−) and higgsino scenarios, shown in Fig. 16 (bottom panels) as a function of the $\widetilde{\chi}_1^0$ and $\widetilde{\chi}_2^0$ masses. The results are obtained by statistically combining the $\mathtt{SR}^{\mathtt{offWZ}}$ and $\mathtt{SR-E}$ contributions, following the prescription outlined above.

In the wino/bino (−) scenario, shown in Fig. 16 (bottom left), observed (expected) lower limits for equal-mass $\widetilde{\chi}_1^{\pm}/\widetilde{\chi}_2^0$ are set at values up to 310 (300) GeV for mass splittings Δm around 80 GeV, and up to 250 (250) GeV for Δm around 40 GeV. For Δm of 10–20 GeV, the impact of the combination of the off-shell WZ and compressed results is the largest, and raises the expected limit to $\widetilde{\chi}_1^{\pm}/\widetilde{\chi}_2^0$ masses of 270 GeV, with the observed limit still showing a mild deficit similar to that visible in the compressed contribution. At a $\widetilde{\chi}_1^{\pm}/\widetilde{\chi}_2^0$ mass of 100 GeV, the observed (expected) exclusion extends down to $\Delta m = 1$ (1.5) GeV.

In the higgsino scenario, shown in Fig. 16 (bottom right), with the $\widetilde{\chi}_1^{\pm}$ mass between that of the $\widetilde{\chi}_1^0$ and $\widetilde{\chi}_2^0$, limits are set for mass splittings Δm up to 60 GeV. For Δm between 30 and 60 GeV, observed (expected) limits extend to around 150–210 (160–215) GeV. The impact of the combination of the off-shell WZ and compressed results is largest in the $\Delta m =$ 15–30 GeV range, improving on the individual result by up to 15 GeV. Below $\Delta m = 20$ GeV, the result is dominated by the compressed contribution, and limits extend down to $\Delta m = 2$ GeV.

Table 16 Summary of the selection criteria for the inclusive SRs in the on-shell WZ and Wh selections

	SR^{WZ} ($m_{\ell\ell} \in [75, 105]$ GeV)			
	$n_{\text{jets}} = 0$		$n_{\text{jets}} > 0$	
m_{T} [GeV]	$E_{\text{T}}^{\text{miss}}$ [GeV]			
[100, 160]	incSR^{WZ}-1: [100, 200]	incSR^{WZ}-2: > 200	incSR^{WZ}-3: [150, 250]	incSR^{WZ}-4: > 250
> 160	incSR^{WZ}-5: > 200		incSR^{WZ}-6: > 200	
	$\text{SR}^{\text{Wh}}_{\text{SFOS}}$ ($m_{\ell\ell} \leq 75$ GeV)			
	$n_{\text{jets}} = 0$		$n_{\text{jets}} > 0$	
m_{T} [GeV]	$E_{\text{T}}^{\text{miss}}$ [GeV]			
[0, 100]	$\text{incSR}^{\text{Wh}}_{\text{SFOS}}$-7: > 50		-	
[100, 160]	$\text{incSR}^{\text{Wh}}_{\text{SFOS}}$-8: > 50		$\text{incSR}^{\text{Wh}}_{\text{SFOS}}$-9: > 75	
> 160	$\text{incSR}^{\text{Wh}}_{\text{SFOS}}$-10: > 50		$\text{incSR}^{\text{Wh}}_{\text{SFOS}}$-11: > 75	
	$\text{SR}^{\text{Wh}}_{\text{DFOS}}$			
	$\text{incSR}^{\text{Wh}}_{\text{DFOS}}$-12: $n_{\text{jets}} \in [0, 2]$, $\Delta R_{\text{OS,near}} < 1.2$, 3rd lepton p_{T} >20 GeV			

Table 17 Summary of the selection criteria for the inclusive SRs in the off-shell WZ selection

$m_{\ell\ell}^{\text{min}}$ [GeV]	$\text{incSR}^{\text{offWZ}}_{\text{high}\not{E}_{\text{T}}}$-nj			
	a	b	c1	c2
	[1, 12]	[12, 15]	[1, 20]	[15, 20]
	$\text{SR}^{\text{offWZ}}_{\text{high}\not{E}_{\text{T}}}$-nj[a]	$\text{SR}^{\text{offWZ}}_{\text{high}\not{E}_{\text{T}}}$-nj[b]	$\text{SR}^{\text{offWZ}}_{\text{high}\not{E}_{\text{T}}}$-nj[a-c]	$\text{SR}^{\text{offWZ}}_{\text{high}\not{E}_{\text{T}}}$-nj[c]
$m_{\ell\ell}^{\text{min}}$ [GeV]	$\text{incSR}^{\text{offWZ}}_{\text{low}\not{E}_{\text{T}}}$		$\text{incSR}^{\text{offWZ}}_{\text{high}\not{E}_{\text{T}}}$	
	b	c	b	c
	[12, 15]	[12, 20]	[12, 15]	[12, 20]
	$\text{SR}^{\text{offWZ}}_{\text{low}\not{E}_{\text{T}}}$-0j[b], $\text{SR}^{\text{offWZ}}_{\text{low}\not{E}_{\text{T}}}$-nj[b]	$\text{SR}^{\text{offWZ}}_{\text{low}\not{E}_{\text{T}}}$-0j[b-c], $\text{SR}^{\text{offWZ}}_{\text{low}\not{E}_{\text{T}}}$-nj[b-c]	$\text{SR}^{\text{offWZ}}_{\text{high}\not{E}_{\text{T}}}$-0j[b], $\text{SR}^{\text{offWZ}}_{\text{high}\not{E}_{\text{T}}}$-nj[b]	$\text{SR}^{\text{offWZ}}_{\text{high}\not{E}_{\text{T}}}$-0j[b-c], $\text{SR}^{\text{offWZ}}_{\text{high}\not{E}_{\text{T}}}$-nj[b-c]
$m_{\ell\ell}^{\text{min}}$ [GeV]	$\text{incSR}^{\text{offWZ}}$				
	d	e1	e2	f1	f2
	[12, 30]	[12, 40]	[20, 40]	[12, 60]	[30, 60]
	$\text{SR}^{\text{offWZ}}_{\text{low}\not{E}_{\text{T}}}$-0j[b-d], $\text{SR}^{\text{offWZ}}_{\text{low}\not{E}_{\text{T}}}$-nj[b-d], $\text{SR}^{\text{offWZ}}_{\text{high}\not{E}_{\text{T}}}$-0j[b-d], $\text{SR}^{\text{offWZ}}_{\text{high}\not{E}_{\text{T}}}$-nj[b-d]	$\text{SR}^{\text{offWZ}}_{\text{low}\not{E}_{\text{T}}}$-0j[b-e], $\text{SR}^{\text{offWZ}}_{\text{low}\not{E}_{\text{T}}}$-nj[b-e], $\text{SR}^{\text{offWZ}}_{\text{high}\not{E}_{\text{T}}}$-0j[b-e], $\text{SR}^{\text{offWZ}}_{\text{high}\not{E}_{\text{T}}}$-nj[b-e]	$\text{SR}^{\text{offWZ}}_{\text{low}\not{E}_{\text{T}}}$-0j[c-e], $\text{SR}^{\text{offWZ}}_{\text{low}\not{E}_{\text{T}}}$-nj[c-e], $\text{SR}^{\text{offWZ}}_{\text{high}\not{E}_{\text{T}}}$-0j[c-e], $\text{SR}^{\text{offWZ}}_{\text{high}\not{E}_{\text{T}}}$-nj[c-e]	$\text{SR}^{\text{offWZ}}_{\text{low}\not{E}_{\text{T}}}$-0j[c-f2], $\text{SR}^{\text{offWZ}}_{\text{low}\not{E}_{\text{T}}}$-nj[c-f2], $\text{SR}^{\text{offWZ}}_{\text{high}\not{E}_{\text{T}}}$-0j[c-f2], $\text{SR}^{\text{offWZ}}_{\text{high}\not{E}_{\text{T}}}$-nj[c-f]	$\text{SR}^{\text{offWZ}}_{\text{low}\not{E}_{\text{T}}}$-0j[e-f2], $\text{SR}^{\text{offWZ}}_{\text{low}\not{E}_{\text{T}}}$-nj[e-f2], $\text{SR}^{\text{offWZ}}_{\text{high}\not{E}_{\text{T}}}$-0j[e-f2], $\text{SR}^{\text{offWZ}}_{\text{high}\not{E}_{\text{T}}}$-nj[e-f]
$m_{\ell\ell}^{\text{min}}$ [GeV]	$\text{incSR}^{\text{offWZ}}$			
	g1	g2	g3	g4
	[12, 75]	[30, 75]	[40, 75]	[60, 75]
	$\text{SR}^{\text{offWZ}}_{\text{low}\not{E}_{\text{T}}}$-0j[b-g2], $\text{SR}^{\text{offWZ}}_{\text{low}\not{E}_{\text{T}}}$-nj[b-g2], $\text{SR}^{\text{offWZ}}_{\text{high}\not{E}_{\text{T}}}$-0j[b-g2], $\text{SR}^{\text{offWZ}}_{\text{high}\not{E}_{\text{T}}}$-nj[b-g]	$\text{SR}^{\text{offWZ}}_{\text{low}\not{E}_{\text{T}}}$-0j[e-g2], $\text{SR}^{\text{offWZ}}_{\text{low}\not{E}_{\text{T}}}$-nj[e-g2], $\text{SR}^{\text{offWZ}}_{\text{high}\not{E}_{\text{T}}}$-0j[e-g2], $\text{SR}^{\text{offWZ}}_{\text{high}\not{E}_{\text{T}}}$-nj[e-g]	$\text{SR}^{\text{offWZ}}_{\text{low}\not{E}_{\text{T}}}$-0j[f1-g2], $\text{SR}^{\text{offWZ}}_{\text{low}\not{E}_{\text{T}}}$-nj[f1-g2], $\text{SR}^{\text{offWZ}}_{\text{high}\not{E}_{\text{T}}}$-0j[f1-g2], $\text{SR}^{\text{offWZ}}_{\text{high}\not{E}_{\text{T}}}$-nj[f1-g]	$\text{SR}^{\text{offWZ}}_{\text{low}\not{E}_{\text{T}}}$-0j[g1-g2], $\text{SR}^{\text{offWZ}}_{\text{low}\not{E}_{\text{T}}}$-nj[g1-g2], $\text{SR}^{\text{offWZ}}_{\text{high}\not{E}_{\text{T}}}$-0j[g1-g2], $\text{SR}^{\text{offWZ}}_{\text{high}\not{E}_{\text{T}}}$-nj[g]

The obtained results for the wino/bino (−) and higgsino scenarios complement the previous compressed result using two-lepton final states as well. These results from the off-shell WZ selection in three-lepton final states make full use of the larger data sample and target a novel phase space in the intermediately compressed $\Delta m(\tilde{\chi}_2^0, \tilde{\chi}_1^0)$ region. The new results extend the exclusion by up to 100 GeV in $\tilde{\chi}_2^0$ mass.

For the wino/bino (+) Wh-mediated model, observed (expected) lower limits for equal-mass $\tilde{\chi}_1^{\pm}/\tilde{\chi}_2^0$ are set at values up to 190 (240) GeV for $\tilde{\chi}_1^0$ masses below 20 GeV, as shown in Fig. 17. The observed exclusion is weaker than the expected exclusion, which is explained by the mild excess found in $\text{SR}^{\text{Wh}}_{\text{DFOS}}$; the limits are, however, compatible within 2σ. The obtained observed (expected) limits show an improvement of up to 40 (80) GeV compared to the previous Run 1, 8 TeV, ATLAS search [17].

10 Recursive Jigsaw Reconstruction selection and results

To follow up on an earlier ATLAS search performed using the Recursive Jigsaw Reconstruction (RJR) technique with the 2015–2016, 36 fb^{-1} dataset [15], the search in this paper includes two signal regions in which the original search observed excesses of three-lepton events. The original search in the two regions is repeated following the same methods,

Table 18 Observed (N_{obs}) yields after the discovery fit and expected (N_{exp}) after the background-only fit, for the inclusive SRs of the on-shell WZ and Wh selections. The third and fourth columns list the 95% CL upper limits on the visible cross section (σ_{vis}^{95}) and on the number of signal events (S_{obs}^{95}). The fifth column (S_{exp}^{95}) shows the 95% CL upper limit on the number of signal events, given the expected number (and $\pm 1\sigma$ excursions of the expectation) of background events. The last two columns indicate the CL_b value, i.e. the confidence level observed for the background-only hypothesis, and the discovery p-value ($p(s = 0)$). If the observed yield is below the expected yield, the p value is capped at 0.5

SR	N_{obs}	N_{exp}	σ_{vis}^{95} [fb]	S_{obs}^{95}	S_{exp}^{95}	CL_b	$p(s = 0)$ (Z)
$\texttt{incSR}^{\texttt{WZ}}\texttt{-1}$	34	38 ± 5	0.10	14	16^{+7}_{-4}	0.32	0.50 (0.00)
$\texttt{incSR}^{\texttt{WZ}}\texttt{-2}$	2	1.2 ± 0.5	0.04	5.0	$4.0^{+1.6}_{-0.7}$	0.76	0.23 (0.73)
$\texttt{incSR}^{\texttt{WZ}}\texttt{-3}$	4	6.5 ± 1.1	0.03	4.8	$6.5^{+2.6}_{-1.8}$	0.19	0.50 (0.00)
$\texttt{incSR}^{\texttt{WZ}}\texttt{-4}$	25	31 ± 6	0.09	12	15^{+6}_{-4}	0.25	0.50 (0.00)
$\texttt{incSR}^{\texttt{WZ}}\texttt{-5}$	1	5.2 ± 1.1	0.03	3.9	$5.8^{+2.2}_{-1.4}$	0.03	0.50 (0.00)
$\texttt{incSR}^{\texttt{WZ}}\texttt{-6}$	23	16.4 ± 1.4	0.12	17.0	$10.3^{+3.9}_{-3.0}$	0.93	0.07 (1.48)
$\texttt{incSR}^{\texttt{Wh}}_{\texttt{SFOS}}\texttt{-7}$	174	150 ± 14	0.41	58	38^{+15}_{-11}	0.90	0.10 (1.27)
$\texttt{incSR}^{\texttt{Wh}}_{\texttt{SFOS}}\texttt{-8}$	53	55 ± 5	0.12	17	18^{+7}_{-5}	0.42	0.50 (0.00)
$\texttt{incSR}^{\texttt{Wh}}_{\texttt{SFOS}}\texttt{-9}$	34	36 ± 4	0.10	14	15^{+6}_{-4}	0.40	0.50 (0.00)
$\texttt{incSR}^{\texttt{Wh}}_{\texttt{SFOS}}\texttt{-10}$	56	55 ± 7	0.16	22	21^{+8}_{-6}	0.55	0.41 (0.22)
$\texttt{incSR}^{\texttt{Wh}}_{\texttt{SFOS}}\texttt{-11}$	41	45 ± 6	0.11	16	18^{+7}_{-5}	0.34	0.50 (0.00)
$\texttt{incSR}^{\texttt{Wh}}_{\texttt{SFOS}}\texttt{-12}$	18	11.5 ± 4.1	0.12	17.0	$10.5^{+4.2}_{-2.7}$	0.92	0.07 (1.48)

Table 19 Observed (N_{obs}) yields after the discovery fit and expected (N_{exp}) after the background-only fit, for the inclusive SRs of the off-shell WZ selection. The third and fourth columns list the 95% CL upper limits on the visible cross section (σ_{vis}^{95}) and on the number of signal events (S_{obs}^{95}). The fifth column (S_{exp}^{95}) shows the 95% CL upper limit on the number of signal events, given the expected number (and $\pm 1\sigma$ excursions of the expectation) of background events. The last two columns indicate the CL_b value, i.e. the confidence level observed for the background-only hypothesis, and the discovery p value ($p(s = 0)$). If the observed yield is below the expected yield, the p-value is capped at 0.5

SR	N_{obs}	N_{exp}	σ_{vis}^{95} [fb]	S_{obs}^{95}	S_{exp}^{95}	CL_b	$p(s = 0)$ (Z)
$\texttt{incSR}^{\texttt{offWZ}}_{\texttt{high}\not{E}_T}\texttt{-nja}$	3	6.0 ± 1.6	0.03	4.6	$6.3^{+2.4}_{-2.0}$	0.16	0.50 (0.00)
$\texttt{incSR}^{\texttt{offWZ}}_{\texttt{high}\not{E}_T}\texttt{-njb}$	2	1.4 ± 0.6	0.03	4.8	$4.0^{+1.6}_{-0.7}$	0.71	0.30 (0.53)
$\texttt{incSR}^{\texttt{offWZ}}_{\texttt{high}\not{E}_T}\texttt{-njc1}$	7	9.5 ± 2.2	0.05	7.0	$8.4^{+2.9}_{-2.2}$	0.28	0.50 (0.00)
$\texttt{incSR}^{\texttt{offWZ}}_{\texttt{high}\not{E}_T}\texttt{-njc2}$	2	2.1 ± 0.8	0.03	4.7	$4.6^{+1.8}_{-1.1}$	0.52	0.50 (0.00)
$\texttt{incSR}^{\texttt{offWZ}}_{\texttt{low}\not{E}_T}\texttt{-b}$	31	36 ± 4	0.09	12	15^{+6}_{-4}	0.25	0.50 (0.00)
$\texttt{incSR}^{\texttt{offWZ}}_{\texttt{high}\not{E}_T}\texttt{-b}$	3	3.0 ± 0.9	0.04	5.4	$5.2^{+2.0}_{-1.3}$	0.53	0.50 (0.00)
$\texttt{incSR}^{\texttt{offWZ}}_{\texttt{low}\not{E}_T}\texttt{-c}$	86	88 ± 7	0.17	23	24^{+9}_{-7}	0.44	0.50 (0.00)
$\texttt{incSR}^{\texttt{offWZ}}_{\texttt{high}\not{E}_T}\texttt{-c}$	9	9.3 ± 1.5	0.06	7.7	$7.7^{+3.4}_{-1.8}$	0.50	0.50 (0.00)
$\texttt{incSR}^{\texttt{offWZ}}\texttt{-d}$	202	184 ± 12	0.37	51	37^{+14}_{-11}	0.84	0.16 (0.99)
$\texttt{incSR}^{\texttt{offWZ}}\texttt{-e1}$	332	308 ± 17	0.49	68	49^{+19}_{-15}	0.84	0.16 (1.00)
$\texttt{incSR}^{\texttt{offWZ}}\texttt{-e2}$	298	269 ± 15	0.50	69	46^{+17}_{-14}	0.90	0.10 (1.29)
$\texttt{incSR}^{\texttt{offWZ}}\texttt{-f1}$	479	457 ± 22	0.56	78	63^{+22}_{-20}	0.77	0.23 (0.75)
$\texttt{incSR}^{\texttt{offWZ}}\texttt{-f2}$	277	272 ± 13	0.33	46	42^{+17}_{-12}	0.60	0.37 (0.34)
$\texttt{incSR}^{\texttt{offWZ}}\texttt{-g1}$	620	593 ± 28	0.69	96	74^{+29}_{-22}	0.77	0.21 (0.79)
$\texttt{incSR}^{\texttt{offWZ}}\texttt{-g2}$	418	408 ± 20	0.46	64	57^{+23}_{-15}	0.65	0.32 (0.47)
$\texttt{incSR}^{\texttt{offWZ}}\texttt{-g3}$	288	285 ± 16	0.35	48	47^{+19}_{-12}	0.55	0.38 (0.30)
$\texttt{incSR}^{\texttt{offWZ}}\texttt{-g4}$	141	136 ± 10	0.25	35	31^{+13}_{-8}	0.64	0.35 (0.39)

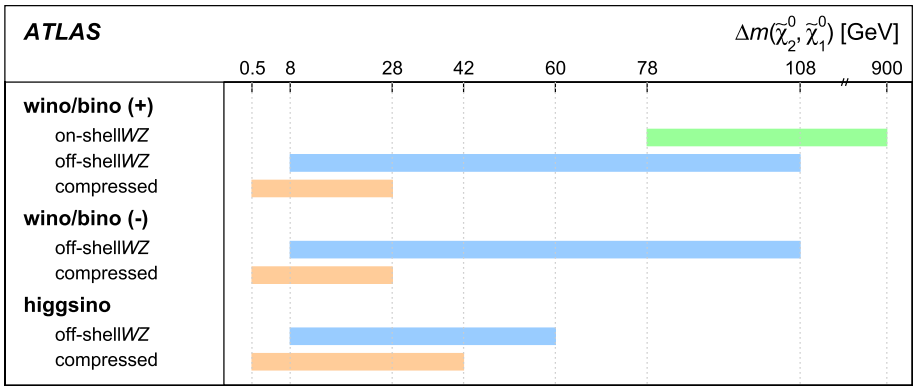

Fig. 15 Illustration of the selections considered for the combined result for each scenario, dependent on Δm

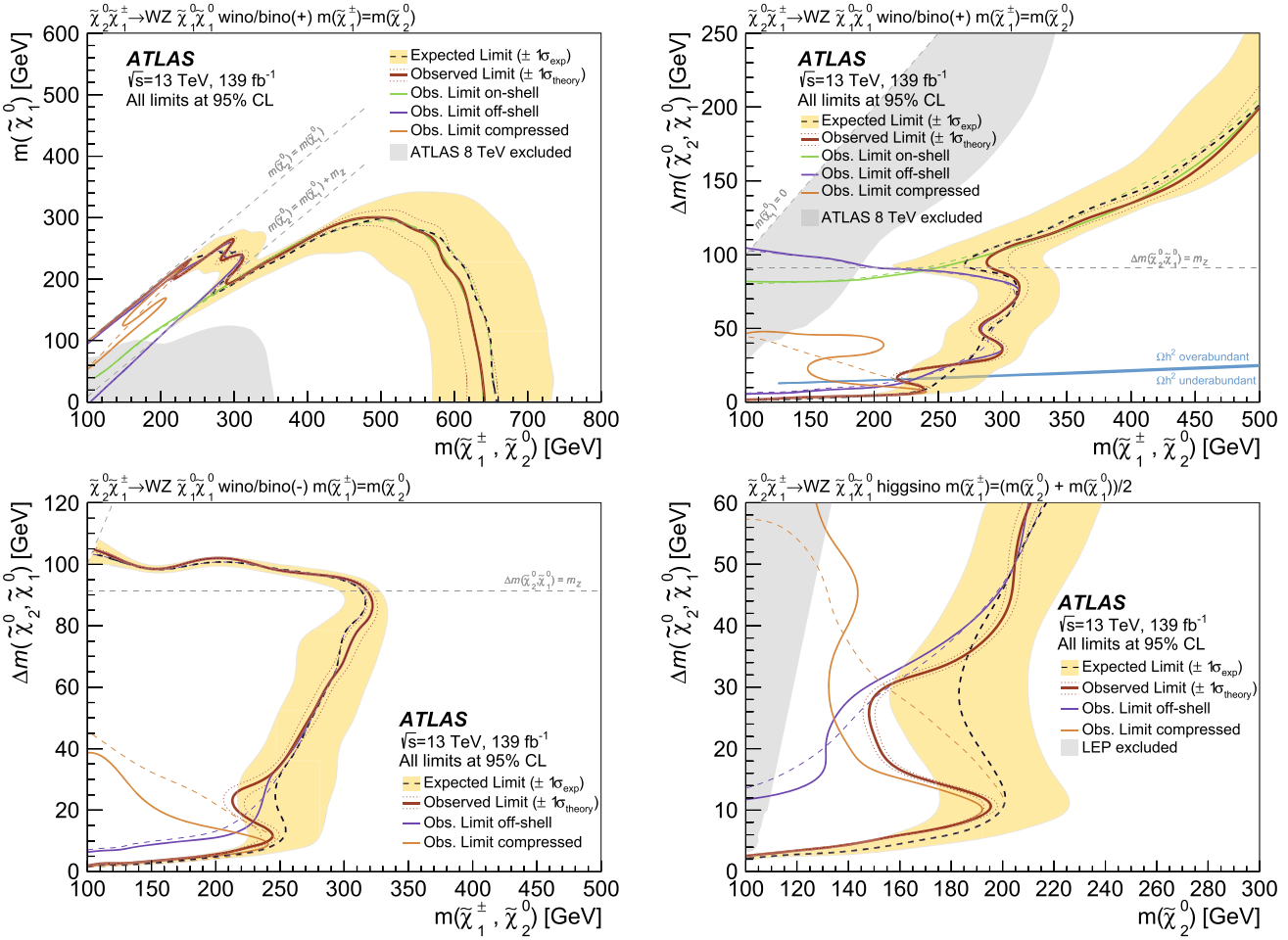

Fig. 16 Exclusion limits obtained for the WZ-mediated models in the (top left and right) wino/bino (+) scenario, (bottom left) the wino/bino (−) scenario, and (bottom right) the higgsino scenario. The expected 95% CL sensitivity (dashed black line) is shown with $\pm 1\sigma_{\text{exp}}$ (yellow band) from experimental systematic uncertainties and statistical uncertainties in the data yields, and the observed limit (red solid line) is shown with $\pm 1\sigma_{\text{theory}}$ (dotted red lines) from signal cross-section uncertainties. The statistical combination of the on-shell WZ, off-shell WZ, and compressed results is shown as the main contour, while the observed (expected) limits for each individual selection are overlaid in green, blue, and orange solid (dashed) lines, respectively. The exclusion is shown projected (top left) onto the $m(\tilde{\chi}_1^\pm,\ \tilde{\chi}_2^0)$ vs $m(\tilde{\chi}_1^0)$ plane or (top right and bottom) onto the $m(\tilde{\chi}_2^0)$ vs Δm plane. The light grey area denotes (top) the constraints obtained by the previous equivalent analysis in ATLAS using the 8 TeV 20.3 fb^{-1} dataset [17], and (bottom right) the LEP lower $\tilde{\chi}_1^\pm$ mass limit [58]. The pale blue line in the top right panel represents the mass-splitting range that yields a dark-matter relic density equal to the observed relic density, $\Omega h^2 = 0.1186 \pm 0.0020$ [176], when the mass parameters of all the decoupled SUSY partners are set to 5 TeV and tan β is chosen such that the lightest Higgs boson's mass is consistent with the observed value of the SM Higgs [45]. The area above (below) the blue line represents a dark-matter relic density larger (smaller) than the observed

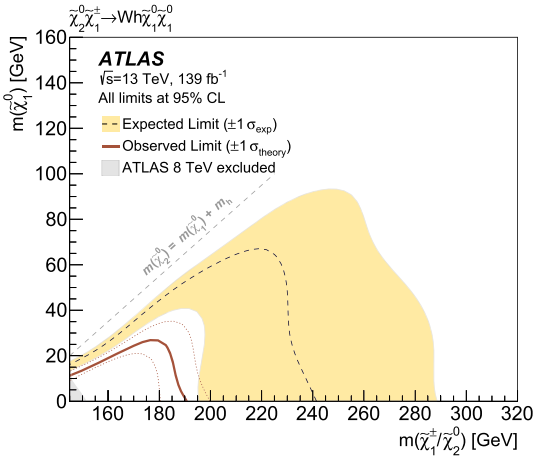

Fig. 17 Exclusion limits obtained for the *Wh*-mediated model in the wino/bino (+) scenario, calculated using the *Wh* SRs and projected onto the $m(\widetilde{\chi}_1^{\pm}, \widetilde{\chi}_2^0)$ vs $m(\widetilde{\chi}_1^0)$ plane. The expected 95% CL sensitivity (dashed black line) is shown with $\pm 1\sigma_{\text{exp}}$ (yellow band) from experimental systematic uncertainties and statistical uncertainties in the data yields, and the observed limit (red solid line) is shown with $\pm 1\sigma_{\text{theory}}$ (dotted red lines) from signal cross-section uncertainties. The light grey area denotes the constraints obtained by the previous equivalent analysis in ATLAS using the 8 TeV 20.3 fb^{-1} dataset [17]

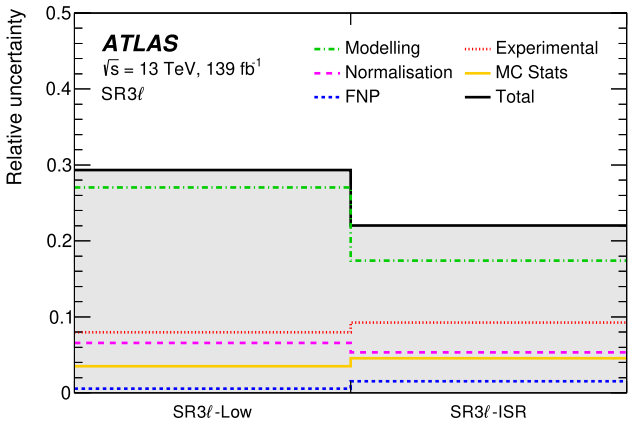

Fig. 19 Breakdown of the total systematic uncertainties in the background prediction for the SRs of the RJR selection

updated to use the full Run 2 dataset. The SR3ℓ-Low region targets low-mass wino/bino (+) $\widetilde{\chi}_1^{\pm}\widetilde{\chi}_2^0$ production, while the SR3ℓ-ISR region targets wino/bino (+) $\widetilde{\chi}_1^{\pm}\widetilde{\chi}_2^0$ production in association with ISR and mass differences Δm near the Z-boson mass. The excesses in SR3ℓ-Low and SR3ℓ-ISR observed in the 36 fb^{-1} result correspond to local significances of 2.1σ and 3.0σ, respectively.

The RJR technique endeavours to resolve the ambiguities inherent in reconstructing original particles for event decays including invisible particles, e.g. SUSY particles. By analysing the event starting from the laboratory frame and boosting back to the parent particle's rest frame, assuming given decay chains, the technique can resolve the $\widetilde{\chi}_1^{\pm}$ and $\widetilde{\chi}_2^0$ particles. For this search, both the standard decay tree applied to a three-lepton final state (representing the decay of pair-produced sparticles into a final state with two invisible objects and three leptons, in the laboratory frame) and the ISR decay tree (representing the decay of an intermediate sparticle into a visible and an invisible component, recoiling from ISR activ-

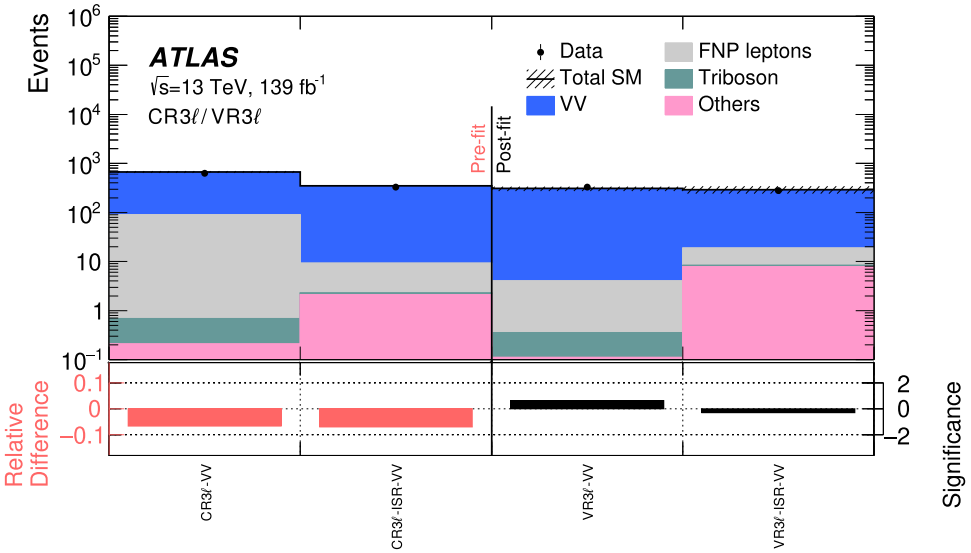

Fig. 18 Comparison of the observed data and expected SM background yields in the CRs and VRs of the RJR selection. The SM prediction is taken from the background-only fit. The 'FNP leptons' category contains backgrounds from $t\bar{t}$, tW, WW and Z + jets processes. The 'Others' category contains backgrounds from Higgs and rare top processes. The hatched band indicates the combined theoretical, experimental, and MC statistical uncertainties. The bottom panel shows the significance of the difference between the observed and expected yields, calculated with the profile likelihood method from Ref. [169], adding a minus sign if the yield is below the prediction

Table 20 Observed and expected yields after the background-only fit in the SRs for the RJR selection. The 'FNP leptons' category contains backgrounds from $t\bar{t}$, tW, WW and Z + jets processes. The 'Others' category contains backgrounds from Higgs and rare top processes. Combined statistical and systematic uncertainties are presented

Region	SR3ℓ-Low	SR3ℓ-ISR
Observed	53	25
Fitted SM	49 ± 14	17 ± 4
Diboson	47 ± 14	16 ± 4
FNP leptons	1.36 ± 0.29	0.83 ± 0.27
Triboson	0.40 ± 0.14	0.14 ± 0.06
Others	0.052 ± 0.029	0.41 ± 0.21

ity, in the centre-of-mass frame) are considered. Using the reconstructed leptons, jets, and missing transverse momentum as inputs, the algorithm assigns each particle to a parent sparticle. ISR jets are selected by minimising the invariant mass of the system formed by the candidate jets and the sparticle system, in the centre-of-mass frame. The algorithm then determines the smallest Lorentz-invariant configuration of the particles' four-momenta guaranteeing a non-negative mass parameter for the invisible particles. Finally, object or frame momenta and derived variables can be considered in each of the different frames of each decay tree.

The search in the RJR selection regions follows a similar strategy for background estimation, systematic uncertainty treatment, and statistical interpretation to that outlined for the on-shell WZ, off-shell WZ, and Wh selections in Sect. 6. For the search in SR3ℓ-Low (SR3ℓ-ISR), the SM diboson background is taken from MC simulation samples and normalised in a dedicated control region CR3ℓ-VV (CR3ℓ-ISR-VV) and validated in a validation region VR3ℓ-VV (VR3ℓ-ISR-VV). The selection criteria for each of the regions follow the original search [15], except for an additional jet-veto ($n_{\text{jets}} = 0$) in CR3ℓ-VV and VR3ℓ-VV which guarantees the orthogonality between the low-mass and ISR regions. The FNP lepton background component, including $t\bar{t}$, tW, WW and Z + jets SM background contributions, is estimated in a data-driven way using the matrix method [177]. The method derives the number of events with one or two FNP leptons by relating the yields for tighter (signal tagged) and looser (baseline tagged) lepton identification criteria. The result is a function of the real-lepton identification efficiencies and the FNP lepton misidentification probabilities. The remaining SM backgrounds, including multiboson and Higgs boson production, and top-pair production in association with a boson, are estimated from MC simulation in all analysis regions. Beyond the treatment of experimental and theoretical systematical uncertainties following the general strategy in Sect. 6.3, uncertainties are assigned to the matrix-method FNP lepton background estimation, accounting for limited numbers of events in the measurement region, potentially different compositions (heavy flavour, light flavour, or conversions) between SRs and CRs, and the uncertainty from the subtraction of prompt-lepton contributions using MC simulation samples.

Performing the background-only fit, diboson normalisation factors of 0.92±0.07 (CR3ℓ-VV) and 0.92±0.05 (CR3ℓ-ISR-VV) are determined. Observed and expected yields for all CRs and VRs are summarised in Fig. 18 and a summary of the considered systematic uncertainties is presented in Fig. 19, grouped as discussed in Sect. 6.3.

The observed data in SR3ℓ-Low and SR3ℓ-ISR are compared with the background expectation obtained by the background-only fit. The results are reported in Table 20 and post-fit distributions of key observables for the SRs are shown in Fig. 20. For the low-mass RJR selection, Fig. 20 shows the leading lepton's transverse momentum, $p_{\text{T}}^{\ell_1}$, and the scalar momentum sum, $H_{3,1}^{\text{PP}}$, of the three visible particles (the leptons) and the invisible particles (the LSPs and the neutrino), in the pair-produced parent sparticle–sparticle (PP) frame and assuming the standard decay tree. For the ISR RJR selection, Fig. 20 shows the vector sum of the transverse momenta of all objects, p_{T}^{CM}, and the fraction of the total momentum of the sparticle system carried by the invisible system, R_{ISR}, in the centre-of-mass (CM) frame and assuming the ISR decay tree. Good agreement with the background-only hypothesis is observed in both SRs. The deviations from the SM expectation as found in the 36 fb^{-1} result are reduced and no longer significant when including the additional 103 fb^{-1} of data from the 2017–2018 datasets.

Model-independent results for SR3ℓ-Low and SR3ℓ-ISR are shown in Table 21. The 95% CL upper limits on the generic BSM cross section are calculated by performing a discovery fit for each target SR and its associated CR, using pseudo-experiments. The table lists the upper limits on the observed (S_{obs}^{95}) and expected (S_{exp}^{95}) number of BSM events in the inclusive SRs, and the visible cross section (σ_{vis}^{95}) reflecting the product of the production cross section, the acceptance, and the selection efficiency for a BSM process; the p-value and significance (Z) for the background-only hypothesis are also presented.

11 Conclusion

Results of a search for chargino–neutralino pair production decaying via WZ, W^*Z^* or Wh into three-lepton final states are presented. A dataset of $\sqrt{s} = 13$ TeV proton–proton collisions corresponding to an integrated luminosity of 139 fb^{-1}, collected by the ATLAS experiment at the CERN LHC, is used. Events with three light-flavour charged leptons and missing transverse momentum are preselected,

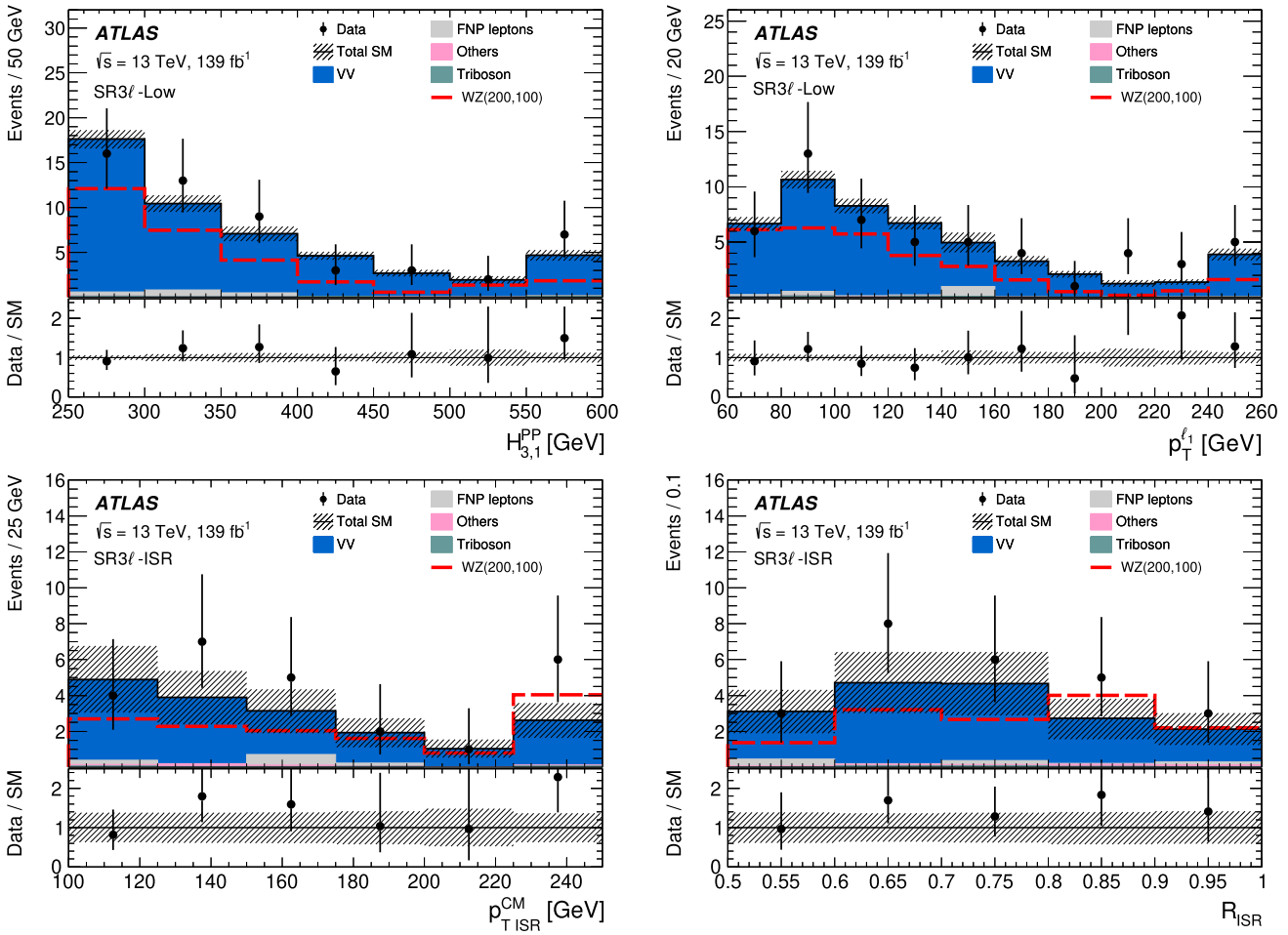

Fig. 20 Example of kinematic distributions after the background-only fit, showing the data and the post-fit expected background, in regions of the RJR selection. The figure shows the (top left) $H_{3,1}^{\mathrm{PP}}$ and (top right) $p_{\mathrm{T}}^{\ell_1}$ distributions in SR3ℓ-Low, and the (bottom left) $p_{\mathrm{T,ISR}}^{\mathrm{CM}}$ and (bottom right) R_{ISR} distributions in SR3ℓ-ISR. The last bin includes overflow. The 'FNP leptons' category contains backgrounds from $t\bar{t}$, tW, WW and Z + jets processes. The 'Others' category contains backgrounds from Higgs and rare top processes. Distributions for wino/bino (+) $\tilde{\chi}_1^{\pm}\tilde{\chi}_2^0 \rightarrow WZ$ signals are overlaid, with mass values given as $(m(\tilde{\chi}_1^{\pm}), m(\tilde{\chi}_1^0))$ GeV. The bottom panel shows the ratio of the observed data to the predicted yields. The hatched bands indicate the combined theoretical, experimental, and MC statistical uncertainties

and three selections are developed with a signal region strategy optimised for chargino–neutralino signals decaying via WZ, W^*Z^* and Wh, respectively. A fourth selection targeting the chargino–neutralino signals decaying via WZ using the Recursive Jigsaw Reconstruction technique is also studied, to follow up on the excesses observed in the previous ATLAS result using the same method and event selection. In all the selections the data are found to be consistent with predictions of the Standard Model. The results are interpreted for simplified models with wino or higgsino production. A statistical combination is performed to include the result of an ATLAS search probing the final state with two soft leptons using the same dataset.

Assuming a simplified model with wino production decaying to a bino LSP, exclusion limits at 95% confidence level are placed on the minimum $\tilde{\chi}_1^{\pm}/\tilde{\chi}_2^0$ mass, extending the reach of previous searches [14–18,21]. Limits are set at 640 GeV for the WZ-mediated model signals in the limit of massless $\tilde{\chi}_1^0$,

Table 21 Results of the discovery fit for the SRs of the RJR selection, calculated using pseudo-experiments. The first and second column list the 95% CL upper limits on the visible cross section ($\sigma_{\mathrm{vis}}^{95}$) and on the number of signal events (S_{obs}^{95}). The third column (S_{exp}^{95}) shows the 95% CL upper limit on the number of signal events, given the expected number (and $\pm 1\sigma$ excursions of the expectation) of background events. The last two columns indicate the $\mathrm{CL_b}$ value, i.e. the confidence level observed for the background-only hypothesis, and the discovery p value ($p(s = 0)$). If the observed yield is below the expected yield, the p-value is capped at 0.5

SR	$\sigma_{\mathrm{vis}}^{95}$ [fb]	S_{obs}^{95}	S_{exp}^{95}	$\mathrm{CL_b}$	$p(s = 0)$ (Z)
SR3ℓ-Low	0.24	33	30^{+10}_{-8}	0.61	0.39 (0.28)
SR3ℓ-ISR	0.14	19	12^{+5}_{-4}	0.89	0.09 (1.32)

improving by about 140 GeV; and at 300 GeV for mass-splittings between $\widetilde{\chi}_1^{\pm}/\widetilde{\chi}_2^0$ and $\widetilde{\chi}_1^0$ close to m_Z, improving by about 100 GeV. In the case of a mass splitting of 5–90 GeV, $\widetilde{\chi}_1^{\pm}/\widetilde{\chi}_2^0$ masses up to 200–300 GeV for the WZ-mediated model are excluded. The limit extends down to a smallest mass splitting of 2 GeV for a $\widetilde{\chi}_1^{\pm}$ mass of 100 GeV. The dependency on a model parameter – the sign of the $m_{\text{eig}}(\tilde{\chi}_2^0) \times m_{\text{eig}}(\tilde{\chi}_1^0)$ product – is also tested, and comparable limits are found for the two scenarios. For the Wh-mediated model signals, the limit on the minimum $\widetilde{\chi}_1^{\pm}/\widetilde{\chi}_2^0$ mass is set at 190 GeV, for $\widetilde{\chi}_1^0$ masses below 20 GeV.

Limits are also set for simplified models with a higgsino LSP triplet, for the first time including results from three-lepton final states, which increases sensitivity to scenarios with moderate mass splittings. Combined with the two-lepton analysis targeting compressed mass spectra, the exclusion limits at 95% confidence level are placed on the minimum $\widetilde{\chi}_2^0$ mass up to 210 GeV for WZ-mediated model signals with a mass splitting of 2–60 GeV. In these models, searches in the three-lepton final state enhance the sensitivity in the experimentally challenging region with mass splitting greater than 30 GeV.

Acknowledgements We thank CERN for the very successful operation of the LHC, as well as the support staff from our institutions without whom ATLAS could not be operated efficiently. We acknowledge the support of ANPCyT, Argentina; YerPhI, Armenia; ARC, Australia; BMWFW and FWF, Austria; ANAS, Azerbaijan; SSTC, Belarus; CNPq and FAPESP, Brazil; NSERC, NRC and CFI, Canada; CERN; ANID, Chile; CAS, MOST and NSFC, China; Minciencias, Colombia; MSMT CR, MPO CR and VSC CR, Czech Republic; DNRF and DNSRC, Denmark; IN2P3-CNRS and CEA-DRF/IRFU, France; SRNSFG, Georgia; BMBF, HGF and MPG, Germany; GSRI, Greece; RGC and Hong Kong SAR, China; ISF and Benoziyo Center, Israel; INFN, Italy; MEXT and JSPS, Japan; CNRST, Morocco; NWO, Netherlands; RCN, Norway; MNiSW and NCN, Poland; FCT, Portugal; MNE/IFA, Romania; JINR; MES of Russia and NRC KI, Russian Federation; MESTD, Serbia; MSSR, Slovakia; ARRS and MIZŠ, Slovenia; DSI/NRF, South Africa; MICINN, Spain; SRC and Wallenberg Foundation, Sweden; SERI, SNSF and Cantons of Bern and Geneva, Switzerland; MOST, Taiwan; TAEK, Turkey; STFC, United Kingdom; DOE and NSF, United States of America. In addition, individual groups and members have received support from BCKDF, CANARIE, Compute Canada and CRC, Canada; COST, ERC, ERDF, Horizon 2020 and Marie Skłodowska-Curie Actions, European Union; Investissements d'Avenir Labex, Investissements d'Avenir Idex and ANR, France; DFG and AvH Foundation, Germany; Herakleitos, Thales and Aristeia programmes co-financed by EU-ESF and the Greek NSRF, Greece; BSF-NSF and GIF, Israel; Norwegian Financial Mechanism 2014-2021, Norway; La Caixa Banking Foundation, CERCA Programme Generalitat de Catalunya and PROMETEO and GenT Programmes Generalitat Valenciana, Spain; Göran Gustafssons Stiftelse, Sweden; The Royal Society and Leverhulme Trust, United Kingdom. The crucial computing support from all WLCG partners is acknowledged gratefully, in particular from CERN, the ATLAS Tier-1 facilities at TRIUMF (Canada), NDGF (Denmark, Norway, Sweden), CC-IN2P3 (France), KIT/GridKA (Germany), INFN-CNAF (Italy), NL-T1 (Netherlands), PIC (Spain), ASGC (Taiwan), RAL (UK) and BNL (USA), the Tier-2 facilities worldwide and large non-WLCG resource providers. Major contributors of computing resources are listed in Ref. [178].

Data Availability Statement This manuscript has no associated data or the data will not be deposited. [Authors' comment: All ATLAS scientific output is published in journals, and preliminary results are made available in Conference Notes. All are openly available, without restriction on use by external parties beyond copyright law and the standard conditions agreed by CERN. Data associated with journal publications are also made available: tables and data from plots (e.g. cross section values, likelihood profiles, selection efficiencies, cross section limits, ...) are stored in appropriate repositories such as HEPDATA (http://hepdata.cedar.ac.uk/). ATLAS also strives to make additional material related to the paper available that allows a reinterpretation of the data in the context of new theoretical models. For example, an extended encapsulation of the analysis is often provided for measurements in the framework of RIVET (http://rivet.hepforge.org/).]

Open Access This article is licensed under a Creative Commons Attribution 4.0 International License, which permits use, sharing, adaptation, distribution and reproduction in any medium or format, as long as you give appropriate credit to the original author(s) and the source, provide a link to the Creative Commons licence, and indicate if changes were made. The images or other third party material in this article are included in the article's Creative Commons licence, unless indicated otherwise in a credit line to the material. If material is not included in the article's Creative Commons licence and your intended use is not permitted by statutory regulation or exceeds the permitted use, you will need to obtain permission directly from the copyright holder. To view a copy of this licence, visit http://creativecommons.org/licenses/by/4.0/.
Funded by SCOAP[3].

References

1. Y. Golfand, E. Likhtman, Extension of the algebra of Poincare group generators and violation of P invariance. JETP Lett. **13**, 323 (1971). [PismaZh. Eksp. Teor. Fiz. **13** , 452 (1971)]
2. D. Volkov, V. Akulov, Is the neutrino a goldstone particle? Phys. Lett. B **46**, 109 (1973)
3. J. Wess, B. Zumino, Supergauge transformations in four dimensions. Nucl. Phys. B **70**, 39 (1974)
4. J. Wess, B. Zumino, Supergauge invariant extension of quantum electrodynamics. Nucl. Phys. B **78**, 1 (1974)
5. S. Ferrara, B. Zumino, Supergauge invariant Yang-Mills theories. Nucl. Phys. B **79**, 413 (1974)
6. A. Salam, J. Strathdee, Super-symmetry and non-Abelian gauges. Phys. Lett. B **51**, 353 (1974)
7. L. Girardello, M.T. Grisaru, Soft breaking of supersymmetry. Nucl. Phys. B **194**, 65 (1982)
8. N. Sakai, Naturalness in supersymmetric GUTS. Z. Phys. C **11**, 153 (1981)
9. S. Dimopoulos, S. Raby, F. Wilczek, Supersymmetry and the scale of unification. Phys. Rev. D **24**, 1681 (1981)
10. L.E. Ibáñez, G.G. Ross, Low-energy predictions in supersymmetric grand unified theories. Phys. Lett. B **105**, 439 (1981)
11. S. Dimopoulos, H. Georgi, Softly broken supersymmetry and SU(5). Nucl. Phys. B **193**, 150 (1981)
12. G.R. Farrar, P. Fayet, Phenomenology of the production, decay, and detection of new hadronic states associated with supersymmetry. Phys. Lett. B **76**, 575 (1978)
13. ATLAS Collaboration, Luminosity determination in pp collisions at $\sqrt{s} = 13$ TeV using the ATLAS detector at the LHC. ATLAS-CONF-2019-021 (2019). https://cds.cern.cn/record/2677054
14. ATLAS Collaboration, Search for electroweak production of supersymmetric particles in final states with two or three leptons

at $\sqrt{s} = 13$ TeV with the ATLAS detector. Eur. Phys. J. C **78**, 995, (2018). arXiv:1803.02762 [hep-ex]
15. ATLAS Collaboration, Search for chargino-neutralino production using recursive jigsaw reconstruction in final states with two or three charged leptons in proton-proton collisions at $\sqrt{s} = 13$ TeV with the ATLAS detector, Phys. Rev. D **98**, 092012 (2018). arXiv:1806.02293 [hep-ex]
16. ATLAS Collaboration, Search for chargino-neutralino production with mass splittings near the electroweak scale in three-lepton final states in $\sqrt{s} = 13$ TeV pp collisions with the ATLAS detector. Phys. Rev. D **101**, 072001 (2020). arXiv:1912.08479 [hep-ex]
17. ATLAS Collaboration, Search for direct production of charginos and neutralinos in events with three leptons and missing transverse momentum in $\sqrt{s} = 8$ TeV pp collisions with the ATLAS detector. JHEP **04**, 169 (2014). arXiv:1402.7029 [hep-ex]
18. ATLAS Collaboration, Searches for electroweak production of supersymmetric particles with compressed mass spectra in $\sqrt{s} = 13$ TeV pp collisions with the ATLAS detector. Phys. Rev. D **101**052005 (2020). arXiv: 1911.12606 [hep-ex]
19. ATLAS Collaboration, Search for chargino and neutralino production in final states with a Higgs boson and missing transverse momentum $\sqrt{s} = 13$ TeV with the ATLAS detector. Phys. Rev. D **100** 012006 (2019). arXiv:1812.09432 [hep-ex]
20. ATLAS Collaboration, Search for direct production of electroweakinos in final states with missing transverse momentum and a Higgs boson decaying into photons in pp collisions at $\sqrt{s} = 13$ TeV with the ATLAS detector. JHEP **10**, 005 (2020). arXiv:2004.10894 [hep-ex]
21. CMS Collaboration, Combined search for electroweak production of charginos and neutralinos in proton-proton collisions at $\sqrt{s} = 13$ TeV. JHEP **03**, 160 (2018). arXiv:1801.03957 [hep-ex]
22. CMS Collaboration, Search for new phenomena in final states with two opposite-charge, same-flavor leptons, jets, and missing transverse momentum in pp collisions at $\sqrt{s} = 13$ TeV. JHEP **03**, 076 (2018). arXiv:1709.08908 [hep-ex]
23. CMS Collaboration, Search for supersymmetry with a compressed mass spectrum in the vector boson fusion topology with 1-lepton and 0-lepton final states in proton-proton collisions at $\sqrt{s} = 13$ TeV. JHEP **08**, 150 (2019). arXiv:1905.13059 [hep-ex]
24. CMS Collaboration, Search for new physics in events with two soft oppositely charged leptons and missing transverse momentum in proton-proton collisions at $\sqrt{s} = 13$ TeV. Phys. Lett. B **782**, 440 (2018). arXiv:1801.01846 [hep-ex]
25. CMS Collaboration, Search for electroweak production of charginos and neutralinos in multilepton final states in proton-proton collisions at $\sqrt{s} = 13$ TeV. JHEP **03**, 166 (2018). arXiv:1709.05406 [hep-ex]
26. CMS Collaboration, Search for electroweak production of charginos and neutralinos in WH events in proton-proton collisions at $\sqrt{s} = 13$ TeV. JHEP **11**, 029 (2017). arXiv:1706.09933 [hep-ex]
27. CMS Collaboration, Search for supersymmetry with Higgs boson to diphoton decays using the razor variables at $\sqrt{s} = 13$ TeV. Phys. Lett. B **779**, 166 (2018). arXiv:1709.00384 [hep-ex]
28. ATLAS Collaboration, Evidence for the associated production of the Higgs boson and a top quark pair with the ATLAS detector. Phys. Rev. D **97**, 072003 (2018). arXiv:1712.08891 [hep-ex]
29. P. Jackson, C. Rogan, M. Santoni, Sparticles in motion: Analyzing compressed SUSY scenarios with a new method of event reconstruction. Phys. Rev. D **95**, 035031 (2017). arXiv: 1607.08307 [hep-ph]
30. P. Jackson, C. Rogan, Recursive jigsaw reconstruction: HEP event analysis in the presence of kinematic and combinatoric ambiguities. Phys. Rev. D **96**, 112007 (2017). arXiv:1705.10733 [hep-ph]
31. P. Fayet, Supersymmetry and weak, electromagnetic and strong interactions. Phys. Lett. B **64**, 159 (1976)
32. P. Fayet, Spontaneously broken supersymmetric theories of weak, electromagnetic and strong interactions. Phys. Lett. B **69**, 489 (1977)
33. H. Goldberg, Constraint on the photino mass from cosmology. Phys. Rev. Lett. **50**, 1419 (2009). Erratum: Phys. Rev. Lett. **103**, 099905 (1983)
34. J. Ellis, J. Hagelin, D.V. Nanopoulos, K.A. Olive, M. Srednicki, Supersymmetric relics from the big bang. Nucl. Phys. B **238**, 453 (1984)
35. A.H. Chamseddine, R.L. Arnowitt, P. Nath, Locally supersymmetric grand unification. Phys. Rev. Lett. **49**, 970 (1982)
36. R. Barbieri, S. Ferrara, C.A. Savoy, Gauge models with spontaneously broken local supersymmetry. Phys. Lett. B **119**, 343 (1982)
37. G.L. Kane, C.F. Kolda, L. Roszkowski, J.D. Wells, Study of constrained minimal supersymmetry. Phys. Rev. D **49**, 6173 (1994). arXiv:hep-ph/9312272
38. T. Albahri et al., Measurement of the anomalous precession frequency of the muon in the Fermilab Muon g-2 Experiment. Phys. Rev. D **103**, 072002 (2021). arXiv:2104.03247 [hep-ex]
39. T. Aoyama et al., The anomalous magnetic moment of the muon in the Standard Model. Phys. Rep. **887**, 1 (2020). arXiv:2006.04822 [hep-ph]
40. T. Moroi, Muon anomalous magnetic dipole moment in the minimal supersymmetric standard model. Phys. Rev. D **53**, 6565 (1996). arXiv:hep-ph/9512396 Erratum: Phys. Rev. D **56**, 4424 (1997)
41. J.L. Feng, T. Moroi, Supernatural supersymmetry: phenomenological implications of anomaly-mediated supersymmetry breaking. Phys. Rev. D **61**, 095004 (2000). arXiv:hep-ph/9907319
42. M. Endo, K. Hamaguchi, S. Iwamoto, T. Kitahara, Muon g-2 vs LHC Run 2 in supersymmetric models. JHEP **04**, 165 (2020). arXiv:2001.11025 [hep-ph]
43. K. Griest, D. Seckel, Three exceptions in the calculation of relic abundances. Phys. Rev. D **43**, 3191 (1991)
44. J. Edsjo, P. Gondolo, Neutralino relic density including coannihilations. Phys. Rev. D **56**, 1879 (1997). arXiv:hep-ph/9704361
45. G.H. Duan, K.-I. Hikasa, J. Ren, L. Wu, J.M. Yang, Probing bino-wino coannihilation dark matter below the neutrino floor at the LHC. Phys. Rev. D **98**, 015010 (2018). arXiv:1804.052 38 [hep-ph]
46. S. Profumo, T. Stefaniak, L. Stephenson Haskins, Not-so-well-tempered neutralino. Phys. Rev. D **96**, 055018 (2017). arXiv:1706.08537 [hep-ph]
47. R. Barbieri, G. Giudice, Upper bounds on supersymmetric particle masses. Nucl. Phys. B **306**, 63 (1988)
48. B. de Carlos, J. Casas, One-loop analysis of the electroweak breaking in supersymmetric models and the fine-tuning problem. Phys. Lett. B **309**, 320 (1993). arXiv:hep-ph/9303291
49. R. Barbieri, D. Pappadopulo, S-particles at their naturalness limits. JHEP **10**, 061 (2009). arXiv:0906.4546 [hep-ph]
50. H. Baer, V. Barger, P. Huang, Hidden SUSY at the LHC: the light higgsino-world scenario and the role of a lepton collider. JHEP **11**, 031 (2011). arXiv:1107.5581 [hep-ph]
51. M. Papucci, J.T. Ruderman, A. Weiler, Natural SUSY endures. JHEP **09**, 035 (2012). arXiv:1110.6926 [hep-ph]
52. H. Baer, V. Barger, P. Huang, A. Mustafayev, X. Tata, Radiative natural supersymmetry with a 125 GeV Higgs boson. Phys. Rev. Lett. **109**, 161802 (2012). arXiv:1207.3343 [hep-ph]
53. J. Alwall, M.-P. Le, M. Lisanti, J.G. Wacker, Searching for directly decaying gluinos at the Tevatron. Phys. Lett. B **666**, 34 (2008). arXiv:0803.0019 [hep-ph]
54. J. Alwall, P. Schuster, N. Toro, Simplified models for a first characterization of new physics at the LHC. Phys. Rev. D **79**, 075020 (2009). arXiv:0810.3921 [hep-ph]

55. D. Alves et al., Simplified models for LHC new physics searches. J. Phys. G **39**, 105005 (2012). arXiv:1105.2838 [hep-ph]
56. B. Fuks, M. Klasen, S. Schmiemann, M. Sunder, Realistic simplified gaugino-higgsino models in the MSSM. Eur. Phys. J. C **78**, 209 (2018). arXiv:1710.09941 [hep-ph]
57. J.F. Gunion, H.E. Haber, Higgs bosons in supersymmetric models (I). Nucl. Phys. B **272**, 76 (1986). Erratum: Nucl. Phys. B **402**, 567 (1993)
58. ALEPH, DELPHI, L3, OPAL Experiments, Combined LEP Chargino Results, up to 208 GeV for low DM, LEPSUSYWG/02-04.1 (2002). http://lepsusy.web.cern.ch/lepsusy/www/inoslowdmsummer02/charginolowdm_pub.html
59. ALEPH Collaboration, Search for scalar leptons in e^+e^- collisions at center-of-mass energies up to 209 GeV. Phys. Lett. B **526**, 206 (2002). arXiv:hep-ex/0112011
60. ALEPH Collaboration, Search for charginos nearly mass degenerate with the lightest neutralino in e^+e^- collisions at center-of-mass energies up to 209 GeV. Phys. Lett. B **533**, 223 (2002). arXiv:hep-ex/0203020
61. ALEPH Collaboration, Absolute lower limits on the masses of selectrons and sneutrinos in the MSSM. Phys. Lett. B, **544**, 73 (2002). arXiv:hep-ex/0207056
62. ALEPH Collaboration, Absolute mass lower limit for the lightest neutralino of the MSSM from e^+e^- data at $\sqrt{s}$ up to 209 GeV. Phys. Lett. B **583**, 247 (2004)
63. DELPHI Collaboration, Searches for supersymmetric particles in e^+e^- collisions up to 208 GeV and interpretation of the results within the MSSM. Eur. Phys. J. C **31**, 421 (2003). arXiv:hep-ex/0311019
64. L3 Collaboration, Search for charginos with a small mass difference with the lightest supersymmetric particle at $\sqrt{s} = 189$ GeV. Phys. Lett. B **482**, 31 (2000). arXiv:hep-ex/0002043
65. L3 Collaboration, Search for scalar leptons and scalar quarks at LEP. Phys. Lett. B **580**, 37 (2004). arXiv:hep-ex/0310007
66. OPAL Collaboration, Search for anomalous production of dilepton events with missing transverse momentum in e^+e^- collisions at $\sqrt{s} = 183 - 209$ GeV. Eur. Phys. J. C **32**, 453 (2004). arXiv:hep-ex/0309014
67. O.P.A.L. Collaboration, Search for nearly mass-degenerate charginos and neutralinos at LEP. Eur. Phys. J. C **29**, 479 (2003). arXiv:hep-ex/0210043
68. ATLAS Collaboration, The ATLAS experiment at the CERN large hadron collider. JINST **3**, S08003 (2008)
69. ATLAS Collaboration, ATLAS Insertable B-Layer Technical Design Report, ATLAS-TDR-19; CERN-LHCC-2010-013 (2010). https://cds.cern.ch/record/1291633. Addendum: ATLAS-TDR-19-ADD-1; CERN-LHCC-2012-009 (2012). https://cds.cern.ch/record/1451888
70. B. Abbott et al., Production and integration of the ATLAS Insertable B-Layer. JINST **13**, T05008 (2018). arXiv:1803.00844 [physics.ins-det]
71. ATLAS Collaboration, Performance of the ATLAS trigger system in 2015. Eur. Phys. J. C **77**, 317 (2017). arXiv:1611.09661 [hep-ex]
72. ATLAS Collaboration, ATLAS data quality operations and performance for 2015–2018 data-taking. JINST **15**, P04003 (2020). arXiv:1911.04632 [physics.ins-det]
73. G. Avoni et al., The new LUCID-2 detector for luminosity measurement and monitoring in ATLAS. JINST **13**, P07017 (2018)
74. ATLAS Collaboration, The ATLAS simulation infrastructure. Eur. Phys. J. C **70**, 823 (2010). arXiv:1005.4568 [physics.ins-det]
75. GEANT4 Collaboration, S. Agostinelli et al., GEANT4—a simulation toolkit. Nucl. Instrum. Methods A **506**, 250 (2003)
76. ATLAS Collaboration, The simulation principle and performance of the ATLAS fast calorimeter simulation FastCaloSim, ATL-PHYS-PUB-2010-013 (2010). https://cds.cern.ch/record/1300517
77. J. Alwall et al., The automated computation of tree-level and next-to-leading order differential cross sections, and their matching to parton shower simulations. JHEP **07**, 079 (2014). arXiv:1405.0301 [hep-ph]
78. R.D. Ball et al., Parton distributions with LHC data. Nucl. Phys. B **867**, 244 (2013). arXiv:1207.1303 [hep-ph]
79. W. Beenakker et al., Production of charginos, neutralinos, and sleptons at hadron colliders. Phys. Rev. Lett. **83**, 3780 (1999). arXiv:hep-ph/9906298. Erratum: Phys. Rev. Lett. **100**, 029901 (2008)
80. J. Debove, B. Fuks, M. Klasen, Threshold resummation for gaugino pair production at hadron colliders. Nucl. Phys. B **842**, 51 (2011). arXiv:1005.2909 [hep-ph]
81. B. Fuks, M. Klasen, D.R. Lamprea, M. Rothering, Gaugino production in proton-proton collisions at a center-of-mass energy of 8 TeV. JHEP **10**, 081 (2012). arXiv:1207.2159 [hep-ph]
82. B. Fuks, M. Klasen, D.R. Lamprea, M. Rothering, Precision predictions for electroweak superpartner production at hadron colliders with RESUMMINO. Eur. Phys. J. C **73**, 2480 (2013). arXiv:1304.0790 [hep-ph]
83. J. Fiaschi, M. Klasen, Neutralino-chargino pair production at NLO+NLL with resummation-improved parton density functions for LHC Run II. Phys. Rev. D **98**, 055014 (2018). arXiv:1805.11322 [hep-ph]
84. C. Borschensky et al., Squark and gluino production cross sections in pp collisions at $\sqrt{s} =$ 13,14,33 and 100 TeV. Eur. Phys. J. C **74**, 3174 (2014). arXiv:1407.5066 [hep-ph]
85. ATLAS Collaboration, Multi-Boson Simulation for 13 TeV ATLAS Analyses, ATL-PHYS-PUB-2017-005 (2017). https://cds.cern.ch/record/2261933
86. E. Bothmann et al., Event generation with Sherpa 2.2. SciPost Phys. **7**, 034 (2019). arXiv:1905.09127 [hep-ph]
87. R.D. Ball et al., Parton distributions for the LHC run II. JHEP **04**, 040 (2015). arXiv:1410.8849 [hep-ph]
88. ATLAS Collaboration, ATLAS simulation of boson plus jets processes in Run 2, ATL-PHYS-PUB-2017-006 (2017). https://cds.cern.ch/record/2261937
89. C. Anastasiou, L.J. Dixon, K. Melnikov, F. Petriello, High precision QCD at hadron colliders: electroweak gauge boson rapidity distributions at next-to-next-to leading order. Phys. Rev. D **69**, 094008 (2004). arXiv:hep-ph/0312266
90. S. Frixione, P. Nason, G. Ridolfi, A positive-weight next-to-leading-order Monte Carlo for heavy flavour hadroproduction. JHEP **09**, 126 (2007). arXiv:0707.3088 [hep-ph]
91. P. Nason, A new method for combining NLO QCD with shower Monte Carlo algorithms. JHEP **11**, 040 (2004). arXiv:hep-ph/0409146
92. S. Frixione, P. Nason, C. Oleari, Matching NLO QCD computations with parton shower simulations: the POWHEG method. JHEP **11**, 070 (2007). arXiv:0709.2092 [hep-ph]
93. S. Alioli, P. Nason, C. Oleari, E. Re, A general framework for implementing NLO calculations in shower Monte Carlo programs: the POWHEG BOX. JHEP **06**, 043 (2010). arXiv:1002.2581 [hep-ph]
94. M. Beneke, P. Falgari, S. Klein, C. Schwinn, Hadronic top-quark pair production with NNLL threshold resummation. Nucl. Phys. B **855**, 695 (2012). arXiv:1109.1536 [hep-ph]
95. M. Cacciari, M. Czakon, M. Mangano, A. Mitov, P. Nason, Top-pair production at hadron colliders with next-to-next-to-leading logarithmic soft-gluon resummation. Phys. Lett. B **710**, 612 (2012). arXiv:1111.5869 [hep-ph]
96. P. Bärnreuther, M. Czakon, A. Mitov, Percent-level-precision physics at the tevatron: next-to-next-to-leading order QCD cor-

rections to $q\bar{q} - t\bar{t} + X$. Phys. Rev. Lett. **109**, 132001 (2012). arXiv:1204.5201 [hep-ph]
97. M. Czakon, A. Mitov, NNLO corrections to top-pair production at hadron colliders: the all-fermionic scattering channels. JHEP **12**, 054 (2012). arXiv:1207.02 36 [hep-ph]
98. M. Czakon, A. Mitov, NNLO corrections to top pair production at hadron colliders: the quark-gluon reaction. JHEP **01**, 080 (2013). arXiv:1210.6832 [hep-ph]
99. M. Czakon, P. Fiedler, A. Mitov, Total top-quark pair-production cross section at hadron colliders through $O\left(\alpha_S^4\right)$. Phys. Rev. Lett. **110**, 252004 (2013). arXiv: 1303.6254 [hep-ph]
100. M. Czakon, A. Mitov, Top++: a program for the calculation of the top-pair cross-section at hadron colliders. Comput. Phys. Commun. **185**, 2930 (2014). arXiv:1112.5675 [hep-ph]
101. E. Re, Single-top Wt-channel production matched with parton showers using the POWHEG method. Eur. Phys. J. C **71**, 1547 (2011). arXiv:1009.2450 [hep-ph]
102. N. Kidonakis, Two-loop soft anomalous dimensions for single top quark associated production with a W^- or H^-. Phys. Rev. D **82**, 054018 (2010). arXiv:1005.4451 [hep-ph]
103. N. Kidonakis, 'Top Quark Production', in *Proceedings, Helmholtz International Summer School on Physics of Heavy Quarks and Hadrons (HQ 2013)* (JINR, Dubna, Russia, 15th–28th July 2013), p. 139. arXiv:1311.0283 [hep-ph]
104. R. Frederix, E. Re, P. Torrielli, Single-top t-channel hadroproduction in the four-flavour scheme with POWHEG and aMC@NLO. JHEP **09**, 130 (2012). arXiv:1207.5391 [hep-ph]
105. S. Alioli, P. Nason, C. Oleari, E. Re, NLO single-top production matched with shower in POWHEG: s- and t-channel contributions. JHEP **09**, 111 (2009). arXiv:0907.4076 [hep-ph]. Erratum: JHEP **02**, 011 (2010)
106. M. Aliev et al., HATHOR—HAdronic Top and Heavy quarks crOss section calculatoR. Comput. Phys. Commun. **182**, 1034 (2011). arXiv:1007.1327 [hep-ph]
107. P. Kant et al., HatHor for single top-quark production: updated predictions and uncertainty estimates for single top-quark production in hadronic collisions. Comput. Phys. Commun. **191**, 74 (2015). arXiv:1406.4403 [hep-ph]
108. H.B. Hartanto, B. Jäger, L. Reina, D. Wackeroth, Higgs boson production in association with top quarks in the POWHEG BOX. Phys. Rev. D **91**, 094003 (2015). arXiv:1501.04498 [hep-ph]
109. D. de Florian et al., Handbook of LHC Higgs Cross Sections: 4. Deciphering the Nature of the Higgs Sector (2016). arXiv:1610.07922 [hep-ph]
110. N. Quintero, J. L. Diaz-Cruz, G. Lopez Castro, Lepton pair emission in the top quark decay $t \to bW^+\ell^-\ell^+$. Phys. Rev. D **89**, 093014 (2014). arXiv:1403.3044 [hep-ph]
111. C. Anastasiou et al., High precision determination of the gluon fusion Higgs boson cross-section at the LHC. JHEP **05**, 058 (2016). arXiv:1602.00695 [hep-ph]
112. C. Anastasiou, C. Duhr, F. Dulat, F. Herzog, B. Mistlberger, Higgs boson gluon-fusion production in QCD at three loops. Phys. Rev. Lett. **114**, 212001 (2015). arXiv:1503. 06056 [hep-ph]
113. F. Dulat, A. Lazopoulos, B. Mistlberger, iHixs 2—inclusive Higgs cross sections. Comput. Phys. Commun. **233**, 243 (2018). arXiv:1802.00827 [hep-ph]
114. U. Aglietti, R. Bonciani, G. Degrassi, A. Vicini, Two-loop light fermion contribution to Higgs production and decays. Phys. Lett. B **595**, 432 (2004). arXiv:hep-ph/0404071
115. S. Actis, G. Passarino, C. Sturm, S. Uccirati, NLO electroweak corrections to Higgs boson production at hadron colliders. Phys. Lett. B **670**, 12 (2008). arXiv:0809.1301 [hep-ph]
116. M. Bonetti, K. Melnikov, L. Tancredi, Higher order corrections to mixed QCD-EWcontributions to Higgs boson production in gluon fusion. Phys. Rev. D , **97**, 056017 (2018). arXiv:1801.10403 [hep-ph]. Erratum: Phys. Rev. D **97**, 099906 (2018)
117. M. Ciccolini, A. Denner, S. Dittmaier, Strong and electroweak corrections to the production of Higgs + 2 jets via weak interactions at the large hadron collider. Phys. Rev. Lett. **99**, 161803 (2007). arXiv:0707.0381 [hep-ph]
118. M. Ciccolini, A. Denner, S. Dittmaier, Electroweak and QCD corrections to Higgs production via vector-boson fusion at the CERN LHC. Phys. Rev. D **77**, 013002 (2008). arXiv:0710. 4749 [hep-ph]
119. P. Bolzoni, F. Maltoni, S.-O. Moch, M. Zaro, Higgs boson production via vector-boson fusion at next-to-next-to-leading order in QCD. Phys. Rev. Lett. **105**, 011801 (2010). arXiv:1003.4451 [hep-ph]
120. T. Sjöstrand et al., An introduction to PYTHIA 8.2. Comput. Phys. Commun. **191**, 159 (2015). arXiv:1410.3012 [hep-ph]
121. ATLAS Collaboration, ATLAS Pythia 8 tunes to 7 TeV data, ATL-PHYS-PUB-2014-021 (2014). https://cds.cern.ch/record/1966419
122. S. Schumann, F. Krauss, A parton shower algorithm based on Catani-Seymour dipole factorisation. JHEP **03**, 038 (2008). arXiv:0709.1027 [hep-ph]
123. J. Pumplin et al., New generation of parton distributions with uncertainties from global QCD analysis. JHEP **07**, 012 (2002). arXiv:hep-ph/0201195
124. ATLAS Collaboration, Measurement of the Z/γ^* boson transverse momentum distribution in pp collisions at $\sqrt{s} = 7$ TeV with the ATLAS detector. JHEP **09**, 145 (2014). arXiv:1406.3660 [hep-ex]
125. P. Artoisenet, R. Frederix, O. Mattelaer, R. Rietkerk, Automatic spin-entangled decays of heavy resonances in Monte Carlo simulations. JHEP **03**, 015 (2013). arXiv:1212.3460 [hep-ph]
126. L. Lönnblad, Correcting the colour-dipole cascade model with fixed order matrix elements. JHEP **05**, 046 (2002). arXiv:hep-ph/0112284
127. L. Lönnblad, S. Prestel, Matching tree-level matrix elements with interleaved showers. JHEP **03**, 019 (2012). arXiv:1109.4829 [hep-ph]
128. U. De Sanctis, T. Lari, S. Montesano, C. Troncon, Perspectives for the detection and measurement of supersymmetry in the focus point region of mSUGRA models with the ATLAS detector at LHC. Eur. Phys. J. C **52**, 743 (2007). arXiv:0704.2515 [hep-ex]
129. T. Gleisberg, S. Höche, Comix, a new matrix element generator. JHEP **12**, 039 (2008). arXiv:0808.3674 [hep-ph]
130. S. Höche, F. Krauss, M. Schönherr, F. Siegert, A critical appraisal of NLO+PS matching methods. JHEP **09**, 049 (2012). arXiv:1111.1220 [hep-ph]
131. S. Catani, F. Krauss, R. Kuhn, B.R. Webber, QCD matrix elements + parton showers. JHEP **11**, 063 (2001). arXiv:hep-ph/0109231
132. S. Höche, F. Krauss, S. Schumann, F. Siegert, QCD matrix elements and truncated showers. JHEP **05**, 053 (2009). arXiv:0903.1219 [hep-ph]
133. S. Höche, F. Krauss, M. Schonherr, F. Siegert, QCD matrix elements + parton showers. The NLO case. JHEP **04**, 027 (2013). arXiv:1207.5030 [hep-ph]
134. F. Cascioli, P. Maierhöfer, S. Pozzorini, Scattering amplitudes with open loops. Phys. Rev. Lett. **108**, 111601 (2012). arXiv:1111.5206 [hep-ph]
135. A. Denner, S. Dittmaier, L. Hofer, Collier: a fortran-based complex one-loop library in extended regularizations. Comput. Phys. Commun. **212**, 220 (2017). arXiv:1604.06792 [hep-ph]
136. ATLAS Collaboration, Studies on top-quark Monte Carlo modelling for Top2016, ATL-PHYS-PUB-2016-020 (2016). https://cds.cern.ch/record/2216168
137. S. Frixione, E. Lænen, P. Motylinski, C. White, B.R. Webber, Single-top hadroproduction in association with a W boson. JHEP **07**, 029 (2008). arXiv:0805.3067 [hep-ph]

138. D.J. Lange, The EvtGen particle decay simulation package. Nucl. Instrum. Methods A **462**, 152 (2001)
139. ATLAS Collaboration, The Pythia 8 A3 tune description of ATLAS minimum bias and inelastic measurements incorporating the Donnachie-Landshoff diffractive model, ATL-PHYS-PUB-2016-017 (2016). https://cds.cern.ch/record/2206965
140. ATLAS Collaboration, Performance of electron and photon triggers in ATLAS during LHC Run 2. Eur. Phys. J. C **80**, 47 (2020). arXiv:1909.00761 [hep-ex]
141. ATLAS Collaboration, Performance of the ATLAS muon triggers in Run 2. JINST, **15**, P09015 (2020). arXiv:2004.13447 [hep-ex]
142. ATLAS Collaboration, Performance of the missing transverse momentum triggers for the ATLAS detector during Run-2 data taking. JHEP, **08**, 080 (2020). arXiv:2005.09554 [hep-ex]
143. ATLAS Collaboration, Vertex Reconstruction Performance of the ATLAS Detector at $\sqrt{s} = 13$ TeV, ATL-PHYS-PUB-2015-026 (2015). https://cds.cern.ch/record/2037717
144. ATLAS Collaboration, Reconstruction of primary vertices at the ATLAS experiment in Run 1 proton-proton collisions at the LHC. Eur. Phys. J. C **77**, 332 (2017). arXiv:1611.10235 [hep-ex]
145. ATLAS Collaboration, Electron and photon performance measurements with the ATLAS detector using the 2015-2017 LHC proton-proton collision data. JINST **14**, P12006 (2019). arXiv:1908.00005 [hep-ex]
146. ATLAS Collaboration, Muon reconstruction and identification efficiency in ATLAS using the full Run 2 pp collision data set at $\sqrt{s} = 13$ TeV (2020). arXiv:2012.00578 [hep-ex]
147. ATLAS Collaboration, Topological cell clustering in the ATLAS calorimeters and its performance in LHC Run 1. Eur. Phys. J. C **77**, 490 (2017). arXiv:1603.02934 [hep-ex]
148. M. Cacciari, G.P. Salam, G. Soyez, The anti-k_t jet clustering algorithm. JHEP **04**, 063 (2008). arXiv:0802.1189 [hep-ph]
149. M. Cacciari, G.P. Salam, G. Soyez, FastJet user manual. Eur. Phys. J. C **72**, 1896 (2012). arXiv:1111.6097 [hep-ph]
150. ATLAS Collaboration, Performance of pile-up mitigation techniques for jets in pp collisions at $\sqrt{s} = 8$ TeV using the ATLAS detector. Eur. Phys. J. C **76**, 581 (2016). arXiv:1510.03823 [hep-ex]
151. ATLAS Collaboration, Jet energy scale measurements and their systematic uncertainties in proton-proton collisions at $\sqrt{s} = 13$ TeV with the ATLAS detector. Phys. Rev. D **96**, 072002 (2017). arXiv:1703.09665 [hep-ex]
152. ATLAS Collaboration, Jet energy scale and resolution measured in proton-proton collisions at $\sqrt{s} = 13$ TeV with the ATLAS detector (2020). arXiv:2007.02645 [hep-ex]
153. ATLAS Collaboration, $E_{\mathrm{T}}^{\mathrm{miss}}$ performance in the ATLAS detector using 2015-2016 LHC pp collisions, ATLAS-CONF-2018-023 (2018). https://cds.cern.ch/record/2625233
154. ATLAS Collaboration, Performance of missing transverse momentum reconstruction with the ATLAS detector using proton-proton collisions at $\sqrt{s} = 13$ TeV. Eur. Phys. J. C **78**, 903 (2018). arXiv:1802.08168 [hep-ex]
155. ATLAS Collaboration, Object-based missing transverse momentum significance in the ATLAS Detector, ATLAS-CONF-2018-038 (2018). https://cds.cern.ch/record/2630948
156. ATLAS Collaboration, Selection of jets produced in 13 TeV proton-proton collisions with the ATLAS detector, ATLAS-CONF-2015-029 (2015). https://cds.cern.ch/record/2037702
157. ATLAS Collaboration, Tagging and suppression of pileup jets with the ATLAS detector, ATLAS-CONF-2014-018 (2014). https://cds.cern.ch/record/1700870
158. ATLAS Collaboration, ATLAS b-jet identification performance and efficiency measurement with $t\bar{t}$ events in pp collisions at $\sqrt{s} = 13$ TeV. Eur. Phys. J. C **79**, 970 (2019). arXiv:1907.05120 [hep-ex]
159. ATLAS Collaboration, Optimisation and performance studies of the ATLAS b-tagging algorithms for the 2017-18 LHC run, ATL-PHYS-PUB-2017-013 (2017). https://cds.cern.ch/record/2273281
160. ATLAS Collaboration, Search for electroweak production of charginos and sleptons decaying into final states with two leptons and missing transverse momentum in $\sqrt{s} = 13$ TeV pp collisions using the ATLAS detector. Eur. Phys. J. C **80**, 123 (2020). arXiv:1908.08215 [hep-ex]
161. ATLAS Collaboration, Search for direct production of electroweakinos in final states with one lepton, missing transverse momentum and a Higgs boson decaying into two b-jets in pp collisions at $\sqrt{s} = 13$ TeV with the ATLAS detector. Eur. Phys. J. C **80**, 691 (2020). arXiv:1909.09226 [hep-ex]
162. ATLAS Collaboration, Measurement of the WW cross section in $\sqrt{s} = 7$ TeV pp collisions with the ATLAS detector and limits on anomalous gauge couplings. Phys. Lett. B **712**, 289 (2012). arXiv:1203.6232 [hep-ex]
163. ATLAS Collaboration, Prospects for Higgs boson searches using the $H \to WW^{(*)} \to \ell\nu\ell\nu$ decay mode with the ATLAS detector at 10 TeV, ATL-PHYS-PUB-2010-005 (2010). https://cds.cern.ch/record/1270568
164. ATLAS Collaboration, Determination of jet calibration and energy resolution in proton-proton collisions at $\sqrt{s} = 8$ TeV using the ATLAS detector. Eur. Phys. J. C **80**, 1104 (2020). arXiv:1910.04482 [hep-ex]
165. M. Bahr et al., Herwig++ physics and manual. Eur. Phys. J. C **58**, 639 (2008). arXiv:0803.0883 [hep-ph]
166. J. Bellm et al., Herwig 7.0/Herwig++ 3.0 release note. Eur. Phys. J. C **76**, 196 (2016). arXiv:1512.01178 [hep-ph]
167. G. Cowan, K. Cranmer, E. Gross, O. Vitells, Asymptotic formulae for likelihood-based tests of new physics. Eur. Phys. J. C **71**, 1554 (2011). arXiv:1007.1727 [physics.data-an]. Erratum: Eur. Phys. J. C **73**, 2501 (2013)
168. M. Baak et al., HistFitter software framework for statistical data analysis. Eur. Phys. J. C **75**, 153 (2015). arXiv:1410.1280 [hep-ex]
169. R.D. Cousins, J.T. Linnemann, J. Tucker, Evaluation of three methods for calculating statistical significance when incorporating a systematic uncertainty into a test of the background-only hypothesis for a Poisson process. Nucl. Instrum. Methods A **595**, 480 (2008). arXiv:physics/0702156
170. A.L. Read, Presentation of search results: the CL_S technique. J. Phys. G **28**, 2693 (2002)
171. L. Heinrich, M. Feickert, G. Stark, K. Cranmer, pyhf: pure-Python implementation of HistFactory statistical models. J. Open Source Softw. **6**, 2823 (2021)
172. L. Heinrich, M. Feickert, G. Stark, scikit-hep/pyhf: v0.5.2 (2020). https://doi.org/10.5281/zenodo.4018115
173. ATLAS Collaboration, Reproducing searches for new physics with the ATLAS experiment through publication of full statistical likelihoods, ATL-PHYS-PUB-2019-029 (2019). https://cds.cern.ch/record/2684863
174. C.G. Lester, D.J. Summers, Measuring masses of semi-invisibly decaying particles pair produced at hadron colliders. Phys. Lett. B **463**, 99 (1999). arXiv:hep-ph/9906349
175. A. Barr, C. Lester, P. Stephens, A variable for measuring masses at hadron colliders when missing energy is expected; m_{T2}: the truth behind the glamour. J. Phys. G **29**, 2343 (2003). arXiv:hep-ph/0304226
176. N. Aghanim et al., Planck 2015 results. XI. CMB power spectra, likelihoods, and robustness of parameters. Astron. Astrophys. **594**, A11 (2016). arXiv:1507.02704 [astro-ph.CO]
177. ATLAS Collaboration, Measurement of the top quark-pair production cross section with ATLAS in pp collisions at $\sqrt{s} = 7$ TeV. Eur. Phys. J. C **71**, 1577 (2011). arXiv:1012.1792 [hep-ex]
178. ATLAS Collaboration, ATLAS Computing Acknowledgements, ATL-SOFT-PUB-2021-003. https://cds.cern.ch/record/2776662

ATLAS Collaboration

G. Aad[99], B. Abbott[126], D. C. Abbott[100], A. Abed Abud[34], K. Abeling[51], D. K. Abhayasinghe[91], S. H. Abidi[27], O. S. AbouZeid[38], H. Abramowicz[159], H. Abreu[158], Y. Abulaiti[5], A. C. Abusleme Hoffman[144a], B. S. Acharya[64a,64b,p], B. Achkar[51], L. Adam[97], C. Adam Bourdarios[4], L. Adamczyk[81a], L. Adamek[164], J. Adelman[118], A. Adiguzel[11c,ae], S. Adorni[52], T. Adye[141], A. A. Affolder[143], Y. Afik[158], C. Agapopoulou[62], M. N. Agaras[12], J. Agarwala[68a,68b], A. Aggarwal[116], C. Agheorghiesei[25c], J. A. Aguilar-Saavedra[137a,137f,ad], A. Ahmad[34], F. Ahmadov[77], W. S. Ahmed[101], X. Ai[44], G. Aielli[71a,71b], S. Akatsuka[83], M. Akbiyik[97], T. P. A. Åkesson[94], A. V. Akimov[108], K. Al Khoury[37], G. L. Alberghi[21b], J. Albert[173], M. J. Alconada Verzini[86], S. Alderweireldt[48], M. Aleksa[34], I. N. Aleksandrov[77], C. Alexa[25b], T. Alexopoulos[9], A. Alfonsi[117], F. Alfonsi[21b,21a], M. Alhroob[126], B. Ali[139], S. Ali[156], M. Aliev[163], G. Alimonti[66a], C. Allaire[34], B. M. M. Allbrooke[154], P. P. Allport[19], A. Aloisio[67a,67b], F. Alonso[86], C. Alpigiani[146], E. Alunno Camelia[71a,71b], M. Alvarez Estevez[96], M. G. Alviggi[67a,67b], Y. Amaral Coutinho[78b], A. Ambler[101], L. Ambroz[132], C. Amelung[34], D. Amidei[103], S. P. Amor Dos Santos[137a], S. Amoroso[44], C. S. Amrouche[52], C. Anastopoulos[147], N. Andari[142], T. Andeen[10], J. K. Anders[18], S. Y. Andrean[43a,43b], A. Andreazza[66a,66b], V. Andrei[59a], S. Angelidakis[8], A. Angerami[37], A. V. Anisenkov[119b,119a], A. Annovi[69a], C. Antel[52], M. T. Anthony[147], E. Antipov[127], M. Antonelli[49], D. J. A. Antrim[16], F. Anulli[70a], M. Aoki[79], J. A. Aparisi Pozo[171], M. A. Aparo[154], L. Aperio Bella[44], N. Aranzabal[34], V. Araujo Ferraz[78a], C. Arcangeletti[49], A. T. H. Arce[47], E. Arena[88], J-F. Arguin[107], S. Argyropoulos[50], J.-H. Arling[44], A. J. Armbruster[34], A. Armstrong[168], O. Arnaez[164], H. Arnold[34], Z. P. Arrubarrena Tame[111], G. Artoni[132], H. Asada[114], K. Asai[124], S. Asai[161], N. A. Asbah[57], E. M. Asimakopoulou[169], L. Asquith[154], J. Assahsah[33d], K. Assamagan[27], R. Astalos[26a], R. J. Atkin[31a], M. Atkinson[170], N. B. Atlay[17], H. Atmani[58b], P. A. Atmasiddha[103], K. Augsten[139], S. Auricchio[67a,67b], V. A. Austrup[179], G. Avolio[34], M. K. Ayoub[13c], G. Azuelos[107,ak], D. Babal[26a], H. Bachacou[142], K. Bachas[160], F. Backman[43a,43b], A. Badea[57], P. Bagnaia[70a,70b], H. Bahrasemani[150], A. J. Bailey[171], V. R. Bailey[170], J. T. Baines[141], C. Bakalis[9], O. K. Baker[180], P. J. Bakker[117], E. Bakos[14], D. Bakshi Gupta[7], S. Balaji[155], R. Balasubramanian[117], E. M. Baldin[119b,119a], P. Balek[140], E. Ballabene[66a,66b], F. Balli[142], W. K. Balunas[132], J. Balz[97], E. Banas[82], M. Bandieramonte[136], A. Bandyopadhyay[17], L. Barak[159], E. L. Barberio[102], D. Barberis[53b,53a], M. Barbero[99], G. Barbour[92], K. N. Barends[31a], T. Barillari[112], M-S. Barisits[34], J. Barkeloo[129], T. Barklow[151], B. M. Barnett[141], R. M. Barnett[16], A. Baroncelli[58a], G. Barone[27], A. J. Barr[132], L. Barranco Navarro[43a,43b], F. Barreiro[96], J. Barreiro Guimarães da Costa[13a], U. Barron[159], S. Barsov[135], F. Bartels[59a], R. Bartoldus[151], G. Bartolini[99], A. E. Barton[87], P. Bartos[26a], A. Basalaev[44], A. Basan[97], I. Bashta[72a,72b], A. Bassalat[62], M. J. Basso[164], C. R. Basson[98], R. L. Bates[55], S. Batlamous[33e], J. R. Batley[30], B. Batool[149], M. Battaglia[143], M. Bauce[70a,70b], F. Bauer[142,*], P. Bauer[22], H. S. Bawa[29], A. Bayirli[11c], J. B. Beacham[47], T. Beau[133], P. H. Beauchemin[167], F. Becherer[50], P. Bechtle[22], H. P. Beck[18,r], K. Becker[175], C. Becot[44], A. J. Beddall[11a], V. A. Bednyakov[77], C. P. Bee[153], T. A. Beermann[179], M. Begalli[78b], M. Begel[27], A. Behera[153], J. K. Behr[44], C. Beirao Da Cruz E Silva[34], J. F. Beirer[51,34], F. Beisiegel[22], M. Belfkir[4], G. Bella[159], L. Bellagamba[21b], A. Bellerive[32], P. Bellos[19], K. Beloborodov[119b,119a], K. Belotskiy[109], N. L. Belyaev[109], D. Benchekroun[33a], Y. Benhammou[159], D. P. Benjamin[5], M. Benoit[27], J. R. Bensinger[24], S. Bentvelsen[117], L. Beresford[132], M. Beretta[49], D. Berge[17], E. Bergeaas Kuutmann[169], N. Berger[4], B. Bergmann[139], L. J. Bergsten[24], J. Beringer[16], S. Berlendis[6], G. Bernardi[133], C. Bernius[151], F. U. Bernlochner[22], T. Berry[91], P. Berta[44], A. Berthold[46], I. A. Bertram[87], O. Bessidskaia Bylund[179], S. Bethke[112], A. Betti[40], A. J. Bevan[90], S. Bhatta[153], D. S. Bhattacharya[174], P. Bhattarai[24], V. S. Bhopatkar[5], R. Bi[136], R. M. Bianchi[136], O. Biebel[111], R. Bielski[34], N. V. Biesuz[69a,69b], M. Biglietti[72a], T. R. V. Billoud[139], M. Bindi[51], A. Bingul[11d], C. Bini[70a,70b], S. Biondi[21b,21a], C. J. Birch-sykes[98], G. A. Bird[19,141], M. Birman[177], T. Bisanz[34], J. P. Biswal[2], D. Biswas[178,k], A. Bitadze[98], C. Bittrich[46], K. Bjørke[131], I. Bloch[44], C. Blocker[24], A. Blue[55], U. Blumenschein[90], J. Blumenthal[97], G. J. Bobbink[117], V. S. Bobrovnikov[119b,119a], D. Bogavac[12], A. G. Bogdanchikov[119b,119a], C. Bohm[43a], V. Boisvert[91], P. Bokan[44], T. Bold[81a], M. Bomben[133], M. Bona[90], M. Boonekamp[142], C. D. Booth[91], A. G. Borbély[55], H. M. Borecka-Bielska[107], L. S. Borgna[92], G. Borissov[87], D. Bortoletto[132], D. Boscherini[21b], M. Bosman[12], J. D. Bossio Sola[101], K. Bouaouda[33a], J. Boudreau[136], E. V. Bouhova-Thacker[87], D. Boumediene[36], R. Bouquet[133], A. Boveia[125], J. Boyd[34], D. Boye[27], I. R. Boyko[77], A. J. Bozson[91], J. Bracinik[19], N. Brahimi[58d,58c], G. Brandt[179], O. Brandt[30], F. Braren[44], B. Brau[100], J. E. Brau[129], W. D. Breaden Madden[55], K. Brendlinger[44],

R. Brener[177], L. Brenner[34], R. Brenner[169], S. Bressler[177], B. Brickwedde[97], D. L. Briglin[19], D. Britton[55], D. Britzger[112], I. Brock[22], R. Brock[104], G. Brooijmans[37], W. K. Brooks[144e], E. Brost[27], P. A. Bruckman de Renstrom[82], B. Brüers[44], D. Bruncko[26b], A. Bruni[21b], G. Bruni[21b], M. Bruschi[21b], N. Bruscino[70a,70b], L. Bryngemark[151], T. Buanes[15], Q. Buat[153], P. Buchholz[149], A. G. Buckley[55], I. A. Budagov[77], M. K. Bugge[131], O. Bulekov[109], B. A. Bullard[57], T. J. Burch[118], S. Burdin[88], C. D. Burgard[44], A. M. Burger[127], B. Burghgrave[7], J. T. P. Burr[44], C. D. Burton[10], J. C. Burzynski[100], V. Büscher[97], P. J. Bussey[55], J. M. Butler[23], C. M. Buttar[55], J. M. Butterworth[92], W. Buttinger[141], C. J. Buxo Vazquez[104], A. R. Buzykaev[119b,119a], G. Cabras[21b], S. Cabrera Urbán[171], D. Caforio[54], H. Cai[136], V. M. M. Cairo[151], O. Cakir[3a], N. Calace[34], P. Calafiura[16], G. Calderini[133], P. Calfayan[63], G. Callea[55], L. P. Caloba[78b], A. Caltabiano[71a,71b], S. Calvente Lopez[96], D. Calvet[36], S. Calvet[36], T. P. Calvet[99], M. Calvetti[69a,69b], R. Camacho Toro[133], S. Camarda[34], D. Camarero Munoz[96], P. Camarri[71a,71b], M. T. Camerlingo[72a,72b], D. Cameron[131], C. Camincher[173], M. Campanelli[92], A. Camplani[38], V. Canale[67a,67b], A. Canesse[101], M. Cano Bret[75], J. Cantero[127], Y. Cao[170], M. Capua[39b,39a], R. Cardarelli[71a], F. Cardillo[171], G. Carducci[39b,39a], T. Carli[34], G. Carlino[67a], B. T. Carlson[136], E. M. Carlson[173,165a], L. Carminati[66a,66b], M. Carnesale[70a,70b], R. M. D. Carney[151], S. Caron[116], E. Carquin[144e], S. Carrá[44], G. Carratta[21b,21a], J. W. S. Carter[164], T. M. Carter[48], D. Casadei[31c], M. P. Casado[12,h], A. F. Casha[164], E. G. Castiglia[180], F. L. Castillo[59a], L. Castillo Garcia[12], V. Castillo Gimenez[171], N. F. Castro[137a,137e], A. Catinaccio[34], J. R. Catmore[131], A. Cattai[34], V. Cavaliere[27], N. Cavalli[21b,21a], V. Cavasinni[69a,69b], E. Celebi[11b], F. Celli[132], K. Cerny[128], A. S. Cerqueira[78a], A. Cerri[154], L. Cerrito[71a,71b], F. Cerutti[16], A. Cervelli[21b], S. A. Cetin[11b], Z. Chadi[33a], D. Chakraborty[118], M. Chala[137f], J. Chan[178], W. S. Chan[117], W. Y. Chan[88], J. D. Chapman[30], B. Chargeishvili[157b], D. G. Charlton[19], T. P. Charman[90], M. Chatterjee[18], C. C. Chau[32], S. Chekanov[5], S. V. Chekulaev[165a], G. A. Chelkov[77,ag], A. Chen[103], B. Chen[159], C. Chen[58a], C. H. Chen[76], H. Chen[13c], H. Chen[27], J. Chen[58a], J. Chen[37], J. Chen[24], S. Chen[134], S. J. Chen[13c], X. Chen[13b], Y. Chen[58a], Y-H. Chen[44], C. L. Cheng[178], H. C. Cheng[60a], H. J. Cheng[13a], A. Cheplakov[77], E. Cheremushkina[44], R. Cherkaoui El Moursli[33e], E. Cheu[6], K. Cheung[61], L. Chevalier[142], V. Chiarella[49], G. Chiarelli[69a], G. Chiodini[65a], A. S. Chisholm[19], A. Chitan[25b], I. Chiu[161], Y. H. Chiu[173], M. V. Chizhov[77,t], K. Choi[10], A. R. Chomont[70a,70b], Y. Chou[100], Y. S. Chow[117], L. D. Christopher[31f], M. C. Chu[60a], X. Chu[13a,13d], J. Chudoba[138], J. J. Chwastowski[82], D. Cieri[112], K. M. Ciesla[82], V. Cindro[89], I. A. Cioară[25b], A. Ciocio[16], F. Cirotto[67a,67b], Z. H. Citron[177,l], M. Citterio[66a], D. A. Ciubotaru[25b], B. M. Ciungu[164], A. Clark[52], P. J. Clark[48], S. E. Clawson[98], C. Clement[43a,43b], L. Clissa[21b,21a], Y. Coadou[99], M. Cobal[64a,64c], A. Coccaro[53b], J. Cochran[76], R. F. Coelho Barrue[137a], R. Coelho Lopes De Sa[100], S. Coelli[66a], H. Cohen[159], A. E. C. Coimbra[34], B. Cole[37], J. Collot[56], P. Conde Muiño[137a,137h], S. H. Connell[31c], I. A. Connelly[55], E. I. Conroy[132], F. Conventi[67a,al], H. G. Cooke[19], A. M. Cooper-Sarkar[132], F. Cormier[172], L. D. Corpe[34], M. Corradi[70a,70b], E. E. Corrigan[94], F. Corriveau[101,aa], M. J. Costa[171], F. Costanza[4], D. Costanzo[147], B. M. Cote[125], G. Cowan[91], J. W. Cowley[30], J. Crane[98], K. Cranmer[123], R. A. Creager[134], S. Crépé-Renaudin[56], F. Crescioli[133], M. Cristinziani[149], M. Cristoforetti[73a,73b,b], V. Croft[167], G. Crosetti[39b,39a], A. Cueto[4], T. Cuhadar Donszelmann[168], H. Cui[13a,13d], A. R. Cukierman[151], W. R. Cunningham[55], S. Czekierda[82], P. Czodrowski[34], M. M. Czurylo[59b], M. J. Da Cunha Sargedas De Sousa[58a], J. V. Da Fonseca Pinto[78b], C. Da Via[98], W. Dabrowski[81a], T. Dado[45], S. Dahbi[31f], T. Dai[103], C. Dallapiccola[100], M. Dam[38], G. D'amen[27], V. D'Amico[72a,72b], J. Damp[97], J. R. Dandoy[134], M. F. Daneri[28], M. Danninger[150], V. Dao[34], G. Darbo[53b], S. Darmora[5], A. Dattagupta[129], S. D'Auria[66a,66b], C. David[165b], T. Davidek[140], D. R. Davis[47], B. Davis-Purcell[32], I. Dawson[90], K. De[7], R. De Asmundis[67a], M. De Beurs[117], S. De Castro[21b,21a], N. De Groot[116], P. de Jong[117], H. De la Torre[104], A. De Maria[13c], D. De Pedis[70a], A. De Salvo[70a], U. De Sanctis[71a,71b], M. De Santis[71a,71b], A. De Santo[154], J. B. De Vivie De Regie[56], D. V. Dedovich[77], J. Degens[117], A. M. Deiana[40], J. Del Peso[96], Y. Delabat Diaz[44], F. Deliot[142], C. M. Delitzsch[6], M. Della Pietra[67a,67b], D. Della Volpe[52], A. Dell'Acqua[34], L. Dell'Asta[66a,66b], M. Delmastro[4], P. A. Delsart[56], S. Demers[180], M. Demichev[77], S. P. Denisov[120], L. D'Eramo[118], D. Derendarz[82], J. E. Derkaoui[33d], F. Derue[133], P. Dervan[88], K. Desch[22], K. Dette[164], C. Deutsch[22], P. O. Deviveiros[34], F. A. Di Bello[70a,70b], A. Di Ciaccio[71a,71b], L. Di Ciaccio[4], C. Di Donato[67a,67b], A. Di Girolamo[34], G. Di Gregorio[69a,69b], A. Di Luca[73a,73b], B. Di Micco[72a,72b], R. Di Nardo[72a,72b], C. Diaconu[99], F. A. Dias[117], T. Dias Do Vale[137a], M. A. Diaz[144a], F. G. Diaz Capriles[22], J. Dickinson[16], M. Didenko[171], E. B. Diehl[103], J. Dietrich[17], S. Díez Cornell[44], C. Diez Pardos[149], A. Dimitrievska[16], W. Ding[13b], J. Dingfelder[22], S. J. Dittmeier[59b], F. Dittus[34], F. Djama[99], T. Djobava[157b], J. I. Djuvsland[15],

M. A. B. Do Vale[145], D. Dodsworth[24], C. Doglioni[94], J. Dolejsi[140], Z. Dolezal[140], M. Donadelli[78c], B. Dong[58c], J. Donini[36], A. D'onofrio[13c], M. D'Onofrio[88], J. Dopke[141], A. Doria[67a], M. T. Dova[86], A. T. Doyle[55], E. Drechsler[150], E. Dreyer[150], T. Dreyer[51], A. S. Drobac[167], D. Du[58b], T. A. du Pree[117], F. Dubinin[108], M. Dubovsky[26a], A. Dubreuil[52], E. Duchovni[177], G. Duckeck[111], O. A. Ducu[34,25b], D. Duda[112], A. Dudarev[34], M. D'uffizi[98], L. Duflot[62], M. Dührssen[34], C. Dülsen[179], A. E. Dumitriu[25b], M. Dunford[59a], S. Dungs[45], A. Duperrin[99], H. Duran Yildiz[3a], M. Düren[54], A. Durglishvili[157b], B. Dutta[44], D. Duvnjak[1], G. I. Dyckes[134], M. Dyndal[81a], S. Dysch[98], B. S. Dziedzic[82], B. Eckerova[26a], M. G. Eggleston[47], E. Egidio Purcino De Souza[78b], L. F. Ehrke[52], T. Eifert[7], G. Eigen[15], K. Einsweiler[16], T. Ekelof[169], Y. El Ghazali[33b], H. El Jarrari[33e], A. El Moussaouy[33a], V. Ellajosyula[169], M. Ellert[169], F. Ellinghaus[179], A. A. Elliot[90], N. Ellis[34], J. Elmsheuser[27], M. Elsing[34], D. Emeliyanov[141], A. Emerman[37], Y. Enari[161], J. Erdmann[45], A. Ereditato[18], P. A. Erland[82], M. Errenst[179], M. Escalier[62], C. Escobar[171], O. Estrada Pastor[171], E. Etzion[159], G. Evans[137a], H. Evans[63], M. O. Evans[154], A. Ezhilov[135], F. Fabbri[55], L. Fabbri[21b,21a], V. Fabiani[116], G. Facini[175], R. M. Fakhrutdinov[120], S. Falciano[70a], P. J. Falke[22], S. Falke[34], J. Faltova[140], Y. Fan[13a], Y. Fang[13a], Y. Fang[13a], G. Fanourakis[42], M. Fanti[66a,66b], M. Faraj[58c], A. Farbin[7], A. Farilla[72a], E. M. Farina[68a,68b], T. Farooque[104], S. M. Farrington[48], P. Farthouat[34], F. Fassi[33e], D. Fassouliotis[8], M. Faucci Giannelli[71a,71b], W. J. Fawcett[30], L. Fayard[62], O. L. Fedin[135,q], M. Feickert[170], L. Feligioni[99], A. Fell[147], C. Feng[58b], M. Feng[13b], M. J. Fenton[168], A. B. Fenyuk[120], S. W. Ferguson[41], J. Ferrando[44], A. Ferrari[169], P. Ferrari[117], R. Ferrari[68a], D. Ferrere[52], C. Ferretti[103], F. Fiedler[97], A. Filipčič[89], F. Filthaut[116], M. C. N. Fiolhais[137a,137c,a], L. Fiorini[171], F. Fischer[111], W. C. Fisher[104], T. Fitschen[19], I. Fleck[149], P. Fleischmann[103], T. Flick[179], B. M. Flierl[111], L. Flores[134], L. R. Flores Castillo[60a], F. M. Follega[73a,73b], N. Fomin[15], J. H. Foo[164], G. T. Forcolin[73a,73b], B. C. Forland[63], A. Formica[142], F. A. Förster[12], A. C. Forti[98], E. Fortin[99], M. G. Foti[132], D. Fournier[62], H. Fox[87], P. Francavilla[69a,69b], S. Francescato[70a,70b], M. Franchini[21b,21a], S. Franchino[59a], D. Francis[34], L. Franco[4], L. Franconi[18], M. Franklin[57], G. Frattari[70a,70b], A. C. Freegard[90], P. M. Freeman[19], B. Freund[107], W. S. Freund[78b], E. M. Freundlich[45], D. Froidevaux[34], J. A. Frost[132], Y. Fu[58a], M. Fujimoto[124], E. Fullana Torregrosa[171], T. Fusayasu[113], J. Fuster[171], A. Gabrielli[21b,21a], A. Gabrielli[34], P. Gadow[44], G. Gagliardi[53b,53a], L. G. Gagnon[16], G. E. Gallardo[132], E. J. Gallas[132], B. J. Gallop[141], R. Gamboa Goni[90], K. K. Gan[125], S. Ganguly[177], J. Gao[58a], Y. Gao[48], Y. S. Gao[29,n], F. M. Garay Walls[144a], C. García[171], J. E. García Navarro[171], J. A. García Pascual[13a], M. Garcia-Sciveres[16], R. W. Gardner[35], D. Garg[75], S. Gargiulo[50], C. A. Garner[164], V. Garonne[131], S. J. Gasiorowski[146], P. Gaspar[78b], G. Gaudio[68a], P. Gauzzi[70a,70b], I. L. Gavrilenko[108], A. Gavrilyuk[121], C. Gay[172], G. Gaycken[44], E. N. Gazis[9], A. A. Geanta[25b], C. M. Gee[143], C. N. P. Gee[141], J. Geisen[94], M. Geisen[97], C. Gemme[53b], M. H. Genest[56], S. Gentile[70a,70b], S. George[91], T. Geralis[42], L. O. Gerlach[51], P. Gessinger-Befurt[97], M. Ghasemi Bostanabad[173], M. Ghneimat[149], A. Ghosh[168], A. Ghosh[75], B. Giacobbe[21b], S. Giagu[70a,70b], N. Giangiacomi[164], P. Giannetti[69a], A. Giannini[67a,67b], S. M. Gibson[91], M. Gignac[143], D. T. Gil[81b], B. J. Gilbert[37], D. Gillberg[32], G. Gilles[179], N. E. K. Gillwald[44], D. M. Gingrich[2,ak], M. P. Giordani[64a,64c], P. F. Giraud[142], G. Giugliarelli[64a,64c], D. Giugni[66a], F. Giuli[71a,71b], I. Gkialas[8,i], E. L. Gkougkousis[12], P. Gkountoumis[9], L. K. Gladilin[110], C. Glasman[96], G. R. Gledhill[129], M. Glisic[129], I. Gnesi[39b,d], M. Goblirsch-Kolb[24], D. Godin[107], S. Goldfarb[102], T. Golling[52], D. Golubkov[120], J. P. Gombas[104], A. Gomes[137a,137b], R. Goncalves Gama[51], R. Gonçalo[137a,137c], G. Gonella[129], L. Gonella[19], A. Gongadze[77], F. Gonnella[19], J. L. Gonski[37], S. González de la Hoz[171], S. Gonzalez Fernandez[12], R. Gonzalez Lopez[88], C. Gonzalez Renteria[16], R. Gonzalez Suarez[169], S. Gonzalez-Sevilla[52], G. R. Gonzalvo Rodriguez[171], R. Y. González Andana[144a], L. Goossens[34], N. A. Gorasia[19], P. A. Gorbounov[121], H. A. Gordon[27], B. Gorini[34], E. Gorini[65a,65b], A. Gorišek[89], A. T. Goshaw[47], M. I. Gostkin[77], C. A. Gottardo[116], M. Gouighri[33b], V. Goumarre[44], A. G. Goussiou[146], N. Govender[31c], C. Goy[4], I. Grabowska-Bold[81a], K. Graham[32], E. Gramstad[131], S. Grancagnolo[17], M. Grandi[154], V. Gratchev[135], P. M. Gravila[25f], F. G. Gravili[65a,65b], H. M. Gray[16], C. Grefe[22], I. M. Gregor[44], P. Grenier[151], K. Grevtsov[44], C. Grieco[12], N. A. Grieser[126], A. A. Grillo[143], K. Grimm[29,m], S. Grinstein[12,x], J.-F. Grivaz[62], S. Groh[97], E. Gross[177], J. Grosse-Knetter[51], Z. J. Grout[92], C. Grud[103], A. Grummer[115], J. C. Grundy[132], L. Guan[103], W. Guan[178], C. Gubbels[172], J. Guenther[34], J. G. R. Guerrero Rojas[171], F. Guescini[112], D. Guest[17], R. Gugel[97], A. Guida[44], T. Guillemin[4], S. Guindon[34], J. Guo[58c], L. Guo[62], Y. Guo[103], R. Gupta[44], S. Gurbuz[22], G. Gustavino[126], M. Guth[50], P. Gutierrez[126], L. F. Gutierrez Zagazeta[134], C. Gutschow[92], C. Guyot[142], C. Gwenlan[132], C. B. Gwilliam[88], E. S. Haaland[131], A. Haas[123], M. Habedank[17],

C. Haber[16], H. K. Hadavand[7], A. Hadef[97], M. Haleem[174], J. Haley[127], J. J. Hall[147], G. Halladjian[104], G. D. Hallewell[99], L. Halser[18], K. Hamano[173], H. Hamdaoui[33e], M. Hamer[22], G. N. Hamity[48], K. Han[58a], L. Han[13c], L. Han[58a], S. Han[16], Y. F. Han[164], K. Hanagaki[79,v], M. Hance[143], M. D. Hank[35], R. Hankache[98], E. Hansen[94], J. B. Hansen[38], J. D. Hansen[38], M. C. Hansen[22], P. H. Hansen[38], K. Hara[166], T. Harenberg[179], S. Harkusha[105], Y. T. Harris[132], P. F. Harrison[175], N. M. Hartman[151], N. M. Hartmann[111], Y. Hasegawa[148], A. Hasib[48], S. Hassani[142], S. Haug[18], R. Hauser[104], M. Havranek[139], C. M. Hawkes[19], R. J. Hawkings[34], S. Hayashida[114], D. Hayden[104], C. Hayes[103], R. L. Hayes[172], C. P. Hays[132], J. M. Hays[90], H. S. Hayward[88], S. J. Haywood[141], F. He[58a], Y. He[162], Y. He[133], M. P. Heath[48], V. Hedberg[94], A. L. Heggelund[131], N. D. Hehir[90], C. Heidegger[50], K. K. Heidegger[50], W. D. Heidorn[76], J. Heilman[32], S. Heim[44], T. Heim[16], B. Heinemann[44,ai], J. G. Heinlein[134], J. J. Heinrich[129], L. Heinrich[34], J. Hejbal[138], L. Helary[44], A. Held[123], S. Hellesund[131], C. M. Helling[143], S. Hellman[43a,43b], C. Helsens[34], R. C. W. Henderson[87], L. Henkelmann[30], A. M. Henriques Correia[34], H. Herde[151], Y. Hernández Jiménez[153], H. Herr[97], M. G. Herrmann[111], T. Herrmann[46], G. Herten[50], R. Hertenberger[111], L. Hervas[34], N. P. Hessey[165a], H. Hibi[80], S. Higashino[79], E. Higón-Rodriguez[171], K. K. Hill[27], K. H. Hiller[44], S. J. Hillier[19], M. Hils[46], I. Hinchliffe[16], F. Hinterkeuser[22], M. Hirose[130], S. Hirose[166], D. Hirschbuehl[179], B. Hiti[89], O. Hladik[138], J. Hobbs[153], R. Hobincu[25e], N. Hod[177], M. C. Hodgkinson[147], B. H. Hodkinson[30], A. Hoecker[34], J. Hofer[44], D. Hohn[50], T. Holm[22], T. R. Holmes[35], M. Holzbock[112], L. B. A. H. Hommels[30], B. P. Honan[98], T. M. Hong[136], J. C. Honig[50], A. Hönle[112], B. H. Hooberman[170], W. H. Hopkins[5], Y. Horii[114], P. Horn[46], L. A. Horyn[35], S. Hou[156], J. Howarth[55], J. Hoya[86], M. Hrabovsky[128], A. Hrynevich[106], T. Hryn'ova[4], P. J. Hsu[61], S.-C. Hsu[146], Q. Hu[37], S. Hu[58c], Y. F. Hu[13a,13d,am], D. P. Huang[92], X. Huang[13c], Y. Huang[58a], Y. Huang[13a], Z. Hubacek[139], F. Hubaut[99], M. Huebner[22], F. Huegging[22], T. B. Huffman[132], M. Huhtinen[34], R. Hulsken[56], N. Huseynov[77,ab], J. Huston[104], J. Huth[57], R. Hyneman[151], S. Hyrych[26a], G. Iacobucci[52], G. Iakovidis[27], I. Ibragimov[149], L. Iconomidou-Fayard[62], P. Iengo[34], R. Ignazzi[38], R. Iguchi[161], T. Iizawa[52], Y. Ikegami[79], A. Ilg[18], N. Ilic[164,164], H. Imam[33a], G. Introzzi[68a,68b], M. Iodice[72a], V. Ippolito[70a,70b], M. Ishino[161], W. Islam[127], C. Issever[17,44], S. Istin[11c,an], J. M. Iturbe Ponce[60a], R. Iuppa[73a,73b], A. Ivina[177], J. M. Izen[41], V. Izzo[67a], P. Jacka[138], P. Jackson[1], R. M. Jacobs[44], B. P. Jaeger[150], C. S. Jagfeld[111], G. Jäkel[179], K. B. Jakobi[97], K. Jakobs[50], T. Jakoubek[177], J. Jamieson[55], K. W. Janas[81a], G. Jarlskog[94], A. E. Jaspan[88], N. Javadov[77,ab], T. Javůrek[34], M. Javurkova[100], F. Jeanneau[142], L. Jeanty[129], J. Jejelava[157a,ac], P. Jenni[50,e], S. Jézéquel[4], J. Jia[153], Z. Jia[13c], Y. Jiang[58a], S. Jiggins[50], J. Jimenez Pena[112], S. Jin[13c], A. Jinaru[25b], O. Jinnouchi[162], H. Jivan[31f], P. Johansson[147], K. A. Johns[6], C. A. Johnson[63], E. Jones[175], R. W. L. Jones[87], T. J. Jones[88], J. Jovicevic[34], X. Ju[16], J. J. Junggeburth[34], A. Juste Rozas[12,x], A. Kaczmarska[82], M. Kado[70a,70b], H. Kagan[125], M. Kagan[151], A. Kahn[37], C. Kahra[97], T. Kaji[176], E. Kajomovitz[158], C. W. Kalderon[27], A. Kaluza[97], A. Kamenshchikov[120], M. Kaneda[161], N. J. Kang[143], S. Kang[76], Y. Kano[114], J. Kanzaki[79], D. Kar[31f], K. Karava[132], M. J. Kareem[165b], I. Karkanias[160], S. N. Karpov[77], Z. M. Karpova[77], V. Kartvelishvili[87], A. N. Karyukhin[120], E. Kasimi[160], C. Kato[58d], J. Katzy[44], K. Kawade[148], K. Kawagoe[85], T. Kawaguchi[114], T. Kawamoto[142], G. Kawamura[51], E. F. Kay[173], F. I. Kaya[167], S. Kazakos[12], V. F. Kazanin[119b,119a], Y. Ke[153], J. M. Keaveney[31a], R. Keeler[173], J. S. Keller[32], D. Kelsey[154], J. J. Kempster[19], J. Kendrick[19], K. E. Kennedy[37], O. Kepka[138], S. Kersten[179], B. P. Kerševan[89], S. Ketabchi Haghighat[164], M. Khandoga[133], A. Khanov[127], A. G. Kharlamov[119b,119a], T. Kharlamova[119b,119a], E. E. Khoda[172], T. J. Khoo[17], G. Khoriauli[174], E. Khramov[77], J. Khubua[157b], S. Kido[80], M. Kiehn[34], A. Kilgallon[129], E. Kim[162], Y. K. Kim[35], N. Kimura[92], A. Kirchhoff[51], D. Kirchmeier[46], J. Kirk[141], A. E. Kiryunin[112], T. Kishimoto[161], D. P. Kisliuk[164], V. Kitali[44], C. Kitsaki[9], O. Kivernyk[22], T. Klapdor-Kleingrothaus[50], M. Klassen[59a], C. Klein[32], L. Klein[174], M. H. Klein[103], M. Klein[88], U. Klein[88], P. Klimek[34], A. Klimentov[27], F. Klimpel[34], T. Klingl[22], T. Klioutchnikova[34], F. F. Klitzner[111], P. Kluit[117], S. Kluth[112], E. Kneringer[74], T. M. Knight[164], A. Knue[50], D. Kobayashi[85], M. Kobel[46], M. Kocian[151], T. Kodama[161], P. Kodys[140], D. M. Koeck[154], P. T. Koenig[22], T. Koffas[32], N. M. Köhler[34], M. Kolb[142], I. Koletsou[4], T. Komarek[128], K. Köneke[50], A. X. Y. Kong[1], T. Kono[124], V. Konstantinides[92], N. Konstantinidis[92], B. Konya[94], R. Kopeliansky[63], S. Koperny[81a], K. Korcyl[82], K. Kordas[160], G. Koren[159], A. Korn[92], S. Korn[51], I. Korolkov[12], E. V. Korolkova[147], N. Korotkova[110], O. Kortner[112], S. Kortner[112], V. V. Kostyukhin[147,163], A. Kotsokechagia[62], A. Kotwal[47], A. Koulouris[8], A. Kourkoumeli-Charalampidi[68a,68b], C. Kourkoumelis[8], E. Kourlitis[5], R. Kowalewski[173], W. Kozanecki[142], A. S. Kozhin[120], V. A. Kramarenko[110], G. Kramberger[89], D. Krasnopevtsev[58a], M. W. Krasny[133], A. Krasznahorkay[34], J. A. Kremer[97], J. Kretzschmar[88], K. Kreul[17], P. Krieger[164], F. Krieter[111],

S. Krishnamurthy[100], A. Krishnan[59b], M. Krivos[140], K. Krizka[16], K. Kroeninger[45], H. Kroha[112], J. Kroll[138], J. Kroll[134], K. S. Krowpman[104], U. Kruchonak[77], H. Krüger[22], N. Krumnack[76], M. C. Kruse[47], J. A. Krzysiak[82], A. Kubota[162], O. Kuchinskaia[163], S. Kuday[3b], D. Kuechler[44], J. T. Kuechler[44], S. Kuehn[34], T. Kuhl[44], V. Kukhtin[77], Y. Kulchitsky[105,af], S. Kuleshov[144c], M. Kumar[31f], N. Kumari[99], M. Kuna[56], A. Kupco[138], T. Kupfer[45], O. Kuprash[50], H. Kurashige[80], L. L. Kurchaninov[165a], Y. A. Kurochkin[105], A. Kurova[109], M. G. Kurth[13a,13d], E. S. Kuwertz[34], M. Kuze[162], A. K. Kvam[146], J. Kvita[128], T. Kwan[101], C. Lacasta[171], F. Lacava[70a,70b], H. Lacker[17], D. Lacour[133], N. N. Lad[92], E. Ladygin[77], R. Lafaye[4], B. Laforge[133], T. Lagouri[144d], S. Lai[51], I. K. Lakomiec[81a], N. Lalloue[56], J. E. Lambert[126], S. Lammers[63], W. Lampl[6], C. Lampoudis[160], E. Lançon[27], U. Landgraf[50], M. P. J. Landon[90], V. S. Lang[50], J. C. Lange[51], R. J. Langenberg[100], A. J. Lankford[168], F. Lanni[27], K. Lantzsch[22], A. Lanza[68a], A. Lapertosa[53b,53a], J. F. Laporte[142], T. Lari[66a], F. Lasagni Manghi[21b], M. Lassnig[34], V. Latonova[138], T. S. Lau[60a], A. Laudrain[97], A. Laurier[32], M. Lavorgna[67a,67b], S. D. Lawlor[91], M. Lazzaroni[66a,66b], B. Le[98], A. Lebedev[76], M. LeBlanc[34], T. LeCompte[5], F. Ledroit-Guillon[56], A. C. A. Lee[92], C. A. Lee[27], G. R. Lee[15], L. Lee[57], S. C. Lee[156], S. Lee[76], L. L. Leeuw[31c], B. Lefebvre[165a], H. P. Lefebvre[91], M. Lefebvre[173], C. Leggett[16], K. Lehmann[150], N. Lehmann[18], G. Lehmann Miotto[34], W. A. Leight[44], A. Leisos[160,w], M. A. L. Leite[78c], C. E. Leitgeb[44], R. Leitner[140], K. J. C. Leney[40], T. Lenz[22], S. Leone[69a], C. Leonidopoulos[48], A. Leopold[133], C. Leroy[107], R. Les[104], C. G. Lester[30], M. Levchenko[135], J. Levêque[4], D. Levin[103], L. J. Levinson[177], D. J. Lewis[19], B. Li[13b], B. Li[103], C. Li[58a], C-Q. Li[58c,58d], H. Li[58a], H. Li[58b], J. Li[58c], K. Li[146], L. Li[58c], M. Li[13a,13d], Q. Y. Li[58a], S. Li[58d,58c,c], X. Li[44], Y. Li[44], Z. Li[58b], Z. Li[132], Z. Li[101], Z. Li[88], Z. Liang[13a], M. Liberatore[44], B. Liberti[71a], K. Lie[60c], K. Lin[104], R. A. Linck[63], R. E. Lindley[6], J. H. Lindon[2], A. Linss[44], A. L. Lionti[52], E. Lipeles[134], A. Lipniacka[15], T. M. Liss[170,aj], A. Lister[172], J. D. Little[7], B. Liu[13a], B. X. Liu[150], J. B. Liu[58a], J. K. K. Liu[35], K. Liu[58d,58c], M. Liu[58a], M. Y. Liu[58a], P. Liu[13a], X. Liu[58a], Y. Liu[44], Y. Liu[13c,13d], Y. L. Liu[103], Y. W. Liu[58a], M. Livan[68a,68b], A. Lleres[56], J. Llorente Merino[150], S. L. Lloyd[90], E. M. Lobodzinska[44], P. Loch[6], S. Loffredo[71a,71b], T. Lohse[17], K. Lohwasser[147], M. Lokajicek[138], J. D. Long[170], R. E. Long[87], I. Longarini[70a,70b], L. Longo[34], R. Longo[170], I. Lopez Paz[12], A. Lopez Solis[44], J. Lorenz[111], N. Lorenzo Martinez[4], A. M. Lory[111], A. Lösle[50], X. Lou[43a,43b], X. Lou[13a], A. Lounis[62], J. Love[5], P. A. Love[87], J. J. Lozano Bahilo[171], G. Lu[13a], M. Lu[58a], S. Lu[134], Y. J. Lu[61], H. J. Lubatti[146], C. Luci[70a,70b], F. L. Lucio Alves[13c], A. Lucotte[56], F. Luehring[63], I. Luise[153], L. Luminari[70a], B. Lund-Jensen[152], N. A. Luongo[129], M. S. Lutz[159], D. Lynn[27], H. Lyons[88], R. Lysak[138], E. Lytken[94], F. Lyu[13a], V. Lyubushkin[77], T. Lyubushkina[77], H. Ma[27], L. L. Ma[58b], Y. Ma[92], D. M. Mac Donell[173], G. Maccarrone[49], C. M. Macdonald[147], J. C. MacDonald[147], R. Madar[36], W. F. Mader[46], M. Madugoda Ralalage Don[127], N. Madysa[46], J. Maeda[80], T. Maeno[27], M. Maerker[46], V. Magerl[50], J. Magro[64a,64c], D. J. Mahon[37], C. Maidantchik[78b], A. Maio[137a,137b,137d], K. Maj[81a], O. Majersky[26a], S. Majewski[129], N. Makovec[62], B. Malaescu[133], Pa. Malecki[82], V. P. Maleev[135], F. Malek[56], D. Malito[39b,39a], U. Mallik[75], C. Malone[30], S. Maltezos[9], S. Malyukov[77], J. Mamuzic[171], G. Mancini[49], J. P. Mandalia[90], I. Mandić[89], L. Manhaes de Andrade Filho[78a], I. M. Maniatis[160], M. Manisha[142], J. Manjarres Ramos[46], K. H. Mankinen[94], A. Mann[111], A. Manousos[74], B. Mansoulie[142], I. Manthos[160], S. Manzoni[117], A. Marantis[160,w], L. Marchese[132], G. Marchiori[133], M. Marcisovsky[138], L. Marcoccia[71a,71b], C. Marcon[94], M. Marjanovic[126], Z. Marshall[16], S. Marti-Garcia[171], T. A. Martin[175], V. J. Martin[48], B. Martin dit Latour[15], L. Martinelli[72a,72b], M. Martinez[12,x], P. Martinez Agullo[171], V. I. Martinez Outschoorn[100], S. Martin-Haugh[141], V. S. Martoiu[25b], A. C. Martyniuk[92], A. Marzin[34], S. R. Maschek[112], L. Masetti[97], T. Mashimo[161], R. Mashinistov[108], J. Masik[98], A. L. Maslennikov[119b,119a], L. Massa[21b], P. Massarotti[67a,67b], P. Mastrandrea[69a,69b], A. Mastroberardino[39b,39a], T. Masubuchi[161], D. Matakias[27], T. Mathisen[169], A. Matic[111], N. Matsuzawa[161], J. Maurer[25b], B. Maček[89], D. A. Maximov[119b,119a], R. Mazini[156], I. Maznas[160], S. M. Mazza[143], C. Mc Ginn[27], J. P. Mc Gowan[101], S. P. Mc Kee[103], T. G. McCarthy[112], W. P. McCormack[16], E. F. McDonald[102], A. E. McDougall[117], J. A. Mcfayden[154], G. Mchedlidze[157b], M. A. McKay[40], K. D. McLean[173], S. J. McMahon[141], P. C. McNamara[102], R. A. McPherson[173,aa], J. E. Mdhluli[31f], Z. A. Meadows[100], S. Meehan[34], T. Megy[36], S. Mehlhase[111], A. Mehta[88], B. Meirose[41], D. Melini[158], B. R. Mellado Garcia[31f], F. Meloni[44], A. Melzer[22], E. D. Mendes Gouveia[137a], A. M. Mendes Jacques Da Costa[19], H. Y. Meng[164], L. Meng[34], S. Menke[112], M. Mentink[34], E. Meoni[39b,39a], S. A. M. Merkt[136], C. Merlassino[132], P. Mermod[52,*], L. Merola[67a,67b], C. Meroni[66a], G. Merz[103], O. Meshkov[110,108], J. K. R. Meshreki[149], J. Metcalfe[5], A. S. Mete[5], C. Meyer[63], J-P. Meyer[142], M. Michetti[17], R. P. Middleton[141], L. Mijović[48], G. Mikenberg[177],

M. Mikestikova[138], M. Mikuž[89], H. Mildner[147], A. Milic[164], C. D. Milke[40], D. W. Miller[35], L. S. Miller[32], A. Milov[177], D. A. Milstead[43a,43b], A. A. Minaenko[120], I. A. Minashvili[157b], L. Mince[55], A. I. Mincer[123], B. Mindur[81a], M. Mineev[77], Y. Minegishi[161], Y. Mino[83], L. M. Mir[12], M. Miralles Lopez[171], M. Mironova[132], T. Mitani[176], V. A. Mitsou[171], M. Mittal[58c], O. Miu[164], P. S. Miyagawa[90], Y. Miyazaki[85], A. Mizukami[79], J. U. Mjörnmark[94], T. Mkrtchyan[59a], M. Mlynarikova[118], T. Moa[43a,43b], S. Mobius[51], K. Mochizuki[107], P. Moder[44], P. Mogg[111], S. Mohapatra[37], G. Mokgatitswane[31f], B. Mondal[149], S. Mondal[139], K. Mönig[44], E. Monnier[99], A. Montalbano[150], J. Montejo Berlingen[34], M. Montella[125], F. Monticelli[86], N. Morange[62], A. L. Moreira De Carvalho[137a], M. Moreno Llácer[171], C. Moreno Martinez[12], P. Morettini[53b], M. Morgenstern[158], S. Morgenstern[175], D. Mori[150], M. Morii[57], M. Morinaga[161], V. Morisbak[131], A. K. Morley[34], A. P. Morris[92], L. Morvaj[34], P. Moschovakos[34], B. Moser[117], M. Mosidze[157b], T. Moskalets[50], P. Moskvitina[116], J. Moss[29,o], E. J. W. Moyse[100], S. Muanza[99], J. Mueller[136], D. Muenstermann[87], G. A. Mullier[94], J. J. Mullin[134], D. P. Mungo[66a,66b], J. L. Munoz Martinez[12], F. J. Munoz Sanchez[98], M. Murin[98], P. Murin[26b], W. J. Murray[175,141], A. Murrone[66a,66b], J. M. Muse[126], M. Muškinja[16], C. Mwewa[27], A. G. Myagkov[120,ag], A. A. Myers[136], G. Myers[63], J. Myers[129], M. Myska[139], B. P. Nachman[16], O. Nackenhorst[45], A. Nag Nag[46], K. Nagai[132], K. Nagano[79], J. L. Nagle[27], E. Nagy[99], A. M. Nairz[34], Y. Nakahama[114], K. Nakamura[79], H. Nanjo[130], F. Napolitano[59a], R. Narayan[40], I. Naryshkin[135], M. Naseri[32], C. Nass[22], T. Naumann[44], G. Navarro[20a], J. Navarro-Gonzalez[171], P. Y. Nechaeva[108], F. Nechansky[44], T. J. Neep[19], A. Negri[68a,68b], M. Negrini[21b], C. Nellist[116], C. Nelson[101], K. Nelson[103], M. E. Nelson[43a,43b], S. Nemecek[138], M. Nessi[34,g], M. S. Neubauer[170], F. Neuhaus[97], J. Neundorf[44], R. Newhouse[172], P. R. Newman[19], C. W. Ng[136], Y. S. Ng[17], Y. W. Y. Ng[168], B. Ngair[33e], H. D. N. Nguyen[99], T. Nguyen Manh[107], R. B. Nickerson[132], R. Nicolaidou[142], D. S. Nielsen[38], J. Nielsen[143], M. Niemeyer[51], N. Nikiforou[10], V. Nikolaenko[120,ag], I. Nikolic-Audit[133], K. Nikolopoulos[19], P. Nilsson[27], H. R. Nindhito[52], A. Nisati[70a], N. Nishu[2], R. Nisius[112], T. Nitta[176], T. Nobe[161], D. L. Noel[30], Y. Noguchi[83], I. Nomidis[133], M. A. Nomura[27], M. B. Norfolk[147], R. R. B. Norisam[92], J. Novak[89], T. Novak[44], O. Novgorodova[46], L. Novotny[139], R. Novotny[115], L. Nozka[128], K. Ntekas[168], E. Nurse[92], F. G. Oakham[32,ak], J. Ocariz[133], A. Ochi[80], I. Ochoa[137a], J. P. Ochoa-Ricoux[144a], K. O'Connor[24], S. Oda[85], S. Odaka[79], S. Oerdek[51], A. Ogrodnik[81a], A. Oh[98], C. C. Ohm[152], H. Oide[162], R. Oishi[161], M. L. Ojeda[164], Y. Okazaki[83], M. W. O'Keefe[88], Y. Okumura[161], A. Olariu[25b], L. F. Oleiro Seabra[137a], S. A. Olivares Pino[144d], D. Oliveira Damazio[27], D. Oliveira Goncalves[78a], J. L. Oliver[1], M. J. R. Olsson[168], A. Olszewski[82], J. Olszowska[82], Ö. O. Öncel[22], D. C. O'Neil[150], A. P. O'neill[132], A. Onofre[137a,137e], P. U. E. Onyisi[10], H. Oppen[131], R. G. Oreamuno Madriz[118], M. J. Oreglia[35], G. E. Orellana[86], D. Orestano[72a,72b], N. Orlando[12], R. S. Orr[164], V. O'Shea[55], R. Ospanov[58a], G. Otero y Garzon[28], H. Otono[85], P. S. Ott[59a], G. J. Ottino[16], M. Ouchrif[33d], J. Ouellette[27], F. Ould-Saada[131], A. Ouraou[142,*], Q. Ouyang[13a], M. Owen[55], R. E. Owen[141], V. E. Ozcan[11c], N. Ozturk[7], S. Ozturk[11c], J. Pacalt[128], H. A. Pacey[30], K. Pachal[47], A. Pacheco Pages[12], C. Padilla Aranda[12], S. Pagan Griso[16], G. Palacino[63], S. Palazzo[48], S. Palestini[34], M. Palka[81b], P. Palni[81a], D. K. Panchal[10], C. E. Pandini[52], J. G. Panduro Vazquez[91], P. Pani[44], G. Panizzo[64a,64c], L. Paolozzi[52], C. Papadatos[107], S. Parajuli[40], A. Paramonov[5], C. Paraskevopoulos[9], D. Paredes Hernandez[60b], S. R. Paredes Saenz[132], B. Parida[177], T. H. Park[164], A. J. Parker[29], M. A. Parker[30], F. Parodi[53b,53a], E. W. Parrish[118], J. A. Parsons[37], U. Parzefall[50], L. Pascual Dominguez[159], V. R. Pascuzzi[16], F. Pasquali[117], E. Pasqualucci[70a], S. Passaggio[53b], F. Pastore[91], P. Pasuwan[43a,43b], J. R. Pater[98], A. Pathak[178], J. Patton[88], T. Pauly[34], J. Pearkes[151], M. Pedersen[131], L. Pedraza Diaz[116], R. Pedro[137a], T. Peiffer[51], S. V. Peleganchuk[119b,119a], O. Penc[138], C. Peng[60b], H. Peng[58a], M. Penzin[163], B. S. Peralva[78a], M. M. Perego[62], A. P. Pereira Peixoto[137a], L. Pereira Sanchez[43a,43b], D. V. Perepelitsa[27], E. Perez Codina[165a], M. Perganti[9], L. Perini[66a,66b], H. Pernegger[34], S. Perrella[34], A. Perrevoort[117], K. Peters[44], R. F. Y. Peters[98], B. A. Petersen[34], T. C. Petersen[38], E. Petit[99], V. Petousis[139], C. Petridou[160], P. Petroff[62], F. Petrucci[72a,72b], M. Pettee[180], N. E. Pettersson[34], K. Petukhova[140], A. Peyaud[142], R. Pezoa[144e], L. Pezzotti[68a,68b], G. Pezzullo[180], T. Pham[102], P. W. Phillips[141], M. W. Phipps[170], G. Piacquadio[153], E. Pianori[16], F. Piazza[66a,66b], A. Picazio[100], R. Piegaia[28], D. Pietreanu[25b], J. E. Pilcher[35], A. D. Pilkington[98], M. Pinamonti[64a,64c], J. L. Pinfold[2], C. Pitman Donaldson[92], D. A. Pizzi[32], L. Pizzimento[71a,71b], A. Pizzini[117], M.-A. Pleier[27], V. Plesanovs[50], V. Pleskot[140], E. Plotnikova[77], P. Podberezko[119b,119a], R. Poettgen[94], R. Poggi[52], L. Poggioli[133], I. Pogrebnyak[104], D. Pohl[22], I. Pokharel[51], G. Polesello[68a], A. Poley[150,165a], A. Policicchio[70a,70b], R. Polifka[140], A. Polini[21b], C. S. Pollard[44], Z. B. Pollock[125], V. Polychronakos[27], D. Ponomarenko[109], L. Pontecorvo[34], S. Popa[25a], G. A. Popeneciu[25d], L. Portales[4], D. M. Portillo Quintero[56],

S. Pospisil[139], P. Postolache[25c], K. Potamianos[132], I. N. Potrap[77], C. J. Potter[30], H. Potti[1], T. Poulsen[44], J. Poveda[171], T. D. Powell[147], G. Pownall[44], M. E. Pozo Astigarraga[34], A. Prades Ibanez[171], P. Pralavorio[99], M. M. Prapa[42], S. Prell[76], D. Price[98], M. Primavera[65a], M. A. Principe Martin[96], M. L. Proffitt[146], N. Proklova[109], K. Prokofiev[60c], F. Prokoshin[77], S. Protopopescu[27], J. Proudfoot[5], M. Przybycien[81a], D. Pudzha[135], P. Puzo[62], D. Pyatiizbyantseva[109], J. Qian[103], Y. Qin[98], A. Quadt[51], M. Queitsch-Maitland[34], G. Rabanal Bolanos[57], F. Ragusa[66a,66b], G. Rahal[95], J. A. Raine[52], S. Rajagopalan[27], K. Ran[13a,13d], D. F. Rassloff[59a], D. M. Rauch[44], S. Rave[97], B. Ravina[55], I. Ravinovich[177], M. Raymond[34], A. L. Read[131], N. P. Readioff[147], D. M. Rebuzzi[68a,68b], G. Redlinger[27], K. Reeves[41], D. Reikher[159], A. Reiss[97], A. Rej[149], C. Rembser[34], A. Renardi[44], M. Renda[25b], M. B. Rendel[112], A. G. Rennie[55], S. Resconi[66a], E. D. Resseguie[16], S. Rettie[92], B. Reynolds[125], E. Reynolds[19], M. Rezaei Estabragh[179], O. L. Rezanova[119b,119a], P. Reznicek[140], E. Ricci[73a,73b], R. Richter[112], S. Richter[44], E. Richter-Was[81b], M. Ridel[133], P. Rieck[112], P. Riedler[34], O. Rifki[44], M. Rijssenbeek[153], A. Rimoldi[68a,68b], M. Rimoldi[44], L. Rinaldi[21b,21a], T. T. Rinn[170], M. P. Rinnagel[111], G. Ripellino[152], I. Riu[12], P. Rivadeneira[44], J. C. Rivera Vergara[173], F. Rizatdinova[127], E. Rizvi[90], C. Rizzi[52], B. A. Roberts[175], S. H. Robertson[101,aa], M. Robin[44], D. Robinson[30], C. M. Robles Gajardo[144e], M. Robles Manzano[97], A. Robson[55], A. Rocchi[71a,71b], C. Roda[69a,69b], S. Rodriguez Bosca[59a], A. Rodriguez Rodriguez[50], A. M. Rodríguez Vera[165b], S. Roe[34], J. Roggel[179], O. Røhne[131], R. A. Rojas[144e], B. Roland[50], C. P. A. Roland[63], J. Roloff[27], A. Romaniouk[109], M. Romano[21b], N. Rompotis[88], M. Ronzani[123], L. Roos[133], S. Rosati[70a], G. Rosin[100], B. J. Rosser[134], E. Rossi[164], E. Rossi[4], E. Rossi[67a,67b], L. P. Rossi[53b], L. Rossini[44], R. Rosten[125], M. Rotaru[25b], B. Rottler[50], D. Rousseau[62], D. Rousso[30], G. Rovelli[68a,68b], A. Roy[10], A. Rozanov[99], Y. Rozen[158], X. Ruan[31f], A. J. Ruby[88], T. A. Ruggeri[1], F. Rühr[50], A. Ruiz-Martinez[171], A. Rummler[34], Z. Rurikova[50], N. A. Rusakovich[77], H. L. Russell[34], L. Rustige[36], J. P. Rutherfoord[6], E. M. Rüttinger[147], M. Rybar[140], E. B. Rye[131], A. Ryzhov[120], J. A. Sabater Iglesias[44], P. Sabatini[171], L. Sabetta[70a,70b], H. F-W. Sadrozinski[143], R. Sadykov[77], F. Safai Tehrani[70a], B. Safarzadeh Samani[154], M. Safdari[151], P. Saha[118], S. Saha[101], M. Sahinsoy[112], A. Sahu[179], M. Saimpert[142], M. Saito[161], T. Saito[161], D. Salamani[52], G. Salamanna[72a,72b], A. Salnikov[151], J. Salt[171], A. Salvador Salas[12], D. Salvatore[39b,39a], F. Salvatore[154], A. Salzburger[34], D. Sammel[50], D. Sampsonidis[160], D. Sampsonidou[58d,58c], J. Sánchez[171], A. Sanchez Pineda[4], V. Sanchez Sebastian[171], H. Sandaker[131], C. O. Sander[44], I. G. Sanderswood[87], J. A. Sandesara[100], M. Sandhoff[179], C. Sandoval[20b], D. P. C. Sankey[141], M. Sannino[53b,53a], Y. Sano[114], A. Sansoni[49], C. Santoni[36], H. Santos[137a,137b], S. N. Santpur[16], A. Santra[177], K. A. Saoucha[147], A. Sapronov[77], J. G. Saraiva[137a,137d], J. Sardain[99], O. Sasaki[79], K. Sato[166], C. Sauer[59b], F. Sauerburger[50], E. Sauvan[4], P. Savard[164,ak], R. Sawada[161], C. Sawyer[141], L. Sawyer[93], I. Sayago Galvan[171], C. Sbarra[21b], A. Sbrizzi[64a,64c], T. Scanlon[92], J. Schaarschmidt[146], P. Schacht[112], D. Schaefer[35], L. Schaefer[134], U. Schäfer[97], A. C. Schaffer[62], D. Schaile[111], R. D. Schamberger[153], E. Schanet[111], C. Scharf[17], N. Scharmberg[98], V. A. Schegelsky[135], D. Scheirich[140], F. Schenck[17], M. Schernau[168], C. Schiavi[53b,53a], L. K. Schildgen[22], Z. M. Schillaci[24], E. J. Schioppa[65a,65b], M. Schioppa[39b,39a], B. Schlag[97], K. E. Schleicher[50], S. Schlenker[34], K. Schmieden[97], C. Schmitt[97], S. Schmitt[44], L. Schoeffel[142], A. Schoening[59b], P. G. Scholer[50], E. Schopf[132], M. Schott[97], J. Schovancova[34], S. Schramm[52], F. Schroeder[179], H-C. Schultz-Coulon[59a], M. Schumacher[50], B. A. Schumm[143], Ph. Schune[142], A. Schwartzman[151], T. A. Schwarz[103], Ph. Schwemling[142], R. Schwienhorst[104], A. Sciandra[143], G. Sciolla[24], F. Scuri[69a], F. Scutti[102], C. D. Sebastiani[88], K. Sedlaczek[45], P. Seema[17], S. C. Seidel[115], A. Seiden[143], B. D. Seidlitz[27], T. Seiss[35], C. Seitz[44], J. M. Seixas[78b], G. Sekhniaidze[67a], S. J. Sekula[40], L. P. Selem[4], N. Semprini-Cesari[21b,21a], S. Sen[47], C. Serfon[27], L. Serin[62], L. Serkin[64a,64b], M. Sessa[58a], H. Severini[126], S. Sevova[151], F. Sforza[53b,53a], A. Sfyrla[52], E. Shabalina[51], R. Shaheen[152], J. D. Shahinian[134], N. W. Shaikh[43a,43b], D. Shaked Renous[177], L. Y. Shan[13a], M. Shapiro[16], A. Sharma[34], A. S. Sharma[1], S. Sharma[44], P. B. Shatalov[121], K. Shaw[154], S. M. Shaw[98], P. Sherwood[92], L. Shi[92], C. O. Shimmin[180], Y. Shimogama[176], M. Shimojima[113], J. D. Shinner[91], I. P. J. Shipsey[132], S. Shirabe[52], M. Shiyakova[77], J. Shlomi[177], M. J. Shochet[35], J. Shojaii[102], D. R. Shope[152], S. Shrestha[125], E. M. Shrif[31f], M. J. Shroff[173], E. Shulga[177], P. Sicho[138], A. M. Sickles[170], E. Sideras Haddad[31f], O. Sidiropoulou[34], A. Sidoti[21b], F. Siegert[46], Dj. Sijacki[14], M. V. Silva Oliveira[34], S. B. Silverstein[43a], S. Simion[62], R. Simoniello[34], S. Simsek[11b], P. Sinervo[164], V. Sinetckii[110], S. Singh[150], S. Sinha[44], S. Sinha[31f], M. Sioli[21b,21a], I. Siral[129], S. Yu. Sivoklokov[110], J. Sjölin[43a,43b], A. Skaf[51], E. Skorda[94], P. Skubic[126], M. Slawinska[82], K. Sliwa[167], V. Smakhtin[177], B. H. Smart[141], J. Smiesko[140], S. Yu. Smirnov[109], Y. Smirnov[109], L. N. Smirnova[110,s], O. Smirnova[94], E. A. Smith[35],

H. A. Smith[132], M. Smizanska[87], K. Smolek[139], A. Smykiewicz[82], A. A. Snesarev[108], H. L. Snoek[117], S. Snyder[27], R. Sobie[173,aa], A. Soffer[159], F. Sohns[51], C. A. Solans Sanchez[34], E. Yu. Soldatov[109], U. Soldevila[171], A. A. Solodkov[120], S. Solomon[50], A. Soloshenko[77], O. V. Solovyanov[120], V. Solovyev[135], P. Sommer[147], H. Son[167], A. Sonay[12], W. Y. Song[165b], A. Sopczak[139], A. L. Sopio[92], F. Sopkova[26b], S. Sottocornola[68a,68b], R. Soualah[64a,64c], A. M. Soukharev[119b,119a], Z. Soumaimi[33e], D. South[44], S. Spagnolo[65a,65b], M. Spalla[112], M. Spangenberg[175], F. Spanò[91], D. Sperlich[50], T. M. Spieker[59a], G. Spigo[34], M. Spina[154], D. P. Spiteri[55], M. Spousta[140], A. Stabile[66a,66b], B. L. Stamas[118], R. Stamen[59a], M. Stamenkovic[117], A. Stampekis[19], M. Standke[22], E. Stanecka[82], B. Stanislaus[34], M. M. Stanitzki[44], M. Stankaityte[132], B. Stapf[44], E. A. Starchenko[120], G. H. Stark[143], J. Stark[99], D. M. Starko[165b], P. Staroba[138], P. Starovoitov[59a], S. Stärz[101], R. Staszewski[82], G. Stavropoulos[42], P. Steinberg[27], A. L. Steinhebel[129], B. Stelzer[150,165a], H. J. Stelzer[136], O. Stelzer-Chilton[165a], H. Stenzel[54], T. J. Stevenson[154], G. A. Stewart[34], M. C. Stockton[34], G. Stoicea[25b], M. Stolarski[137a], S. Stonjek[112], A. Straessner[46], J. Strandberg[152], S. Strandberg[43a,43b], M. Strauss[126], T. Strebler[99], P. Strizenec[26b], R. Ströhmer[174], D. M. Strom[129], L. R. Strom[44], R. Stroynowski[40], A. Strubig[43a,43b], S. A. Stucci[27], B. Stugu[15], J. Stupak[126], N. A. Styles[44], D. Su[151], S. Su[58a], W. Su[58d,146,58c], X. Su[58a], N. B. Suarez[136], K. Sugizaki[161], V. V. Sulin[108], M. J. Sullivan[88], D. M. S. Sultan[52], S. Sultansoy[3c], T. Sumida[83], S. Sun[103], S. Sun[178], X. Sun[98], O. Sunneborn Gudnadottir[169], C. J. E. Suster[155], M. R. Sutton[154], M. Svatos[138], M. Swiatlowski[165a], T. Swirski[174], I. Sykora[26a], M. Sykora[140], T. Sykora[140], D. Ta[97], K. Tackmann[44,y], A. Taffard[168], R. Tafirout[165a], E. Tagiev[120], R. H. M. Taibah[133], R. Takashima[84], K. Takeda[80], T. Takeshita[148], E. P. Takeva[48], Y. Takubo[79], M. Talby[99], A. A. Talyshev[119b,119a], K. C. Tam[60b], N. M. Tamir[159], A. Tanaka[161], J. Tanaka[161], R. Tanaka[62], Z. Tao[172], S. Tapia Araya[76], S. Tapprogge[97], A. Tarek Abouelfadl Mohamed[104], S. Tarem[158], K. Tariq[58b], G. Tarna[25b,f], G. F. Tartarelli[66a], P. Tas[140], M. Tasevsky[138], E. Tassi[39b,39a], G. Tateno[161], Y. Tayalati[33e], G. N. Taylor[102], W. Taylor[165b], H. Teagle[88], A. S. Tee[87], R. Teixeira De Lima[151], P. Teixeira-Dias[91], H. Ten Kate[34], J. J. Teoh[117], K. Terashi[161], J. Terron[96], S. Terzo[12], M. Testa[49], R. J. Teuscher[164,aa], N. Themistokleous[48], T. Theveneaux-Pelzer[17], D. W. Thomas[91], J. P. Thomas[19], E. A. Thompson[44], P. D. Thompson[19], E. Thomson[134], E. J. Thorpe[90], Y. Tian[51], V. O. Tikhomirov[108,ah], Yu. A. Tikhonov[119b,119a], S. Timoshenko[109], P. Tipton[180], S. Tisserant[99], S. H. Tlou[31f], A. Tnourji[36], K. Todome[21b,21a], S. Todorova-Nova[140], S. Todt[46], M. Togawa[79], J. Tojo[85], S. Tokár[26a], K. Tokushuku[79], E. Tolley[125], R. Tombs[30], M. Tomoto[79,114], L. Tompkins[151], P. Tornambe[100], E. Torrence[129], H. Torres[46], E. Torró Pastor[171], M. Toscani[28], C. Tosciri[35], J. Toth[99,z], D. R. Tovey[147], A. Traeet[15], C. J. Treado[123], T. Trefzger[174], A. Tricoli[27], I. M. Trigger[165a], S. Trincaz-Duvoid[133], D. A. Trischuk[172], W. Trischuk[164], B. Trocmé[56], A. Trofymov[62], C. Troncon[66a], F. Trovato[154], L. Truong[31c], M. Trzebinski[82], A. Trzupek[82], F. Tsai[153], A. Tsiamis[160], P. V. Tsiareshka[105,af], A. Tsirigotis[160,w], V. Tsiskaridze[153], E. G. Tskhadadze[157a], M. Tsopoulou[160], I. I. Tsukerman[121], V. Tsulaia[16], S. Tsuno[79], O. Tsur[158], D. Tsybychev[153], Y. Tu[60b], A. Tudorache[25b], V. Tudorache[25b], A. N. Tuna[34], S. Turchikhin[77], D. Turgeman[177], I. Turk Cakir[3b,u], R. J. Turner[19], R. Turra[66a], P. M. Tuts[37], S. Tzamarias[160], P. Tzanis[9], E. Tzovara[97], K. Uchida[161], F. Ukegawa[166], G. Unal[34], M. Unal[10], A. Undrus[27], G. Unel[168], F. C. Ungaro[102], K. Uno[161], J. Urban[26b], P. Urquijo[102], G. Usai[7], R. Ushioda[162], M. Usman[107], Z. Uysal[11d], V. Vacek[139], B. Vachon[101], K. O. H. Vadla[131], T. Vafeiadis[34], C. Valderanis[111], E. Valdes Santurio[43a,43b], M. Valente[165a], S. Valentinetti[21b,21a], A. Valero[171], L. Valéry[44], R. A. Vallance[19], A. Vallier[99], J. A. Valls Ferrer[171], T. R. Van Daalen[12], P. Van Gemmeren[5], S. Van Stroud[92], I. Van Vulpen[117], M. Vanadia[71a,71b], W. Vandelli[34], M. Vandenbroucke[142], E. R. Vandewall[127], D. Vannicola[70a,70b], L. Vannoli[53b,53a], R. Vari[70a], E. W. Varnes[6], C. Varni[53b,53a], T. Varol[156], D. Varouchas[62], K. E. Varvell[155], M. E. Vasile[25b], L. Vaslin[36], G. A. Vasquez[173], F. Vazeille[36], D. Vazquez Furelos[12], T. Vazquez Schroeder[34], J. Veatch[51], V. Vecchio[98], M. J. Veen[117], I. Veliscek[132], L. M. Veloce[164], F. Veloso[137a,137c], S. Veneziano[70a], A. Ventura[65a,65b], A. Verbytskyi[112], M. Verducci[69a,69b], C. Vergis[22], M. Verissimo De Araujo[78b], W. Verkerke[117], A. T. Vermeulen[117], J. C. Vermeulen[117], C. Vernieri[151], P. J. Verschuuren[91], M. L. Vesterbacka[123], M. C. Vetterli[150,ak], N. Viaux Maira[144e], T. Vickey[147], O. E. Vickey Boeriu[147], G. H. A. Viehhauser[132], L. Vigani[59b], M. Villa[21b,21a], M. Villaplana Perez[171], E. M. Villhauer[48], E. Vilucchi[49], M. G. Vincter[32], G. S. Virdee[19], A. Vishwakarma[48], C. Vittori[21b,21a], I. Vivarelli[154], V. Vladimirov[175], E. Voevodina[112], M. Vogel[179], P. Vokac[139], J. Von Ahnen[44], S. E. von Buddenbrock[31f], E. Von Toerne[22], V. Vorobel[140], K. Vorobev[109], M. Vos[171], J. H. Vossebeld[88], M. Vozak[98], N. Vranjes[14], M. Vranjes Milosavljevic[14], V. Vrba[139,*], M. Vreeswijk[117], N. K. Vu[99], R. Vuillermet[34], I. Vukotic[35], S. Wada[166], C. Wagner[100], P. Wagner[22],

W. Wagner[179], S. Wahdan[179], H. Wahlberg[86], R. Wakasa[166], M. Wakida[114], V. M. Walbrecht[112], J. Walder[141], R. Walker[111], S. D. Walker[91], W. Walkowiak[149], A. M. Wang[57], A. Z. Wang[178], C. Wang[58a], C. Wang[58c], H. Wang[16], J. Wang[60a], P. Wang[40], R.-J. Wang[97], R. Wang[57], R. Wang[118], S. M. Wang[156], S. Wang[58b], T. Wang[58a], W. T. Wang[58a], W. X. Wang[58a], X. Wang[170], Y. Wang[58a], Z. Wang[103], C. Wanotayaroj[34], A. Warburton[101], C. P. Ward[30], R. J. Ward[19], N. Warrack[55], A. T. Watson[19], M. F. Watson[19], G. Watts[146], B. M. Waugh[92], A. F. Webb[10], C. Weber[27], M. S. Weber[18], S. A. Weber[32], S. M. Weber[59a], C. Wei[58a], Y. Wei[132], A. R. Weidberg[132], J. Weingarten[45], M. Weirich[97], C. Weiser[50], T. Wenaus[27], B. Wendland[45], T. Wengler[34], S. Wenig[34], N. Wermes[22], M. Wessels[59a], K. Whalen[129], A. M. Wharton[87], A. S. White[57], A. White[7], M. J. White[1], D. Whiteson[168], W. Wiedenmann[178], C. Wiel[46], M. Wielers[141], N. Wieseotte[97], C. Wiglesworth[38], L. A. M. Wiik-Fuchs[50], D. J. Wilbern[126], H. G. Wilkens[34], L. J. Wilkins[91], D. M. Williams[37], H. H. Williams[134], S. Williams[30], S. Willocq[100], P. J. Windischhofer[132], I. Wingerter-Seez[4], F. Winklmeier[129], B. T. Winter[50], M. Wittgen[151], M. Wobisch[93], A. Wolf[97], R. Wölker[132], J. Wollrath[168], M. W. Wolter[82], H. Wolters[137a,137c], V. W. S. Wong[172], A. F. Wongel[44], S. D. Worm[44], B. K. Wosiek[82], K. W. Woźniak[82], K. Wraight[55], J. Wu[13a,13d], S. L. Wu[178], X. Wu[52], Y. Wu[58a], Z. Wu[142,58a], J. Wuerzinger[132], T. R. Wyatt[98], B. M. Wynne[48], S. Xella[38], J. Xiang[60c], X. Xiao[103], X. Xie[58a], I. Xiotidis[154], D. Xu[13a], H. Xu[58a], H. Xu[58a], L. Xu[58a], R. Xu[134], W. Xu[103], Y. Xu[13b], Z. Xu[58b], Z. Xu[151], B. Yabsley[155], S. Yacoob[31a], N. Yamaguchi[85], Y. Yamaguchi[162], M. Yamatani[161], H. Yamauchi[166], T. Yamazaki[16], Y. Yamazaki[80], J. Yan[58c], Z. Yan[23], H. J. Yang[58c,58d], H. T. Yang[16], S. Yang[58a], T. Yang[60c], X. Yang[58a], X. Yang[13a], Y. Yang[161], Z. Yang[103,58a], W-M. Yao[16], Y. C. Yap[44], H. Ye[13c], J. Ye[40], S. Ye[27], I. Yeletskikh[77], M. R. Yexley[87], P. Yin[37], K. Yorita[176], K. Yoshihara[76], C. J. S. Young[34], C. Young[151], R. Yuan[58b,j], X. Yue[59a], M. Zaazoua[33e], B. Zabinski[82], G. Zacharis[9], E. Zaffaroni[52], A. M. Zaitsev[120,ag], T. Zakareishvili[157b], N. Zakharchuk[32], S. Zambito[34], D. Zanzi[50], S. V. Zeißner[45], C. Zeitnitz[179], G. Zemaityte[132], J. C. Zeng[170], O. Zenin[120], T. Ženiš[26a], S. Zenz[90], S. Zerradi[33a], D. Zerwas[62], M. Zgubič[132], B. Zhang[13c], D. F. Zhang[13b], G. Zhang[13b], J. Zhang[5], K. Zhang[13a], L. Zhang[13c], M. Zhang[170], R. Zhang[178], S. Zhang[103], X. Zhang[58c], X. Zhang[58b], Z. Zhang[62], P. Zhao[47], Y. Zhao[143], Z. Zhao[58a], A. Zhemchugov[77], Z. Zheng[103], D. Zhong[170], B. Zhou[103], C. Zhou[178], H. Zhou[6], N. Zhou[58c], Y. Zhou[6], C. G. Zhu[58b], C. Zhu[13a,13d], H. L. Zhu[58a], H. Zhu[13a], J. Zhu[103], Y. Zhu[58a], X. Zhuang[13a], K. Zhukov[108], V. Zhulanov[119b,119a], D. Zieminska[63], N. I. Zimine[77], S. Zimmermann[50,*], M. Ziolkowski[149], L. Živković[14], A. Zoccoli[21b,21a], K. Zoch[52], T. G. Zorbas[147], O. Zormpa[42], W. Zou[37], L. Zwalinski[34]

[1] Department of Physics, University of Adelaide, Adelaide, Australia
[2] Department of Physics, University of Alberta, Edmonton, AB, Canada
[3] [(a)]Department of Physics, Ankara University, Ankara, Turkey; [(b)]Application and Research Center for Advanced Studies, Istanbul Aydin University, Istanbul, Turkey; [(c)]Division of Physics, TOBB University of Economics and Technology, Ankara, Turkey
[4] LAPP, Univ. Savoie Mont Blanc, CNRS/IN2P3, Annecy , France
[5] High Energy Physics Division, Argonne National Laboratory, Argonne, IL, USA
[6] Department of Physics, University of Arizona, Tucson, AZ, USA
[7] Department of Physics , University of Texas at Arlington, Arlington, TX, USA
[8] Physics Department, National and Kapodistrian University of Athens, Athens, Greece
[9] Physics Department, National Technical University of Athens, Zografou, Greece
[10] Department of Physics, University of Texas at Austin, Austin, TX, USA
[11] [(a)]Faculty of Engineering and Natural Sciences, Bahcesehir University, Istanbul, Turkey; [(b)]Faculty of Engineering and Natural Sciences, Istanbul Bilgi University, Istanbul, Turkey; [(c)]Department of Physics, Bogazici University, Istanbul, Turkey; [(d)]Department of Physics Engineering, Gaziantep University, Gaziantep, Turkey
[12] Institut de Física d'Altes Energies (IFAE), Barcelona Institute of Science and Technology, Barcelona, Spain
[13] [(a)]Institute of High Energy Physics, Chinese Academy of Sciences, Beijing, China; [(b)]Physics Department, Tsinghua University, Beijing, China; [(c)]Department of Physics, Nanjing University, Nanjing, China; [(d)]University of Chinese Academy of Science (UCAS), Beijing, China
[14] Institute of Physics, University of Belgrade, Belgrade, Serbia
[15] Department for Physics and Technology, University of Bergen, Bergen, Norway
[16] Physics Division, Lawrence Berkeley National Laboratory and University of California, Berkeley, CA, USA

[17] Institut für Physik, Humboldt Universität zu Berlin, Berlin, Germany
[18] Albert Einstein Center for Fundamental Physics and Laboratory for High Energy Physics, University of Bern, Bern, Switzerland
[19] School of Physics and Astronomy, University of Birmingham, Birmingham, UK
[20] [(a)]Facultad de Ciencias y Centro de Investigaciónes, Universidad Antonio Nariño, Bogotá, Colombia; [(b)]Departamento de Física, Universidad Nacional de Colombia, Bogotá, Colombia
[21] [(a)]Dipartimento di Fisica e Astronomia A. Righi, Università di Bologna, Bologna, Italy; [(b)]INFN Sezione di Bologna, Bologna, Italy
[22] Physikalisches Institut, Universität Bonn, Bonn, Germany
[23] Department of Physics, Boston University, Boston, MA, USA
[24] Department of Physics, Brandeis University, Waltham, MA, USA
[25] [(a)]Transilvania University of Brasov, Brasov, Romania; [(b)]Horia Hulubei National Institute of Physics and Nuclear Engineering, Bucharest, Romania; [(c)]Department of Physics, Alexandru Ioan Cuza University of Iasi, Iasi, Romania; [(d)]Physics Department, National Institute for Research and Development of Isotopic and Molecular Technologies, Cluj-Napoca, Romania; [(e)]University Politehnica Bucharest, Bucharest, Romania; [(f)]West University in Timisoara, Timisoara, Romania
[26] [(a)]Faculty of Mathematics, Physics and Informatics, Comenius University, Bratislava, Slovak Republic; [(b)]Department of Subnuclear Physics, Institute of Experimental Physics of the Slovak Academy of Sciences, Kosice, Slovak Republic
[27] Physics Department, Brookhaven National Laboratory, Upton, NY, USA
[28] Departamento de Física (FCEN) and IFIBA, Universidad de Buenos Aires and CONICET, Buenos Aires, Argentina
[29] California State University, Long Beach, CA, USA
[30] Cavendish Laboratory, University of Cambridge, Cambridge, UK
[31] [(a)]Department of Physics, University of Cape Town, Cape Town, South Africa; [(b)]iThemba Labs, Western Cape, South Africa; [(c)]Department of Mechanical Engineering Science, University of Johannesburg, Johannesburg, South Africa; [(d)]National Institute of Physics, University of the Philippines Diliman (Philippines), Quezon, Philippines; [(e)]Department of Physics, University of South Africa, Pretoria, South Africa; [(f)]School of Physics, University of the Witwatersrand, Johannesburg, South Africa
[32] Department of Physics, Carleton University, Ottawa, ON, Canada
[33] [(a)]Faculté des Sciences Ain Chock, Réseau Universitaire de Physique des Hautes Energies-Université Hassan II, Casablanca, Morocco; [(b)]Faculté des Sciences, Université Ibn-Tofail, Kenitra, Morocco; [(c)]Faculté des Sciences Semlalia, Université Cadi Ayyad, LPHEA-Marrakech, Marrakech, Morocco; [(d)]LPMR, Faculté des Sciences, Université Mohamed Premier, Oujda, Morocco; [(e)]Faculté des sciences, Université Mohammed V, Rabat, Morocco; [(f)]Mohammed VI Polytechnic University, Ben Guerir, Morocco
[34] CERN, Geneva, Switzerland
[35] Enrico Fermi Institute, University of Chicago, Chicago, IL, USA
[36] LPC, CNRS/IN2P3, Université Clermont Auvergne, Clermont-Ferrand, France
[37] Nevis Laboratory, Columbia University, Irvington, NY, USA
[38] Niels Bohr Institute, University of Copenhagen, Copenhagen, Denmark
[39] [(a)]Dipartimento di Fisica, Università della Calabria, Rende, Italy; [(b)]INFN Gruppo Collegato di Cosenza, Laboratori Nazionali di Frascati, Frascati, Italy
[40] Physics Department, Southern Methodist University, Dallas, TX, USA
[41] Physics Department, University of Texas at Dallas, Richardson, TX, USA
[42] National Centre for Scientific Research "Demokritos", Agia Paraskevi, Greece
[43] [(a)]Department of Physics, Stockholm University, Stockholm, Sweden; [(b)]Oskar Klein Centre, Stockholm, Sweden
[44] Deutsches Elektronen-Synchrotron DESY, Hamburg and Zeuthen, Germany
[45] Lehrstuhl für Experimentelle Physik IV, Technische Universität Dortmund, Dortmund, Germany
[46] Institut für Kern- und Teilchenphysik, Technische Universität Dresden, Dresden, Germany
[47] Department of Physics, Duke University, Durham, NC, USA
[48] SUPA-School of Physics and Astronomy, University of Edinburgh, Edinburgh, UK
[49] INFN e Laboratori Nazionali di Frascati, Frascati, Italy
[50] Physikalisches Institut, Albert-Ludwigs-Universität Freiburg, Freiburg, Germany
[51] II. Physikalisches Institut, Georg-August-Universität Göttingen, Göttingen, Germany
[52] Département de Physique Nucléaire et Corpusculaire , Université de Genève, Geneva, Switzerland

[53] [(a)]Dipartimento di Fisica, Università di Genova, Genoa, Italy; [(b)]INFN Sezione di Genova, Genoa, Italy
[54] II. Physikalisches Institut, Justus-Liebig-Universität Giessen, Giessen, Germany
[55] SUPA-School of Physics and Astronomy, University of Glasgow, Glasgow, UK
[56] LPSC, Université Grenoble Alpes, CNRS/IN2P3, Grenoble INP, Grenoble, France
[57] Laboratory for Particle Physics and Cosmology, Harvard University, Cambridge, MA, USA
[58] [(a)]Department of Modern Physics and State Key Laboratory of Particle Detection and Electronics, University of Science and Technology of China, Hefei, China; [(b)]Key Laboratory of Particle Physics and Particle Irradiation (MOE), Institute of Frontier and Interdisciplinary Science, Shandong University, Qingdao, China; [(c)]Key Laboratory for Particle Astrophysics and Cosmology (MOE), SKLPPC, School of Physics and Astronomy, Shanghai Jiao Tong University, Shanghai, China; [(d)]Tsung-Dao Lee Institute, Shanghai, China
[59] [(a)]Kirchhoff-Institut für , Physik Ruprecht-Karls-Universität Heidelberg, Heidelberg, Germany; [(b)]Physikalisches Institut, Ruprecht-Karls-Universität Heidelberg, Heidelberg, Germany
[60] [(a)]Department of Physics, Chinese University of Hong Kong, Shatin, NT, Hong Kong; [(b)]Department of Physics, University of Hong Kong, Hong Kong, China; [(c)]Department of Physics and Institute for Advanced Study, Hong Kong University of Science and Technology, Clear Water Bay, Kowloon, Hong Kong, China
[61] Department of Physics, National Tsing Hua University, Hsinchu, Taiwan
[62] IJCLab, Université Paris-Saclay, CNRS/IN2P3, 91405 Orsay, France
[63] Department of Physics, Indiana University, Bloomington, IN, USA
[64] [(a)]INFN Gruppo Collegato di Udine, Sezione di Trieste, Udine, Italy; [(b)]ICTP, Trieste, Italy; [(c)]Dipartimento Politecnico di Ingegneria e Architettura, Università di Udine, Udine, Italy
[65] [(a)]INFN Sezione di Lecce, Lecce, Italy; [(b)]Dipartimento di Matematica e Fisica, Università del Salento, Lecce, Italy
[66] [(a)]INFN Sezione di Milano, Milan, Italy; [(b)]Dipartimento di Fisica, Università di Milano, Milan, Italy
[67] [(a)]INFN Sezione di Napoli, Naples, Italy; [(b)]Dipartimento di Fisica, Università di Napoli, Naples, Italy
[68] [(a)]INFN Sezione di Pavia, Pavia, Italy; [(b)]Dipartimento di Fisica, Università di Pavia, Pavia, Italy
[69] [(a)]INFN Sezione di Pisa, Pisa, Italy; [(b)]Dipartimento di Fisica E. Fermi, Università di Pisa, Pisa, Italy
[70] [(a)]INFN Sezione di Roma, Rome, Italy; [(b)]Dipartimento di Fisica, Sapienza Università di Roma, Rome, Italy
[71] [(a)]INFN Sezione di Roma Tor Vergata, Rome, Italy; [(b)]Dipartimento di Fisica, Università di Roma Tor Vergata, Rome, Italy
[72] [(a)]INFN Sezione di Roma Tre, Rome, Italy; [(b)]Dipartimento di Matematica e Fisica, Università Roma Tre, Rome, Italy
[73] [(a)]INFN-TIFPA, Trento, Italy; [(b)]Università degli Studi di Trento, Trento, Italy
[74] Institut für Astro- und Teilchenphysik, Leopold-Franzens-Universität, Innsbruck, Austria
[75] University of Iowa, Iowa City, IA, USA
[76] Department of Physics and Astronomy, Iowa State University, Ames, IA, USA
[77] Joint Institute for Nuclear Research, Dubna, Russia
[78] [(a)]Departamento de Engenharia Elétrica, Universidade Federal de Juiz de Fora (UFJF), Juiz de Fora, Brazil; [(b)]Universidade Federal do Rio De Janeiro COPPE/EE/IF, Rio de Janeiro, Brazil; [(c)]Instituto de Física, Universidade de São Paulo, São Paulo, Brazil
[79] KEK, High Energy Accelerator Research Organization, Tsukuba, Japan
[80] Graduate School of Science, Kobe University, Kobe, Japan
[81] [(a)]Faculty of Physics and Applied Computer Science, AGH University of Science and Technology, Kraków, Poland; [(b)]Marian Smoluchowski Institute of Physics, Jagiellonian University, Kraków, Poland
[82] Institute of Nuclear Physics Polish Academy of Sciences, Kraków, Poland
[83] Faculty of Science, Kyoto University, Kyoto, Japan
[84] Kyoto University of Education, Kyoto, Japan
[85] Department of Physics, Research Center for Advanced Particle Physics, Kyushu University, Fukuoka , Japan
[86] Instituto de Física La Plata, Universidad Nacional de La Plata and CONICET, La Plata, Argentina
[87] Physics Department, Lancaster University, Lancaster, UK
[88] Oliver Lodge Laboratory, University of Liverpool, Liverpool, UK
[89] Department of Experimental Particle Physics, Jožef Stefan Institute and Department of Physics, University of Ljubljana, Ljubljana, Slovenia
[90] School of Physics and Astronomy, Queen Mary University of London, London, UK
[91] Department of Physics, Royal Holloway University of London, Egham, UK
[92] Department of Physics and Astronomy, University College London, London, UK

[93] Louisiana Tech University, Ruston LA, USA
[94] Fysiska Institutionen, Lunds Universitet, Lund, Sweden
[95] Centre de Calcul de l'Institut National de Physique Nucléaire et de Physique des Particules (IN2P3), Villeurbanne, France
[96] Departamento de Física Teorica C-15 and CIAFF, Universidad Autónoma de Madrid, Madrid, Spain
[97] Institut für Physik, Universität Mainz, Mainz, Germany
[98] School of Physics and Astronomy, University of Manchester, Manchester, UK
[99] CPPM, Aix-Marseille Université, CNRS/IN2P3, Marseille, France
[100] Department of Physics, University of Massachusetts, Amherst, MA, USA
[101] Department of Physics, McGill University, Montreal, QC, Canada
[102] School of Physics, University of Melbourne, Victoria, Australia
[103] Department of Physics, University of Michigan, Ann Arbor, MI, USA
[104] Department of Physics and Astronomy, Michigan State University, East Lansing, MI, USA
[105] B.I. Stepanov Institute of Physics, National Academy of Sciences of Belarus, Minsk, Belarus
[106] Research Institute for Nuclear Problems of Byelorussian State University, Minsk, Belarus
[107] Group of Particle Physics, University of Montreal, Montreal, QC, Canada
[108] P.N. Lebedev Physical Institute of the Russian Academy of Sciences, Moscow, Russia
[109] National Research Nuclear University MEPhI, Moscow, Russia
[110] D.V. Skobeltsyn Institute of Nuclear Physics, M.V. Lomonosov Moscow State University, Moscow, Russia
[111] Fakultät für Physik, Ludwig-Maximilians-Universität München, Munich, Germany
[112] Max-Planck-Institut für Physik (Werner-Heisenberg-Institut), Munich, Germany
[113] Nagasaki Institute of Applied Science, Nagasaki, Japan
[114] Graduate School of Science and Kobayashi-Maskawa Institute, Nagoya University, Nagoya, Japan
[115] Department of Physics and Astronomy, University of New Mexico, Albuquerque, NM, USA
[116] Institute for Mathematics, Astrophysics and Particle Physics, Radboud University/Nikhef, Nijmegen, The Netherlands
[117] Nikhef National Institute for Subatomic Physics and University of Amsterdam, Amsterdam, The Netherlands
[118] Department of Physics, Northern Illinois University, DeKalb, IL, USA
[119] [(a)]Budker Institute of Nuclear Physics and NSU, SB RAS, Novosibirsk, Russia; [(b)]Novosibirsk State University, Novosibirsk, Russia
[120] Institute for High Energy Physics of the National Research Centre Kurchatov Institute, Protvino, Russia
[121] Institute for Theoretical and Experimental Physics named by A.I. Alikhanov of National Research Centre "Kurchatov Institute";, Moscow, Russia
[122] [(a)]New York University Abu Dhabi, Abu Dhabi, United Arab Emirates; [(b)]United Arab Emirates University, Al Ain, United Arab Emirates; [(c)]University of Sharjah, Sharjah, United Arab Emirates
[123] Department of Physics, New York University, New York, NY, USA
[124] Ochanomizu University, Bunkyo-ku, Otsuka, Tokyo, Japan
[125] Ohio State University, Columbus, OH, USA
[126] Homer L. Dodge Department of Physics and Astronomy, University of Oklahoma, Norman, OK, USA
[127] Department of Physics, Oklahoma State University, Stillwater, OK, USA
[128] Palacký University, Joint Laboratory of Optics, Olomouc, Czech Republic
[129] Institute for Fundamental Science, University of Oregon, Eugene, OR, USA
[130] Graduate School of Science, Osaka University, Osaka, Japan
[131] Department of Physics, University of Oslo, Oslo, Norway
[132] Department of Physics , Oxford University, Oxford, UK
[133] LPNHE, Sorbonne Université, Université de Paris CNRS/IN2P3, Paris, France
[134] Department of Physics, University of Pennsylvania, Philadelphia, PA, USA
[135] Konstantinov Nuclear Physics Institute of National Research Centre "Kurchatov Institute", PNPI, St. Petersburg, Russia
[136] Department of Physics and Astronomy, University of Pittsburgh, Pittsburgh, PA, USA
[137] [(a)]Laboratório de Instrumentação e Física Experimental de Partículas-LIP, Lisbon, Portugal; [(b)]Departamento de Física, Faculdade de Ciências, Universidade de Lisboa, Lisbon, Portugal; [(c)]Departamento de Física, Universidade de Coimbra, Coimbra, Portugal; [(d)]Centro de Física Nuclear da Universidade de Lisboa, Lisbon, Portugal; [(e)]Departamento de Física, Universidade do Minho, Braga, Portugal; [(f)]Departamento de Física Teórica y del Cosmos, Universidad de Granada,

Granada, Spain; [g]Dep Física and CEFITEC of Faculdade de Ciências e Tecnologia, Universidade Nova de Lisboa, Caparica, Portugal; [h]Instituto Superior Técnico, Universidade de Lisboa, Lisbon, Portugal
[138] Institute of Physics of the Czech Academy of Sciences, Prague, Czech Republic
[139] Czech Technical University in Prague, Prague, Czech Republic
[140] Faculty of Mathematics and Physics, Charles University, Prague, Czech Republic
[141] Particle Physics Department, Rutherford Appleton Laboratory, Didcot, UK
[142] IRFU, CEA, Université Paris-Saclay, Gif-sur-Yvette, France
[143] Santa Cruz Institute for Particle Physics, University of California Santa Cruz, Santa Cruz, CA, USA
[144] [a]Departamento de Física, Pontificia Universidad Católica de Chile, Santiago, Chile; [b]Universidad de la Serena, La Serena, Chile; [c]Department of Physics, Universidad Andres Bello, Santiago, Chile; [d]Instituto de Alta Investigación, Universidad de Tarapacá, Arica, Chile; [e]Departamento de Física, Universidad Técnica Federico Santa María, Valparaiso, Chile
[145] Universidade Federal de São João del Rei (UFSJ), São João del Rei, Brazil
[146] Department of Physics, University of Washington, Seattle, WA, USA
[147] Department of Physics and Astronomy, University of Sheffield, Sheffield, UK
[148] Department of Physics, Shinshu University, Nagano, Japan
[149] Department Physik, Universität Siegen, Siegen, Germany
[150] Department of Physics, Simon Fraser University, Burnaby, BC, Canada
[151] SLAC National Accelerator Laboratory, Stanford, CA, USA
[152] Department of Physics, Royal Institute of Technology, Stockholm, Sweden
[153] Departments of Physics and Astronomy, Stony Brook University, Stony Brook, NY, USA
[154] Department of Physics and Astronomy, University of Sussex, Brighton, UK
[155] School of Physics, University of Sydney, Sydney, Australia
[156] Institute of Physics, Academia Sinica, Taipei, Taiwan
[157] [a]E. Andronikashvili Institute of Physics, Iv. Javakhishvili Tbilisi State University, Tbilisi, Georgia; [b]High Energy Physics Institute, Tbilisi State University, Tbilisi, Georgia
[158] Department of Physics, Technion, Israel Institute of Technology, Haifa, Israel
[159] Raymond and Beverly Sackler School of Physics and Astronomy, Tel Aviv University, Tel Aviv, Israel
[160] Department of Physics, Aristotle University of Thessaloniki, Thessaloníki, Greece
[161] International Center for Elementary Particle Physics and Department of Physics, University of Tokyo, Tokyo, Japan
[162] Department of Physics, Tokyo Institute of Technology, Tokyo, Japan
[163] Tomsk State University, Tomsk, Russia
[164] Department of Physics, University of Toronto, Toronto, ON, Canada
[165] [a]TRIUMF, Vancouver, BC, Canada; [b]Department of Physics and Astronomy, York University, Toronto, ON, Canada
[166] Division of Physics and Tomonaga Center for the History of the Universe, Faculty of Pure and Applied Sciences, University of Tsukuba, Tsukuba, Japan
[167] Department of Physics and Astronomy, Tufts University, Medford, MA, USA
[168] Department of Physics and Astronomy, University of California Irvine, Irvine, CA, USA
[169] Department of Physics and Astronomy, University of Uppsala, Uppsala, Sweden
[170] Department of Physics, University of Illinois, Urbana, IL, USA
[171] Instituto de Física Corpuscular (IFIC), Centro Mixto Universidad de Valencia-CSIC, Valencia, Spain
[172] Department of Physics, University of British Columbia, Vancouver, BC, Canada
[173] Department of Physics and Astronomy, University of Victoria, Victoria, BC, Canada
[174] Fakultät für Physik und Astronomie, Julius-Maximilians-Universität Würzburg, Würzburg, Germany
[175] Department of Physics, University of Warwick, Coventry, UK
[176] Waseda University, Tokyo, Japan
[177] Department of Particle Physics and Astrophysics, Weizmann Institute of Science, Rehovot, Israel
[178] Department of Physics, University of Wisconsin, Madison, WI, USA
[179] Fakultät für Mathematik und Naturwissenschaften, Fachgruppe Physik, Bergische Universität Wuppertal, Wuppertal, Germany
[180] Department of Physics, Yale University, New Haven, CT, USA

[a] Also at Borough of Manhattan Community College, City University of New York, New York, NY, USA

[b] Also at Bruno Kessler Foundation, Trento, Italy
[c] Also at Center for High Energy Physics, Peking University, Beijing, China
[d] Also at Centro Studi e Ricerche Enrico Fermi, Rome, Italy
[e] Also at CERN, Geneva, Switzerland
[f] Also at CPPM, Aix-Marseille Université, CNRS/IN2P3, Marseille, France
[g] Also at Département de Physique Nucléaire et Corpusculaire, Université de Genève, Geneva, Switzerland
[h] Also at Departament de Fisica de la Universitat Autonoma de Barcelona, Barcelona, Spain
[i] Also at Department of Financial and Management Engineering, University of the Aegean, Chios, Greece
[j] Also at Department of Physics and Astronomy, Michigan State University, East Lansing, MI, USA
[k] Also at Department of Physics and Astronomy, University of Louisville, Louisville, KY, USA
[l] Also at Department of Physics, Ben Gurion University of the Negev, Beer Sheva, Israel
[m] Also at Department of Physics, California State University, East Bay, USA
[n] Also at Department of Physics, California State University, Fresno, USA
[o] Also at Department of Physics, California State University, Sacramento, USA
[p] Also at Department of Physics, King's College London, London, UK
[q] Also at Department of Physics, St. Petersburg State Polytechnical University, St. Petersburg, Russia
[r] Also at Department of Physics, University of Fribourg, Fribourg, Switzerland
[s] Also at Faculty of Physics, M.V. Lomonosov Moscow State University, Moscow, Russia
[t] Also at Faculty of Physics, Sofia University, 'St. Kliment Ohridski', Sofia, Bulgaria
[u] Also at Giresun University, Faculty of Engineering, Giresun, Turkey
[v] Also at Graduate School of Science, Osaka University, Osaka, Japan
[w] Also at Hellenic Open University, Patras, Greece
[x] Also at Institucio Catalana de Recerca i Estudis Avancats, ICREA, Barcelona, Spain
[y] Also at Institut für Experimentalphysik, Universität Hamburg, Hamburg, Germany
[z] Also at Institute for Particle and Nuclear Physics, Wigner Research Centre for Physics, Budapest, Hungary
[aa] Also at Institute of Particle Physics (IPP), Victoria, Canada
[ab] Also at Institute of Physics, Azerbaijan Academy of Sciences, Baku, Azerbaijan
[ac] Also at Institute of Theoretical Physics, Ilia State University, Tbilisi, Georgia
[ad] Also at Instituto de Fisica Teorica, IFT-UAM/CSIC, Madrid, Spain
[ae] Also at Department of Physics, Istanbul University, Istanbul, Turkey
[af] Also at Joint Institute for Nuclear Research, Dubna, Russia
[ag] Also at Moscow Institute of Physics and Technology State University, Dolgoprudny, Russia
[ah] Also at National Research Nuclear University MEPhI, Moscow, Russia
[ai] Also at Physikalisches Institut, Albert-Ludwigs-Universität Freiburg, Freiburg, Germany
[aj] Also at The City College of New York, New York, NY, USA
[ak] Also at TRIUMF, Vancouver, BC, Canada
[al] Also at Universita di Napoli Parthenope, Naples, Italy
[am] Also at University of Chinese Academy of Sciences (UCAS), Beijing, China
[an] Also at Yeditepe University, Physics Department, Istanbul, Turkey
[*] Deceased